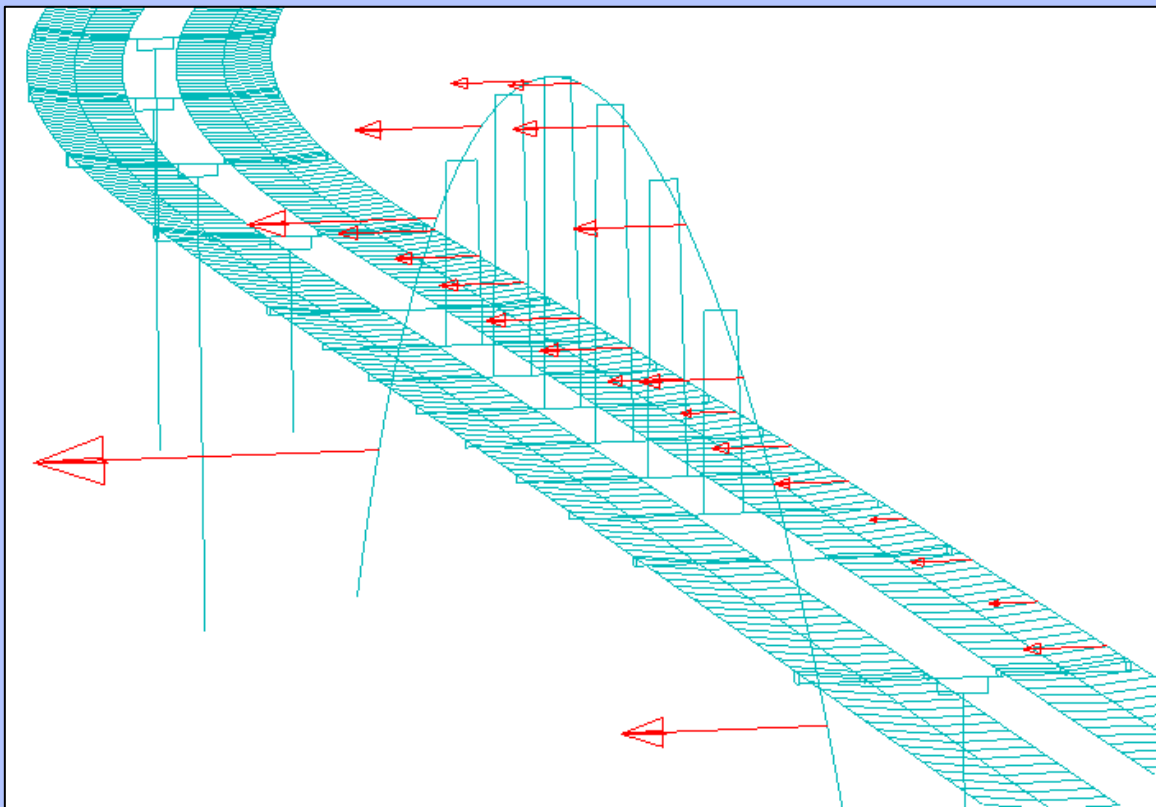




KTH Byggetenskap



Wind Response of The New Svinesund Bridge

MATTEO GIUMELLI

Examensarbete 251
Brobyggnad
ISSN 1103-4297

Brobyggnad
KTH Byggetenskap
KTH, SE 100 44 Stockholm
www.byv.kth.se

Abstract

Very high or long structures characterized by a relevant slenderness, low weight and a small damping ratio, like towers or long suspended bridges, can be particularly susceptible to wind actions. The effect of the wind on this type of structures has to be studied through a dynamic approach. This thesis deals with the response of the New Svinesund Bridge to wind actions. The slenderness of its single concrete arch and the long main span suspended to the arch through a system of hangers make the structure sensible to problem of vibrations during its operating time. Due to the complexity of the structural design and the importance of the bridge a monitoring program was developed in order to control the structural behaviour during the construction phase, the testing phase and the first years of its service life. The aim of this work is to make a comparison between numerical results and experimental measurements. At first the structure is modelled by a FE model, which is based on the structural model produced by the bridge contractor and regards the arch, the hangers, the piers and the superstructure, all modelled by beam elements. At the same time the identification of the dynamic parameters of the structure from the output measurements is carried out; this step permits the evaluation of the frequencies and modes of the structure and allows a comparison with the results extracted from the FE eigenvalue analysis. The measured damping ratio is determined later and permits the updating of the FE model for the simulations. The wind data from in-situ measurements are analysed and a reference wind velocity history is chosen. The wind and the related actions can be represented by a random multivariate stationary Gaussian process and the simulation of this random process is carried out by the random phase method. The along-wind forces are calculated through the aerodynamic static coefficients: for the bridge deck the values are deduced from the wind tunnel tests; for the arch, instead, approximate values have to be assumed. A preliminary study of the wind effects induced on a simplified beam model is examined in order to point out the influence of some relevant parameters involved in the simulations. The simulations are then made varying the wind characteristic parameters and taking into account their influence on the final response obtained. The results from each simulation can be compared with the measurements and this comparison has to be made in statistical terms by a mean maximum displacement evaluated for any section considered. The estimated difference is expressed as a percentage value. Finally an analysis with equivalent

static forces and a dynamic simulation are carried out, both assuming an high mean wind velocity as reference; the results obtained can be compared making considerations on the validity of the performed analyses.

Table of contents

Abstract.....	i
Chapter 1 Description of the bridge and monitoring program	1
1.1 Introduction.....	1
1.2 Description of the bridge	1
1.3 Construction of the bridge	3
1.3.1 Construction of the arch	4
1.3.2 Construction of the superstructure.....	5
1.4 Description of the monitoring program	6
1.4.1 Instrumentation of the arch.....	6
1.4.2 Wind speed measurements	9
1.5 Aim and scope of the study.....	11
Chapter 2 Theory on dynamics of structures and wind actions	14
2.1 Structural dynamics	14
2.2 Undamped free vibration	16
2.3 Damped free vibration	18
2.4 Undamped system: harmonic excitation.....	20
2.5 Damped system: harmonic excitation.....	21
2.6 Half power (Band width) method	23
2.7 Methods of numerical integration.....	23
2.7.1 Newmark "Beta" method	25
2.7.2 Hilbert-Huge-Taylor alpha method	26
2.8 Eigenvalue problem	26
2.9 Rayleigh damping	28
2.10 Wind profile	29
2.11 Aerodynamic forces and coefficients.....	31
2.12 Wind tunnel tests.....	33
2.13 Along-wind forces on the bridge	40
2.14 Fourier analysis.....	43
2.15 Power spectral density function (PSD).....	45
2.16 N-varied stationary random process	48
2.17 Discrete Fourier Transform (DFT)	49
2.18 Aliasing	50
2.19 Fast Fourier Transform	51

Chapter 3 FE model of the bridge	53
3.1 Creating a model in ABAQUS/CAE.....	53
3.1.1 Modules	53
3.1.2 Analysis type	54
3.1.2.1 General static analysis	54
3.1.2.2 Linear eigenvalue analysis	55
3.1.2.3 Implicit dynamic analysis.....	55
3.1.2.4 Explicit dynamic analysis.....	56
3.1.3 Elements	57
3.1.3.1 Beam elements	58
3.1.3.2 Material damping	58
3.2 FE model of the New Svinesund Bidge.....	59
3.2.1 General description.....	60
3.2.2 Different parts of the model.....	61
3.2.3 Boundary conditions and constraints.....	62
3.3 Model of the wind forces	63
3.4 Analysis steps.....	65
Chapter 4 Simulations and analysis of the results	66
4.1 Dynamic identification of civil structures.....	66
4.1.1 Peak-picking method	67
4.2 Identification of the natural frequencies	68
4.2.1 Numerical results	72
4.2.2 Identification of the modes	75
4.2.3 Comparison between numerical and measured results.....	78
4.3 Simulation of random stationary normal processes	81
4.3.1 Mono-variate processes	81
4.3.2 Multi-variate processes.....	83
4.3.3 Spectral turbulence model	84
4.3.4 Spectral models, model errors and parameter uncertainties	87
4.4 Wind velocity history	88
4.5 Analysis with correlated forces.....	92
4.5.1 Damping ratio from the Eurocode	93
4.5.2 Filtering	94
4.5.3 Determination of the roughness length.....	98
4.5.4 Results	99
4.6 Numerical simulation of wind velocity histories along the bridge.....	102
4.7 Evaluation of the measured damping ratio	106

4.8	Distribution of the maximum displacement.....	108
4.9	Study of a simplified beam model	109
4.10	Analysis of the results from the simulations.....	115
4.10.1	Influence of the number of nodes.....	115
4.10.2	Influence of the drag coefficient of the arch	116
4.10.3	Influence of the coherence	118
4.10.4	Influence of the roughness length	120
4.10.5	Drag forces divided in equal parts between the two deck girders.....	122
4.10.6	Contribution of the vertical turbulence	124
4.10.7	Coherence between different turbulence components.....	126
4.11	Eurocode method to calculate the static equivalent forces	130
4.11.1	Basic wind velocity	130
4.11.2	Mean wind velocity	131
4.11.3	Wind turbulence.....	132
4.11.4	Peak velocity pressure	132
4.11.5	Wind pressure on external surfaces	133
4.11.6	Wind forces.....	133
4.11.7	Structural factor	135
4.11.8	Equivalent static forces on the bridge	135
4.12	Equivalent static forces from the wind tunnel tests	136
4.13	Analysis with high mean wind velocity.....	137
Chapter 5 Conclusions and suggestions for further research.....		140
5.1	Conclusions.....	140
5.2	Suggestions for further research	142
Bibliography		144

Chapter 1 Description of the bridge and monitoring program

1.1 Introduction

This report presents a study of the dynamic response of the New Svinesund Bridge subjected to wind load. The structure is a new road bridge which joins Sweden and Norway across the Ide Fjord at Svinesund and it is part of the European highway E6 which is the main route for all road traffic between Gothenburg and Oslo. The particular design of the bridge combines a very slender construction with a special structural form. In particular the single arch and the position of the columns closest to the arch which are not located on its foundations make the structure susceptible to problem of instability both during the construction phase and during the service life. Due to this structural complexity and the importance of the bridge a monitoring programme was developed through the collaboration between the Swedish National Road Administration, the Royal Institute of Technology (KTH), the Norwegian Geotechnical Institute (NGI) and the Norwegian Public Roads Administration. The study of the effects of the wind is a significant part in the general description of the structural behaviour of the bridge and allows making a comparison with the measurements.

1.2 Description of the bridge

The New Svinesund Bridge is a highway bridge 704 m long made up of a substructure in ordinary reinforced concrete, a steel bridge deck and a single ordinary reinforced concrete arch. The bridge has eight spans; the length of the main span is 247 m and is carried by the arch. The bridge deck is connected to the arch at approximately half its height and increases its lateral stability preventing out of plane buckling.

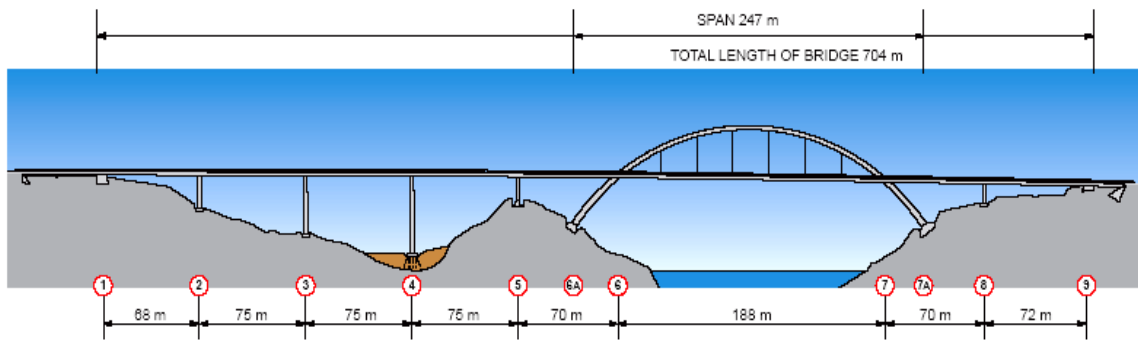


Figure 1.1 Sketch of the New Svinesund Bridge, showing numbering of the support lines and approximate dimensions of the spans.

The bridge deck consists of two box-girders, one on either side of the arch, with a total width of approximately 28 m. Each box-girder is composed of two steel prefabricated elements 5.5 m wide and 24 m long, welded together for a total width of 11 m. The steel plates of the box-girder are 12-40 mm thick and are stiffened with longitudinal profiles. The arch is joined to the bridge deck by stiff connections at the intersections and between these intersections, where the arch rises above the bridge deck, the two box-girders are joined by transverse beams supported by hangers which are in turn connected to the concrete arch. The transverse beams are positioned at 25.5 m intervals and are carried by six pairs of hangers. In the land spans the transverse beams, connecting the two box-girders, are positioned in correspondence of the columns and abutments.



Figure 1.2 Section of the bridge deck.

The level of the top of the arch and the bridge deck are approximately +91 m and +60 m respectively on the sea level. The section of the arch is a rectangular hollow section that decreases from the abutment to the crown in both width and height. The section at the abutments is approximately 6.2 m wide and 4.2 m high with a wall thickness of 1.5 m and 1.1 m respectively. Close to the crown the section is approximately 4 m wide and 2.7 m high with a wall thickness of 0.6 m and 0.45 m. In addition to the abutments on each side of the fjord the superstructure is supported by five intermediate supporting piers made of reinforced concrete, four on the Swedish side and one on the Norwegian. All of the substructures have foundations in the rock except the pier 4 (see Figure 1.1) which is supported by steel core piles in a peat bog. The section of the piers is a rectangular hollow section 6.2 m wide, which is the gap between the two box-girders of the bridge deck, and the height varies from 11 to 47 m. Due to the large uplift reaction on the supporting piers the transverse beams are anchored with tendons inside the piers. The main span instead is suspended in the arch.

1.3 Construction of the bridge

The construction of the bridge, started during 2003, is finished in the spring of 2005 after 36 months. During 2003 the work was concentrated on the construction of the arch, the piers and the superstructure on the southern side. In 2004 the superstructure and all the construction work connected with the arch were completed. The bridge was opened for traffic on 10th of May as part of the celebrations for the 100-year anniversary of Norway independence from Sweden. The monitoring program will continue until 2010 to control the behaviour of the structure and the response to traffic loads, temperature and wind effects.

1.3.1 Construction of the arch

The construction of the arch was started at the same time on both sides of the fjord with the foundations at the abutments of the arch. The construction was carried out in 24 successive arch segments for each side finally linked together at the crown of the arch. The first segments were cast using traditional scaffolding. Then the subsequent segments were cast by a climbing formwork using a cantilever construction method with temporary cable-stayed supporting as shown in the Figure 1.3.

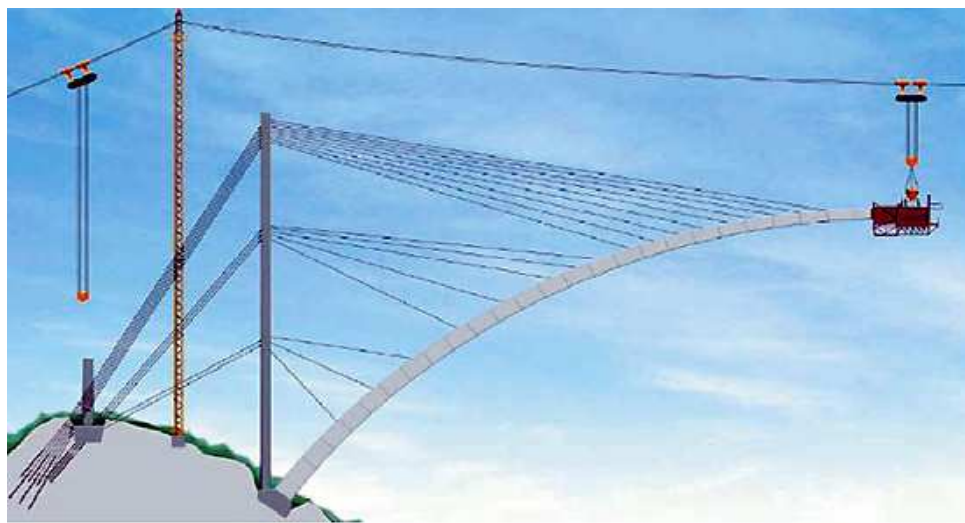


Figure 1.3 Phase of the arch launching.

The system is a hydraulic climbing formwork that was anchored to the previous completed arch segment. When the cast of a segment was finished the climbing formwork was moved forward to prepare the casting of the next segment; after the completion of the first three segments supporting steel cables were used to hold the followings in their position. These cables were anchored to two temporarily towers, one on each side of the fjord, and passed through the reinforced concrete towers anchoring themselves at the back of the towers. The towers were back-anchored into the rock by cables which passed through the towers and were anchored at the front of these. After 13 segments each segment needed to be supported by cables in order to correct the position of the arch, compensating the deflection of the structure from its original position due to its self-weight.

1.3.2 Construction of the superstructure

Each bridge deck is composed of two 5.5 m wide and 24 m long prefabricated steel element which were welded together on site to produce the resulting 11 m wide decks. Two different methods were used to assembly the superstructure elements on the Swedish and on the Norwegian side. On the Swedish side the sections were welded together and then the bridge deck was launched out over the bridge supports using hydraulic jacks that pushed the structure 0.5 m above its final position; after the entire structure reached its position it was brought down to its final level on the piers supports. On the Norwegian side a more traditional method was used welding the sections directly in their final position and keeping them in a fixed scaffold. The last part of the bridge deck installed was the suspended central part carried by the arch. The central section was welded together in Halden harbour and then transported on the sea by barges to bridge site where it was lift by jacks mounted on temporary cables hanging from the arch (see Figure 1.4). When it reached its final position, it was connected to the permanent pairs of hangers from the arch and to the rest of the bridge deck.



Figure 1.4 The central section of the bridge is lift in its final position.

1.4 Description of the monitoring program

The monitoring program was developed to measure the structural behaviour of the bridge during the construction phase, the testing phase and it will continue for the first 5 years of the service life. It is coordinated by the Royal Institute of Technology (KTH), project manager Dr. Raid Karoumi, which is the responsible for the analysis and the documentation of the project. The instrumentation is carried out by the Norwegian Geotechnical Institute which is responsible for the measurements. During the construction phase the main objective of the measurements was to check that the bridge was built as designed and to verify the agreement of the design assumptions with reality. When the bridge was completed static and dynamic load testing were conducted to quantify global stiffness and dynamic properties such as damping ratio, eigenfrequencies and vibration mode shapes. Thus comparing the measurements with the analytical and theoretical results it is possible to understand more about the structural behaviour of the bridge.

1.4.1 Instrumentation of the arch

The sensors were positioned at the critical sections of the arch. The first segments at the abutments of the arch were chosen, the segment at the top of the arch and the segments at the arch-bridge deck junctions were identified as critical; but then it was judged that local effects may influence the measurements and make these meaningless so it was decided to choose for the instrumentation the segments immediately below these. All the sensors were positioned within the box section of the arch close to the axes of symmetry of the section (Figure 1.5). The data acquisition system was designed and delivered by NGI for the specific purposes of this monitoring program; the system consists of two separate data sub control units located at the base of the arch on respectively the Swedish and Norwegian side. The sub-control system on the Swedish side contains the central computers which are connected by a telephone link for data transmittal to the computers facilities at NGI/KTH. The logged data on the Norwegian side are transmitted to the central computer on the Swedish side through a radio link. The logging procedure provides sampling of all sensors

continuously at 50 Hz with the exception of the temperature sensors which have a sampling of once per 20 seconds or 1/20 Hz. At the end of each 10 minute sampling period, statistical data such as mean, maximum, minimum and standard deviation are calculated for each sensor and stored in a statistical data file having a file name that identifies the date and time period when the data was recorded.

Making a summary of the type, location and number of the sensors installed on the arch it is possible to distinguish:

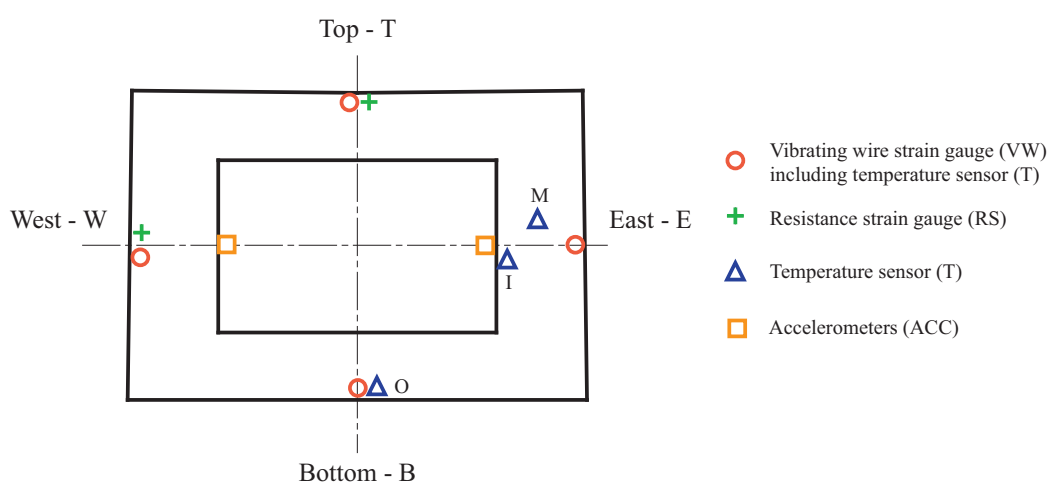


Figure 1.5 A sketch which shows the general positioning of the sensors within the box section of the arch.

- Two different types of strain gauges were installed for the measurement of the internal strains: vibrating wire strain and resistance strain gauges. Both of these sensors are preassembled on normal reinforcement bars, called ‘sister bars’, placed along the main reinforcement. The length of the sister bars is such to ensure a full bonding with the concrete at both ends of the bars.
- Inside the concrete were installed 28 temperature gauges to measure the temperature within the concrete arch. The air temperature is monitored by a separate sensor that is part of the SMHI (Swedish Meteorological and Hydrological System) wind monitoring system.

- In order to measure the accelerations two boxes were used, each box including two linear servo accelerometers. One accelerometer was oriented vertically, along the z-axis and the other one horizontally along the y-axis, perpendicular to the longitudinal bridge axis. The boxes were moved during the construction phase towards the centre of the bridge and when the arch was completed they were placed in their final position: one at the midpoint of the arch and one at the Swedish quarter point of the arch. The acceleration data are recorded with a frequency of 50 Hz.

The final position of the accelerometers is shown in the Figure below.

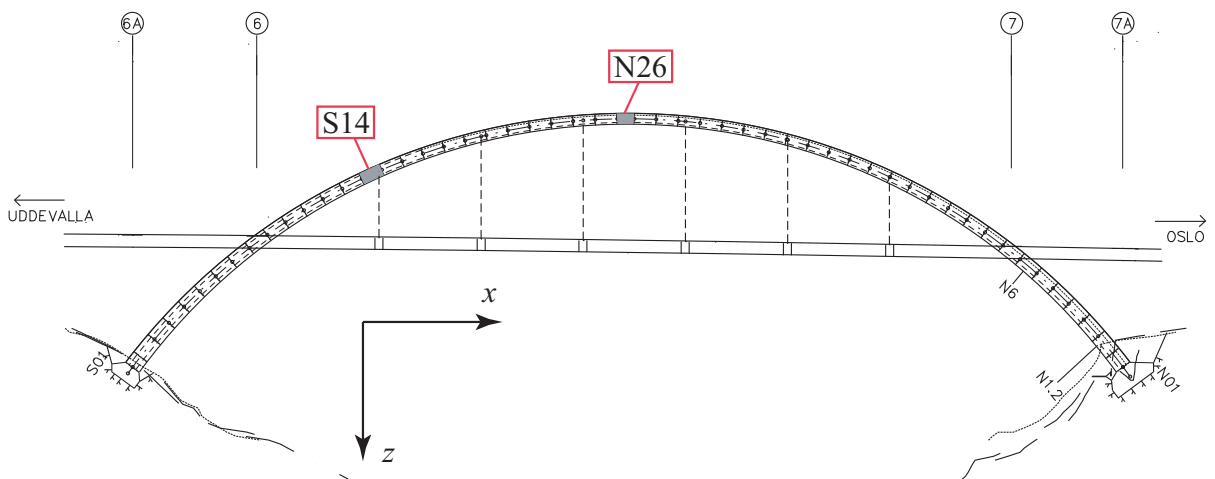


Figure 1.6 An elevation of the bridge showing the final position of the accelerometers installed in segment S14 at the Swedish side of the arch and in segment N26 at the top of the arch

The use of the letters S and N refer to the Swedish and Norwegian side respectively. The numbering 1-25 starts at the abutment and proceeds to the crown of the arch, with the segment N26 forming the crown itself.

1.4.2 Wind speed measurements

The wind speed and direction is measured using a 3-directional ultrasonic anemometer which can measure the wind speed in three directions. Installed before the beginning of the construction of the bridge by the SMHI, it was removed from its original position in December 2003 and installed on the top of a special mast positioned in correspondence of the pier, on the Swedish side, closest to the arch. The mast is 20 m high and the resulting position of the anemometer is at 65 m on the sea level, 4 m above the bridge deck level. Originally the intention was to place the instrument at a certain distance from the bridge to avoid distorted wind measurements; then practical reasons made impossible this positioning. The wind speed data are measured with a frequency of 5 Hz.

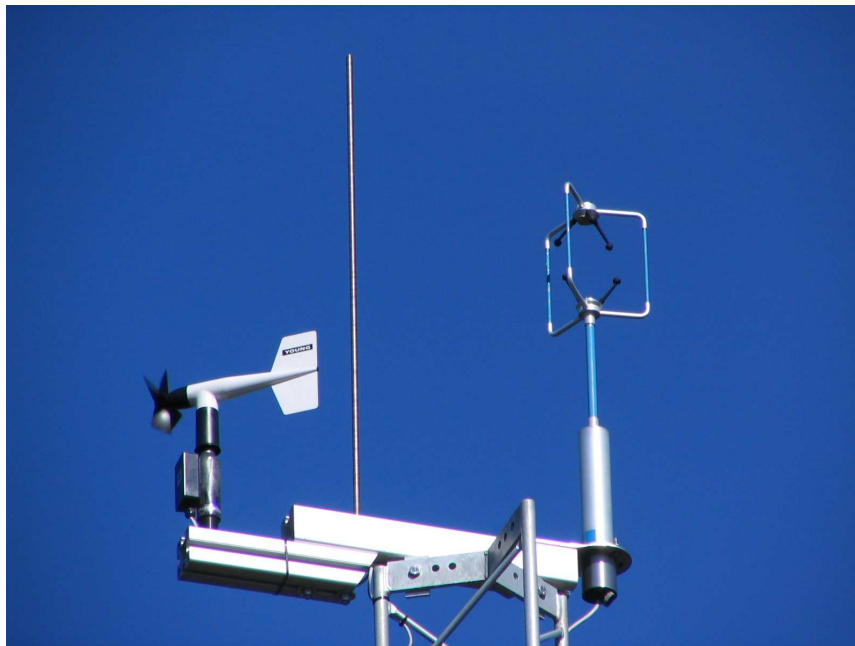


Figure 1.7 Detail of the anemometric station.

In the next table the specifications of the transducer are summarised:

<i>Anemometer type</i>	3-axis GILL Windmaster
<i>Wind speed</i>	
Measuring range	0 - 60 m/s
Accuracy	1.5 % rms (0 – 20 m/s)
Resolution	0.01 m/s
<i>Direction</i>	
Measuring range	0 - 359°
Accuracy	<25 m/s $\pm 2^\circ$, >25 m/s $\pm 4^\circ$
Resolution	1°
<i>Sampling rate</i>	5 Hz

Table 1.1 Characteristics of the anemometer.



Figure 1.8 The mast on which the anemometer is installed.

1.5 Aim and scope of the study

The aim of this work is to study the response of the New Svinesund Bridge subjected to wind load and try to improve the knowledge of the wind effects on the structure comparing numerical results with measurements; since the wind and the correspondent action on the structure represents a random process, the results obtained have to be treated and compared with the measurements in statistical terms. In order to interpret the analysis carried out in a correct way it is necessary to consider the simplifications made in the model and the uncertainties of many parameters involved in the simulation. All of these aspects will be dealt in the next chapters, but it could be important to focalize the attention on them from the beginning.

The wind velocity is measured in a point close to the bridge and the measurements are certainly affected by the presence of the structure. At the beginning of the study the registrations of wind velocities considered were about west winds; since the anemometer is installed on the east side of the structure the measurements resulted clearly affected by the disturbance of the structure. So it was decided to consider a time-history of wind velocity for east wind.

It is necessary also to note the anomaly that the anemometer is positioned on the east side of the bridge and the accelerometers, which measure the horizontal accelerations of the bridge deck, are positioned on its west side. This demonstrates a few attention given to the specific wind effect in the general monitoring program.

The aerodynamic static coefficients are known exactly only for the bridge deck by the wind tunnel test. It is necessary to consider that these values are determined in the wind tunnel for high values of the wind velocity and for a laminar flow; for low velocities with a turbulent content the experimental data have a larger dispersion. For the arch on the approximate values have to be taken, having not precise results from the wind tunnel tests but just a not clear value indicated in the calculation of the quasi static loads in the final report of the wind tunnel tests. So approximate constant values are assumed for the whole arch, but in reality each cross section of the arch varies its inclination with respect to the

wind flow, supposed perpendicular to the longitudinal bridge axis. So different values should be determined but this problem results rather difficult. Furthermore it has to be noticed that the drag coefficient of the arch will prove to be one of the most influential parameter in the structural response.

Uncertainties exist in the model of the wind field; for example the roughness length, which represents the characteristics of the bridge site, has a big uncertainty even if its value doesn't influence so much the final structural response.

Uncertainties affect the dynamic characteristics of the structure like the damping ratio. At first a value based on the expression proposed by the Eurocode was assumed; then a more accurate value was evaluated from the measurements and it permits to update the FE model.

During the simulations of the wind field coherence functions of the turbulence components at different points of the structure and coherence functions of different turbulence components in the same point are assumed, based on literature models; their characteristic parameters are those proposed by literature and derived from experimental data; it is necessary to take into account the uncertainty of these values and the large influence that they have on the results of the analyses.

Assuming that the response to the wind actions is fundamentally on the first shape mode, which showed to interest only the central part of the bridge, the wind forces are applied on the arch and on the mid part of the bridge deck included between the first two piers from the arch. This assumption, even if simplifies the real configuration of the whole structure subjected to the wind action, can be considered reliable taking into account the previous consideration and the positions of the sensors; moreover it aids to decrease the computational effort of the analysis.

Finally it is necessary to consider the limit of the quasi-static theory considered in the calculation of the along-wind forces. This theory works well for high wind velocities, but

in the case considered the reference velocity is low and probably this approach is at the limit of its validity.

Chapter 2 Theory on dynamics of structures and wind actions

2.1 Structural dynamic

The purpose of this section is to introduce some of the theoretical basics of structural dynamic used in this thesis. The concept of a dynamic analysis is to study the response in the time (displacements, stresses, reaction forces etc.) of a system subjected to a load that is time-varying. Two fundamental approaches are available for evaluating structural response to dynamic loads: deterministic and nondeterministic. The type of the analysis depends upon the nature of the load; if the time variation of the load is fully known a deterministic analysis will be carried out and a deterministic displacement time-history will be obtained, from which then it is possible to calculate other aspects of the response such as stresses, strains, internal forces etc; if the time variation of the load is not completely known, it must be defined in statistical terms and a random dynamic analysis will be carried out.

Thus the first basic difference of a structural dynamic problem from a static problem is the time-varying nature of the problem. However a more fundamental distinction results from the inertia forces which resist accelerations of the structure; thus the internal forces in the system must equilibrate not only the externally applied force but also the inertia forces resulting from the accelerations of the structure. The closed cycle of cause and effect, for which the inertia forces result from the structural displacements which in turn are influenced by the magnitudes of the inertia forces, can be solved only by formulating the problem in terms of differential equations.

The number of independent coordinates necessary to specify the configuration or position of a system at any time represents the number of degrees of freedom of the structure (DOF). A continuous structure has an infinite number of degrees of freedom, but selecting an appropriate mathematical model of the structure it is possible to reduce the number of degrees of freedom to a discrete number or to just a single degree of freedom.

There are different procedures to reduce the number of degrees of freedom and they permit to express the displacements of any given structure in terms of a finite number of discrete displacements coordinates. For simplicity it is considered the case of a one dimensional structure represented by a simple beam. The Lumped-Mass procedure concentrates the

mass of the beam in discrete points or lumped and therefore it is necessary to define the displacements and the accelerations only at these discrete points. In case where the mass of the system is quite uniformly distributed throughout an alternative method is preferable. This procedure assumes that the deflection shape of the beam can be expressed as the sum of a series of specified displacement patterns; these patterns become the displacement coordinates of the structure. A simple example is to express the deflection of the beam as the sum of independent sine wave contributions:

$$v(x) = \sum_{n=1}^{\infty} b_n \sin \frac{n\pi x}{l} \quad (2.1)$$

where the amplitudes of the sine waves may be considered to be the coordinates of the system. In general any arbitrary shape compatible with the boundary conditions can be represented by an infinite series of such sine wave components. The advantage of the method is that a good approximation to the actual shape of the beam can be achieved by a truncated series of sine wave components. A generalized expression for the displacements of any one dimensional structure can be written as:

$$v(x) = \sum_n Z_n \psi_n(x) \quad (2.2)$$

where $\psi_n(x)$ represents any shape function, compatible with the support-geometric conditions, and Z_n the amplitude terms referred to as the generalized coordinates. A third method is the Finite Element Method which combines certain features of both the precedent methods. The first step in the finite element method is to divide the structure, for example the beam, in an appropriate number of elements. The points of connection between the elements are called nodes and the displacements of these nodal points represent the generalized coordinates of the structure. The displacements of the complete structure are expressed in terms of nodal displacements by means of appropriate displacement functions, using an expression similar to the equation (2.2). The displacement functions are called interpolation functions because they define the shape between the specified nodal displacements. In principle these interpolation functions could be any curve

which is internally continuous and which satisfies the geometric displacements conditions imposed by the nodal displacements. For one dimensional element it is convenient to use the shapes which would be produced by the nodal displacements in a uniform beam (these are cubic hermitian polynomials).

The Finite-Element procedure provides the most efficient procedure for expressing the displacements of arbitrary structural configurations by means of a discrete set of coordinates for the following reasons:

- Any desired number of generalized coordinates can be introduced merely by dividing the structure into an appropriate number of segments.
- Since the displacement functions chosen for each element may be identical, computations are simplified.
- The equations which are developed by this approach are largely uncoupled because each nodal displacement affects only the neighbour elements; thus the solution process is greatly simplified.

2.2 Undamped free vibration

Considering a structure modelled with a single degree of freedom, the displacement coordinate $u(t)$ completely defines the position of the system.

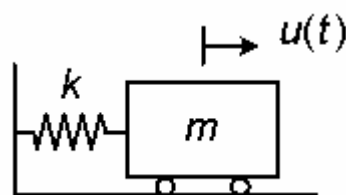


Figure 2.1 Simple undamped oscillator.

Each element in the system represents a single property: the mass m represents the property of inertia and the spring k represents the elasticity. The structure is disturbed from its static equilibrium by either an initial displacement $u(0)$ or velocity $\dot{u}(0)$ and then vibrates without any applied load .

The application of D'Alembert Principle to the system allows to obtain the equation of motion as an equilibrium equation of the forces in the u direction:

$$m\ddot{u} + ku = 0 \quad (2.3)$$

The equation of motion is a differential equation of second order, linear, homogeneous with constant coefficients; the displacement of the system is a simple harmonic and oscillatory about its static equilibrium and has the solution:

$$u(t) = u_0 \cos \omega_n t + \frac{\dot{u}_0}{\omega_n} \sin \omega_n t \quad (2.4)$$

It can be written in an equivalent form:

$$u(t) = C \sin(\omega_n t + \theta) \quad (2.5)$$

Where $C = \sqrt{u_0^2 + \left(\frac{\dot{u}_0}{\omega_n}\right)^2}$, $\sin(\theta) = \frac{u_0}{C}$ and $\cos(\theta) = \frac{\dot{u}_0}{\omega_n C}$

The value of C is the amplitude of the motion and θ is the phase angle.

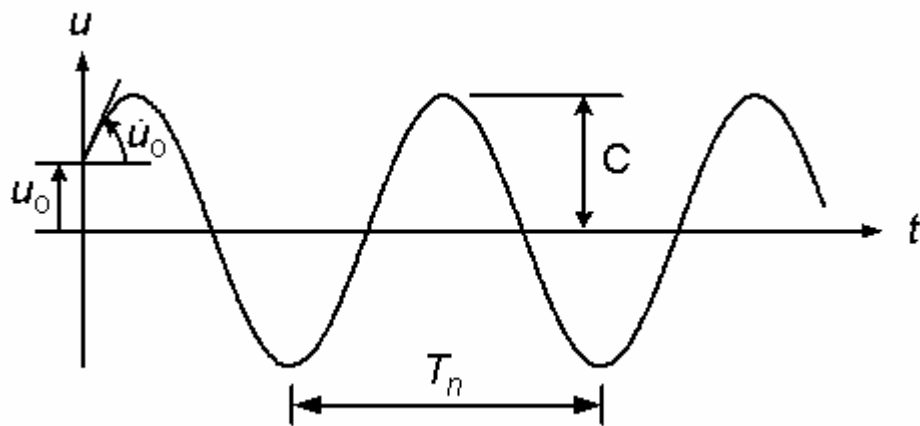


Figure 2.2 Undamped free vibration response.

The circular natural frequency or angular natural frequency is ω_n and is measured in radians per second [rad/sec].

The natural frequency (or frequency of the motion) is $f_n = \frac{\omega_n}{2\pi}$ and is expressed in hertz [Hz] or cycles per second [cps].

The reciprocal of the natural frequency is the natural period of the motion $T_n = \frac{1}{f_n} = \frac{2\pi}{\omega_n}$ and is expressed in seconds per cycle or simply in seconds [s] with the implicit understanding that is per cycle.

2.3 Damped free vibration

The simple oscillator under ideal conditions of no damping once excited will oscillate indefinitely with constant amplitude and its natural frequency. But damping forces which dissipate energy are always present in any physical system in motion. Usually viscous damping forces are assumed, these forces are proportional to the magnitude of the velocity and opposite to the direction of motion; there are two fundamental reasons for the use of viscous damping forces: the mathematical equation which describes the motion is easy; this model gives results which are often in very good agreement with experiments.

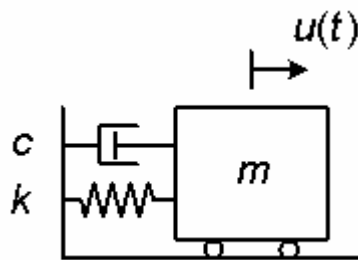


Figure 2.3 Viscous damped oscillator.

k is the spring constant and c is the viscous damping coefficient. Using the D'Alembert Principle the equation of motion results:

$$m\ddot{u} + c\dot{u} + ku = 0 \quad (2.6)$$

The solution for an underdamped system with $c < c_{cr} = 2\sqrt{km}$ is:

$$u(t) = e^{-\xi\omega_n t} \left(u_0 \cos \omega_D t + \frac{\dot{u}_0 + \xi\omega_n u_0}{\omega_D} \sin \omega_D t \right) \quad (2.7)$$

It can be written in an equivalent form:

$$u(t) = C e^{-\xi\omega_n t} \sin(\omega_D t + \theta) \quad (2.8)$$

Where $C = \sqrt{u_0^2 + \frac{(\dot{u}_0 + \xi\omega_n u_0)^2}{\omega_D^2}}$, $\sin(\theta) = \frac{u_0}{C}$ and $\cos(\theta) = \frac{\dot{u}_0 + \xi\omega_n u_0}{C\omega_D}$

The damping ratio of the system is defined as $\xi = \frac{c}{c_{cr}} = \frac{c}{2\sqrt{km}}$ and the damped frequency

of the system is $\omega_D = \omega_n \sqrt{1 - \xi^2}$.

The motion is oscillatory but not periodic. The amplitude of the oscillations decreases for successive cycles, nevertheless the oscillations occur at equal intervals of time with a

damped period of vibration: $T_D = \frac{2\pi}{\omega_D} = \frac{2\pi}{\omega_n \sqrt{1 - \xi^2}}$

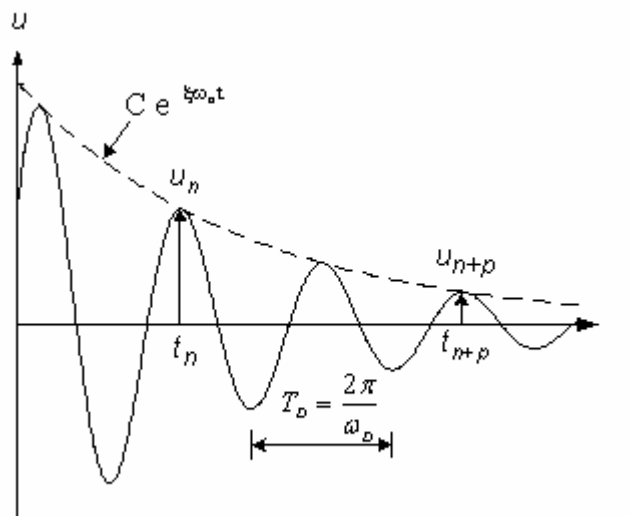


Figure 2.4 Free vibration response of an underdamped system.

The value of the damping coefficient for real structures is much less than the critical damping coefficient and usually ranges between 2 to 10 % of the critical value. In practice the natural frequency for a damped system may be taken to be equal to the undamped natural frequency.

2.4 Undamped system: harmonic excitation

It's important to study the response of the structures to harmonic excitations because even in cases when the excitation is not a harmonic function, the response of the structure may be obtained using Fourier Method as the superposition of individual responses to the harmonic components of the external excitation. The simple oscillator is subjected to a harmonic load equal to $p_0 \sin \omega t$.

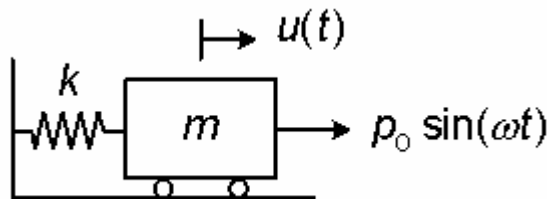


Figure 2.5 Undamped oscillator harmonically excited.

$$m\ddot{u} + ku = p_0 \sin(\omega t) \quad (2.9)$$

The solution can be expressed as the sum of $u_h(t)$, satisfying the homogeneous equation, and a particular solution $u_p(t)$.

$$u(t) = u_h(t) + u_p(t) \quad (2.10)$$

with $u_h(t) = C \sin(\omega_n t + \theta)$ and $u_p(t) = A \sin(\omega t)$

The resulting solution is:

$$u(t) = C \sin(\omega_n t + \theta) + \frac{p_0/k}{1 - (\omega/\omega_n)^2} \sin(\omega t) \quad (2.11)$$

where:

$u_h(t)$ is the transient response and the damping implies that this term disappears after some time.

$u_p(t)$ is the steady state response and ω represents the frequency of the external excitation.

p_0/k is the static deformation due to a static load p_0 .

ω/ω_n is the ratio of the applied forced frequency to the natural frequency of vibration of the system.

$\frac{1}{1 - (\omega/\omega_n)^2}$ is the magnification factor.

2.5 Damped system: harmonic excitation

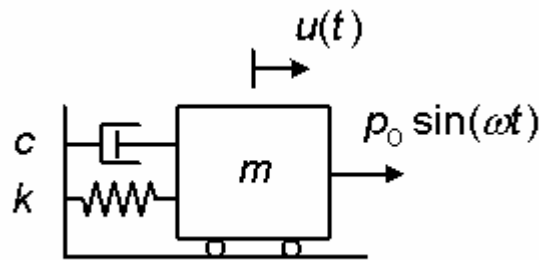


Figure 2.6 Damped oscillator harmonically excited.

The equation of motion is:

$$m\ddot{u} + c\dot{u} + ku = p_0 \sin(\omega t) \quad (2.12)$$

The homogeneous solution (transient response) $u_h(t)$ is given by:

$$u_h(t) = Ce^{-\xi\omega_n t} (\sin \omega_d t + \theta) \quad (2.13)$$

But after some time the transient response disappears (when the effect of the initial conditions vanishes), so $u(t) = u_p(t)$ (steady state response) and the structure vibrates with the same frequency as the applied force.

$$u_p(t) = \frac{p_0/k}{\sqrt{[1-(\omega/\omega_n)^2]^2 + [2\xi(\omega/\omega_n)]^2}} \sin(\omega t - \varphi) \quad (2.14)$$

with $\tan \varphi = \frac{2\xi(\omega/\omega_n)}{1-(\omega/\omega_n)^2}$

The amplitudes of the vibration is equal to the product of the static deformation $u_{st} = \frac{p_0}{k}$

with a dimensionless dynamic magnification factor R_d :

$$R_d(\xi, \omega/\omega_n) = \frac{1}{\sqrt{[1-(\omega/\omega_n)^2]^2 + [2\xi(\omega/\omega_n)]^2}} \quad (2.15)$$

It can be represented as function of the ratio ω/ω_n for different values of the damping ratio ξ :

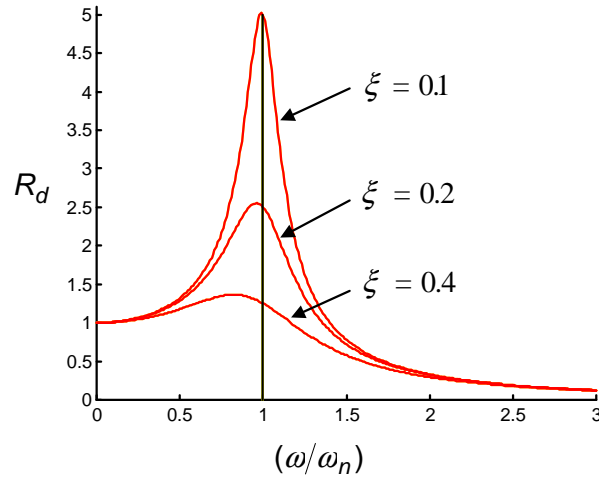


Figure 2.7 Dynamic magnification factor.

For $\omega/\omega_n < 0.25 \Rightarrow R_d \approx 1$ “quasi static” response.

If $\omega \rightarrow \omega_n$ the amplitude of the vibrations becomes large, increases with the reducing of the damping ratio and for $\xi = 0$ tends to infinity; this regime is called Resonance.

For example assuming a damping ratio ξ equal to 1% it means that the dynamic deformation at resonance frequency is 50 times larger than the static one.

2.6 Half-power (Band-width) method

It is a method to determine the damping ratio ξ from the measured response.

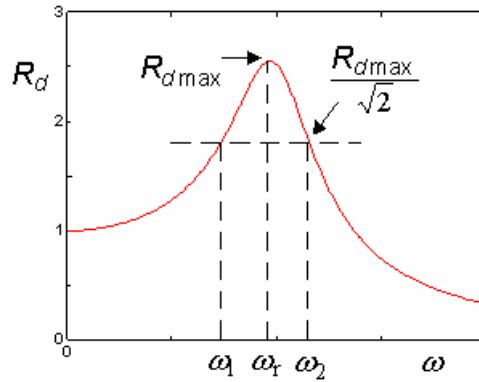


Figure 2.8 Band-width method resulting from the curve of R_d as function of ω .

The response of the structure is studied in the frequency domain. The structure is excited by a harmonic load and the frequency of the load is increased step by step. The curve R_d is then obtained experimentally as a function of ω .

The damping ratio is determined from the frequencies at which the response amplitude is equal to $1/\sqrt{2}$ times the resonant amplitude by the relation:

$$\xi \approx \frac{\omega_2 - \omega_1}{\omega_2 + \omega_1} \quad (2.16)$$

It can be noted how the damping ratio controls not only the amplitude of the dynamic magnification factor but also the width of the curve of R_d versus the frequency ω .

2.7 Methods of numerical integration

The problem of the damped forced vibrations is expressed by the relation:

$$m\ddot{u} + c\dot{u} + ku = p(t) \quad (2.17)$$

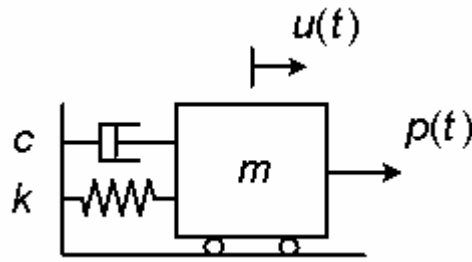


Figure 2.9 Damped oscillator externally excited.

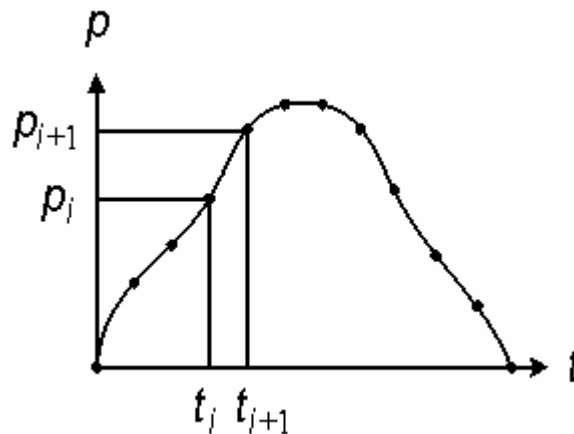


Figure 2.10 Load's time-history $p(t)$.

The equation of motion (2.17) can be integrated directly in the time domain through different techniques. The load p is time discretised and the purpose is to solve the equation and calculate u (and \dot{u}, \ddot{u} if required) at the discrete time instants. The solution is found by recursive algorithms; it means that, if the solution is known in the step times up to a certain step time t , the algorithm gives the solution at the next step $t + \Delta t$. The integration methods can be classified as explicit or implicit. In the explicit methods the dynamic equilibrium is imposed at the time t and the result depends only on the quantities obtained in the previous step. The implicit methods instead impose the dynamic equilibrium at the time $t + \Delta t$ and so include quantities which are linked to this step time and they need to be guessed by successive iterations. Furthermore the integration methods may be unconditionally stable if the dynamic solution doesn't increase without limits for any time increment Δt ; on the other hand they are conditionally stable if the time increment is $\Delta t < \Delta t_{crit}$, where Δt_{crit} represents the limit of stability.

The accuracy of the solution as well as the computational effort of the procedure are closely related to the selected time interval Δt ; this interval must be small enough to get a good accuracy and long enough to be computationally efficient.

One useful technique for selecting the time step of the integration is to solve the problem with a value that seems to be reasonable and then repeat the solution with a smaller one and finally compare the results; the process must be continued until when the solutions are close enough and seem to converge to the same values.

2.7.1 Newmark “Beta” Method

It is a recursive algorithm with the equation of motion considered at the step time $t + \Delta t$ and the velocity and the displacement at $t + \Delta t$ connected to those at t by the relations:

$$\dot{u}(t + \Delta t) = \dot{u}(t) + \{(1 - \gamma)\ddot{u}(t) + \gamma\ddot{u}(t + \Delta t)\}\Delta t \quad (2.18)$$

$$u(t + \Delta t) = u(t) + \dot{u}(t)\Delta t + \left\{ \left(\frac{1}{2} - \beta \right) \ddot{u}(t) + \beta \ddot{u}(t + \Delta t) \right\} \Delta t^2 \quad (2.19)$$

The factor γ provides a linearly weighting between the influence of the initial and final accelerations on the change of the velocity and the factor β provides the same weighting between the initial and the final acceleration for the displacement. Studies of this formulation have shown that the factor γ controls the amount of the artificial damping induced by the step procedure and if $\gamma = 1/2$ there is not artificial damping.

If $\gamma = 1/2$, $\beta = 1/6$ and $\vartheta = 1$ is the “Theta” Method of Wilson which assumes a linear variation of the acceleration between t and $t + \vartheta\Delta t$.

If $\gamma = 1/2$ and $\beta = 1/4$ is the Trapezoidal rule.

The stability condition for the Newmark’s method is given by:

$$\frac{\Delta t}{T_n} \leq \frac{1}{\pi\sqrt{2}} \frac{1}{\sqrt{\gamma - 2\beta}} \quad (2.20)$$

For the Trapezoidal rule the condition becomes: $\frac{\Delta t}{T_n} < \infty$

It means that the Trapezoidal rule is unconditionally stable and any time increment can be chosen.

2.7.2 Hilbert-Huges –Taylor Alpha Method

This method is used when damping is introduced in the Newmark's method without degrading the order of accuracy. The method is based on the Newmark's equations, whereas the time discrete equations are modified by averaging elastic, inertial and external forces between both time instants. The parameters γ and β are defined as:

$$\gamma = \frac{1-2\alpha}{2} \quad (2.21)$$

$$\beta = \frac{(1-\alpha)^2}{4} \quad (2.22)$$

Where the parameter α is taken in the interval: $\alpha \in \left[-\frac{1}{3}, 0\right]$

This unconditionally stable method represents the logical replacement of Newmark's method for non-linear problems in which it is necessary to control the damping during the integration.

2.8 Eigenvalue problem

The free undamped vibrations of a multi degree of freedom (MDOF) system are expressed by the system of n-differential equations (n is equal to the number of degrees of freedom of the system):

$$\mathbf{M}\ddot{\mathbf{u}}(t) + \mathbf{K}\mathbf{u}(t) = \mathbf{0} \quad (2.23)$$

with the correlated initial conditions: $\mathbf{u}(0) = \mathbf{u}_0$, $\dot{\mathbf{u}}(0) = \dot{\mathbf{u}}_0$

\mathbf{M} is the mass matrix; it is real, defined positive and diagonal.

\mathbf{K} is the stiffness matrix; it is real, symmetric, tridiagonal and defined positive if the system is statically determined.

The solution can be searched in the form:

$$\mathbf{u}(t) = \mathbf{\Psi} f(t) \quad (2.24)$$

In the equation $f(t)$ represents a generic function of time and $\mathbf{\Psi}$ is a vector of constant values. The substitution of (2.24) in the equation of motion (2.23) leads to a system of n linear homogeneous equations:

$$(\mathbf{K} - \omega_n^2 \mathbf{M}) \mathbf{\Psi} = \mathbf{0} \quad (2.25)$$

This system has one trivial solution $\mathbf{\Psi} = \mathbf{0}$ that corresponds to equilibrium (no motion).

Other solutions can be found if the following condition is respected:

$$\det([\mathbf{K}] - \omega_n^2 [\mathbf{M}]) = 0 \quad (2.26)$$

From this condition the characteristic equation is obtained from which the eigenvalues, corresponding to the square of the natural circular frequencies of the structure, are calculated. For each eigenvalue an eigenmode $\mathbf{\Psi}_n$ is associated; the free vibration of the structure determined by an initial deflection corresponding to an eigenmode $\mathbf{\Psi}_n$ causes a motion of the structure that is harmonic, with the circular frequency ω_n and a deflected shape that is constant in time and corresponds to the n-eigenmode.

2.9 Rayleigh Damping

The forced damped vibrations of an MDOF system are expressed by the system of differential equations:

$$\mathbf{M} \ddot{\mathbf{q}}(t) + \mathbf{C} \dot{\mathbf{q}}(t) + \mathbf{K} \mathbf{q}(t) = \mathbf{f}(t) \quad (2.27)$$

where \mathbf{C} is the damping matrix.

Under general conditions it represents a system of coupled differential equations. The Rayleigh method assumes that the damping matrix can be expressed as a linear combination of the mass and stiffness matrices as:

$$\mathbf{C} = a_0 \mathbf{M} + a_1 \mathbf{K} \quad (2.28)$$

The application of the modal coordinates transformation and the assumption of the damping matrix as in (2.28) leads to a diagonal modal damping matrix and so to uncoupled differential equations of motion. The damping ratio depends on the frequency through the relation:

$$\xi_n = \frac{a_0}{2} \frac{1}{\omega_n} + \frac{a_1}{2} \omega_n \quad (2.29)$$

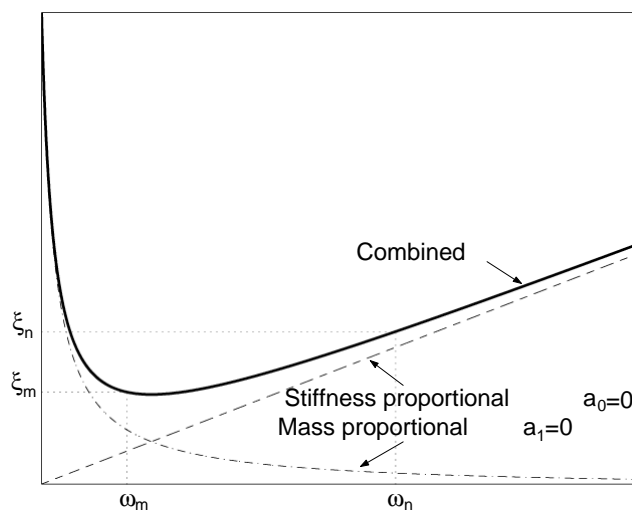


Figure 2.11 Relationship between damping ratio and frequency for Rayleigh damping.

The proportional coefficients a_0 and a_1 control the material damping and have the units respectively of s^{-1} and s . They can be evaluated by the solution of a pair of simultaneous equations if two damping ratios ξ_m and ξ_n are known. The two modes with the specified damping ratios ξ_m and ξ_n should be chosen to ensure reasonable values for the other damping ratios. From the equation written for the two eigenfrequencies ω_m and ω_n the proportional constants can be obtained as:

$$\begin{Bmatrix} a_0 \\ a_1 \end{Bmatrix} = \frac{2\omega_n\omega_m}{\omega_n^2 - \omega_m^2} \begin{bmatrix} \omega_n & -\omega_m \\ -1/\omega_n & 1/\omega_m \end{bmatrix} \begin{Bmatrix} \xi_m \\ \xi_n \end{Bmatrix} \quad (2.30)$$

Because a detailed variation of the damping ratio with the frequency is seldom available, usually it is assumed that $\xi_m = \xi_n = \xi$ which leads to:

$$\begin{Bmatrix} a_0 \\ a_1 \end{Bmatrix} = \frac{2\xi}{\omega_m + \omega_n} \begin{Bmatrix} \omega_m\omega_n \\ 1 \end{Bmatrix} \quad (2.31)$$

2.10 Wind profile

Two basic assumptions are made on the wind field:

- According to international meteorological practice a 10-minute observation period is used and during this period the wind field is normally considered to be stationary.
- In the atmospheric boundary layer due to the frictional forces close to the ground, the wind direction changes systematically from ground to geostrophic height z_g generating the Ekman spiral. However except very high structures and structures which are unusually sensitive to wind direction an excellent approximation is obtained even though directional changing is not taken into account and thus assuming a planar wind profile.

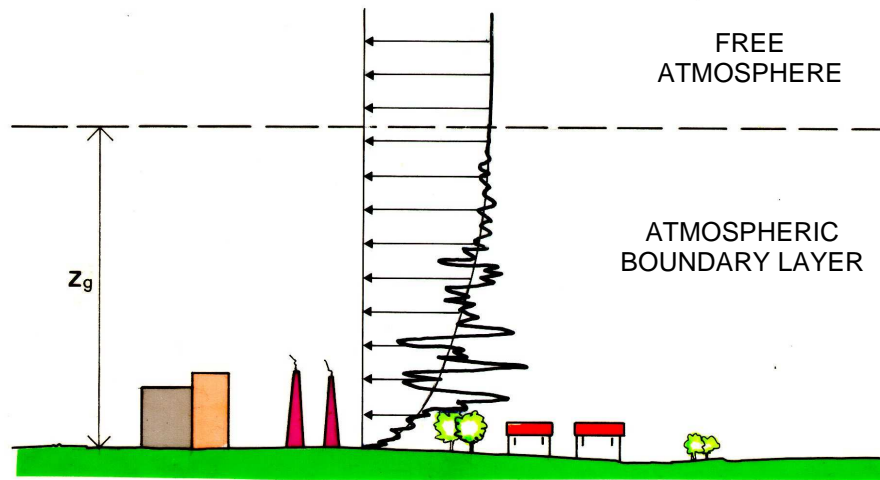


Figure 2.12 Mean wind velocity profile and longitudinal component of the atmospheric turbulence.

The logarithmic law is assumed to model the mean wind velocity profile. It is expressed in the form:

$$V_m(z) = \frac{1}{\chi} u_* \ln \left(\frac{z}{z_0} \right) \quad (2.32)$$

where:

V_m is the mean wind velocity at height z in m/s.

z is the height on the sea level in m.

z_0 is the roughness length in m.

χ is the Von Karman constant ≈ 0.4

u_* is the shear velocity in m/s.

The heights z on the sea level considered are those at which the concentrated forces, simulating the wind actions, are calculated: these values are variable for the points on the arch and constant equal to 60 m for the points on the bridge deck.

Eurocode 1, “Actions on structures”, in the part 1-4 deals with the wind actions on structures. The terrain is divided in different categories of roughness:

Roughness category	z_0 (m)	k_r
Sea and sea coast	0.003	0.16
Lakes, area without vegetation	0.01	0.17
Open country with few isolated obstacles	0.05	0.19
Area with regular vegetation, suburban and industrial zone	0.3	0.21
Urban area	1.0	0.23

Table 2.1 Roughness categories based on Eurocode 1.

k_r is the roughness factor depending on, likewise z_0 , the soil roughness.

2.11 Aerodynamic forces and coefficients

The distribution of the pressures on the surface of a structure immersed in a fluid flow is generally represented by the punctual values of the dimensionless pressure coefficient C_p which is defined as:

$$C_p = \frac{p - p_0}{\frac{1}{2} \rho V^2} \quad (2.33)$$

where:

p is the pressure on the surface of the structure.

p_0 is the reference pressure or environment pressure.

ρ is the density of the air, equal to 1.25 kg/m^3 .

V is the velocity of the undisturbed flow upstream of the structure.

If $p > p_0$ the resultant force works towards the surface; instead if $p < p_0$ the surface is subjected to a depression and the resultant force works from the surface to the fluid. If the pressure coefficient is known as well as the undisturbed velocity of the flow, immediately it is possible to calculate from the equation (2.33) the distribution of the pressure and then, integrating on the surface of the structure, the resultant force. Generally it is not necessary to calculate the exact distribution of the pressure on the external surface of the structure but, especially in presence of structures with aerodynamic profile like bridge decks, it is enough to calculate the resultant aerodynamic forces for unit of length.

The drag force D is the force for unit of length in the direction of the undisturbed flow; the lift force L is the force for unit of length normal to the direction of the flow; the torsion moment M is the moment for unit of length around the axis normal to the section of the structure. These forces are defined in the terms of the exact distribution of pressure by the relation:

$$\begin{aligned}
 D &= \int_S (p - p_0)_x ds \\
 L &= \int_S (p - p_0)_y ds \\
 M &= \int_S [x(p - p_0)_y - y(p - p_0)_x] ds
 \end{aligned}
 \tag{2.34}$$

where:

$(p - p_0)_x$ and $(p - p_0)_y$ are the components of $(p - p_0)$ in the direction respectively of $D(x)$ and $L(y)$.

x and y are the distances of the application point of $(p - p_0)$ from the origin of the axes.

S is the perimeter of the section.

The dimensionless drag coefficient C_D , lift coefficient C_L and moment coefficient C_M are defined as:

$$\begin{aligned}
 C_D &= \frac{D}{\frac{1}{2} \rho B V^2} \\
 C_L &= \frac{L}{\frac{1}{2} \rho B V^2} \\
 C_M &= \frac{M}{\frac{1}{2} \rho B^2 V^2}
 \end{aligned}
 \tag{2.35}$$

or in terms of the pressure coefficient as:

$$\begin{aligned}
 C_D &= \frac{1}{B} \int_s C_{px} ds \\
 C_L &= \frac{1}{B} \int_s C_{py} ds \\
 C_M &= \frac{1}{B^2} \int_s (x C_{py} - y C_{px}) ds
 \end{aligned} \tag{2.36}$$

where C_{px} and C_{py} are the components of C_p in the direction of $D(x)$ and $L(y)$. If the dimensionless aerodynamic coefficients and the velocity of the undisturbed flow are known it is possible to calculate immediately the aerodynamic forces D , L and M using the equations (2.35).

The term B at the denominator represents a characteristic dimension of the section. For the bridge deck it is taken equal to 28 m, the width deck perpendicular to the bridge axis; for the arch this term represents the height of the section and varies from 4.2 m at the abutments to 2.7 m at the crown of the arch.

2.12 Wind tunnel tests

The wind tunnel tests were performed by PSP Technologien im Bauwesen GmbH together with the Institute of Steel Construction RWTH Aachen. Two kinds of tests were carried out:

- Static tests
- Aeroelastic tests

Static tests on a section model of the bridge deck were carried out in order to measure the aerodynamic forces and coefficients. The scale of the section model is 1:50. The required 10-minute mean wind velocity was obtained by using a logarithmic profile; a reference velocity was taken equal to $V_{ref} = 25 [m/s]$, corresponding to a return period of 100 years, and a roughness length $z_0 = 0.025 [m]$. For wind directions perpendicular to the bridge axis (westerly winds) the mean wind profile above the sea level could be defined as :

$$V_m(z) = V_{ref} k_r \ln \left(\frac{z}{z_0} \right), \quad \text{for } z_{min} \leq z \leq z_{max} \tag{2.37}$$

$$V_m(z) = V_{ref} k_r \ln\left(\frac{z_{min}}{z_0}\right), \text{ for } z < z_{min} \quad (2.38)$$

where:

k_r is the terrain factor depending on the roughness length z_0 .

z_{min} depends on the terrain category as z_0 (EC1, Table 4.1).

z_{max} is to be taken as 200 [m], unless otherwise specified in the National Annex.

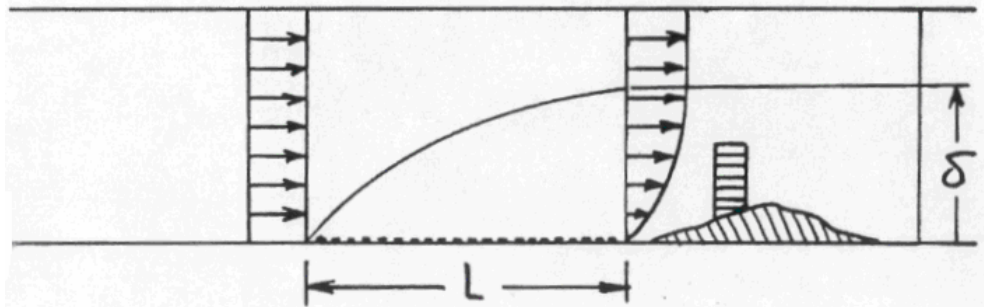


Figure 2.13 Mean wind profile in the wind tunnel.

Along the bridge axis the profile will change due to the influence of terrain, which can reach heights up to approximately 50 [m] above sea level. In order to take into account this effect the mean velocity profile was modified as:

$$V_m(z) = V_{ref} k_r \ln\left(\frac{z - h_{terrain}}{z_0}\right) \quad (2.39)$$

The quasi-static loads perpendicular and along the bridge axis were calculated using this definition of the mean wind profile.

The section model was installed into a test frame, located in front of the wind tunnel test section. The model was supported by two 3D-force balances, which allow to measure lift, drag and moment forces simultaneously.

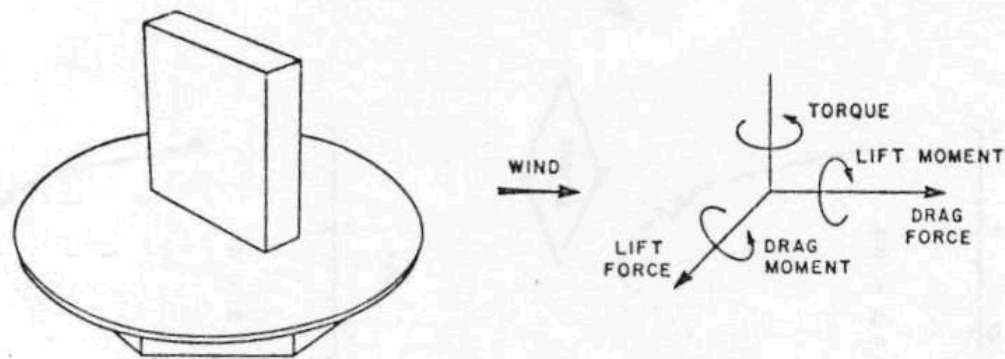


Figure 2.14 Sketch of the forces measured by a rigid 3D-force balance.

The tests were performed for two different configuration of the cross section:

- Construction phase, without screen
- Bridge in operation, with screen

The forces measured, for unit of length, were used to determine the aerodynamic dimensionless coefficients using the formulas (2.35). The tests were performed varying the onflow angle α of the velocity, for the entire girder and for each box separately (see Figure 2.13).

The role of the screens in the aerodynamic behaviour of the bridge deck is fundamental and it will be difficult to calculate reliable wind induced forces on the bridge deck without knowing the aerodynamic coefficients C_D , C_L , and C_M from wind tunnel tests.

For the evaluation of the drag and lift coefficients the configuration of the global cross section with screen and an onflow angle α equal to zero (see Figure 2.15) is considered; the final values assumed for the drag coefficient is equal to 0.15 (see Figure 2.17) and for the lift coefficient is equal to -0.2 (see Figure 2.18)

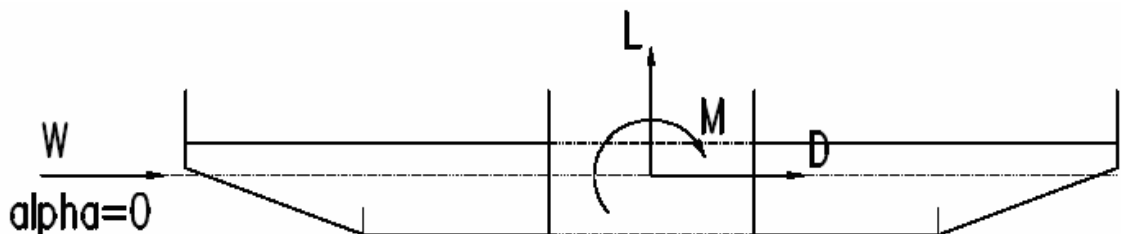


Figure 2.15 Positive directions of the aerodynamic forces for an onflow angle of 0° .



Figure 2.16 Model of the cross section during modification for the tests on each box separately.

The results for the entire cross section are shown in the Figure 2.17-2.18 for the section during the erection (without screen) and in its final configuration (with screen).

The results for each girder considered separately, in their final configuration with screen, are shown in the Figure 2.19-2.20. In the same graphs the results of the summation of the values for the two girders and of the coefficient for the entire cross section are represented.

In the table below the reference values of the aerodynamic coefficients for a nil onflow angle and for the configurations described before are summarized:

Configuration	C_D	C_L
Windward	0.09	0.05
Leeward	0.06	-0.25
Entire section	0.15	-0.2

Table 2.2 Drag and lift coefficients.

The summation of the values for each box girder considered separately coincides with the value measured on the entire section.

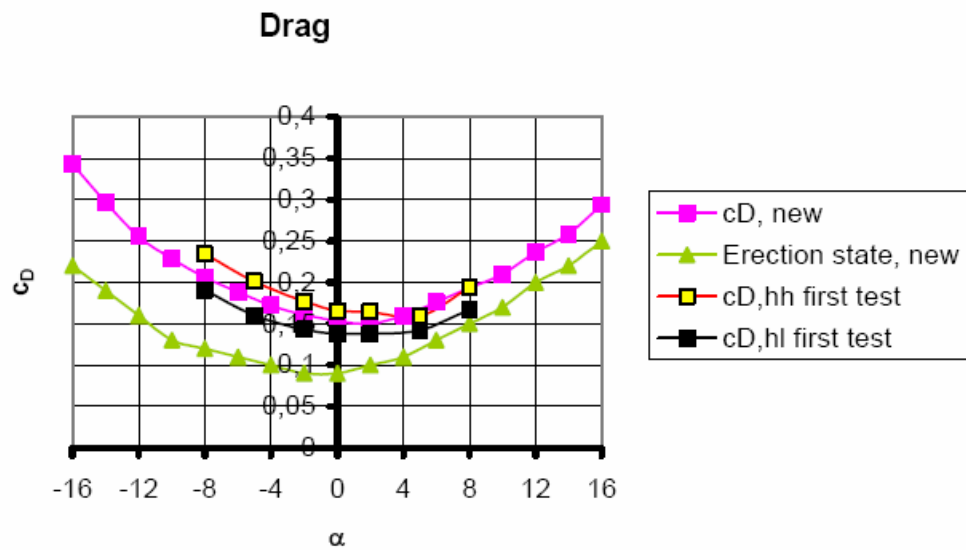


Figure 2.17 Drag coefficients of the cross section versus the onflow angle α .

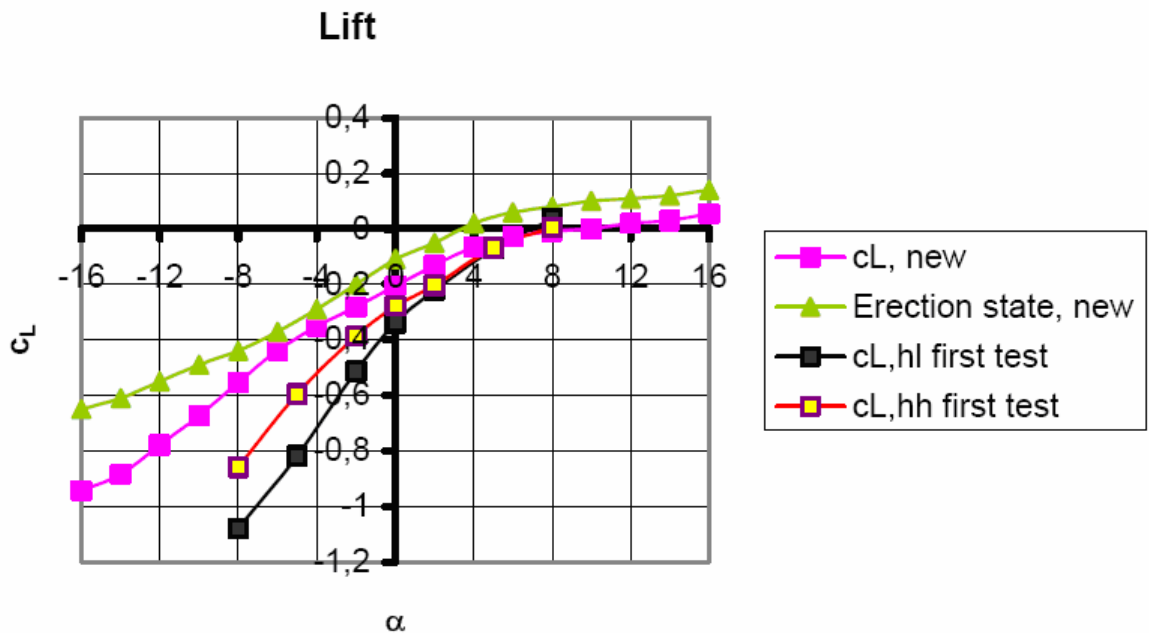


Figure 2.18 Lift coefficients of the cross section versus the onflow angle α .

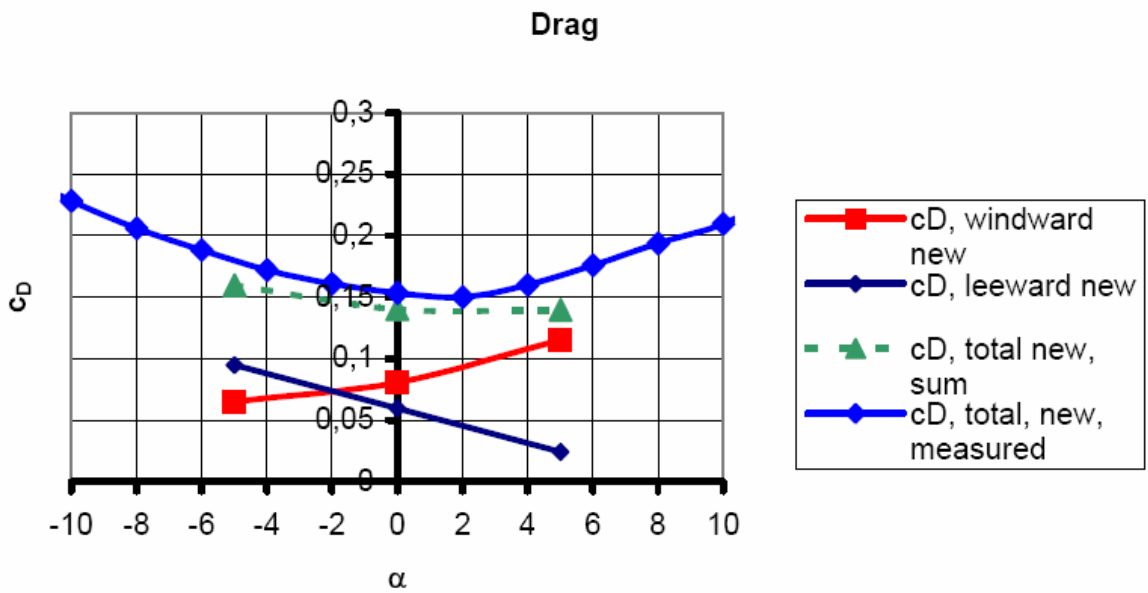


Figure 2.19 Drag coefficients for the entire cross section and each girder separately versus the onflow angle α .

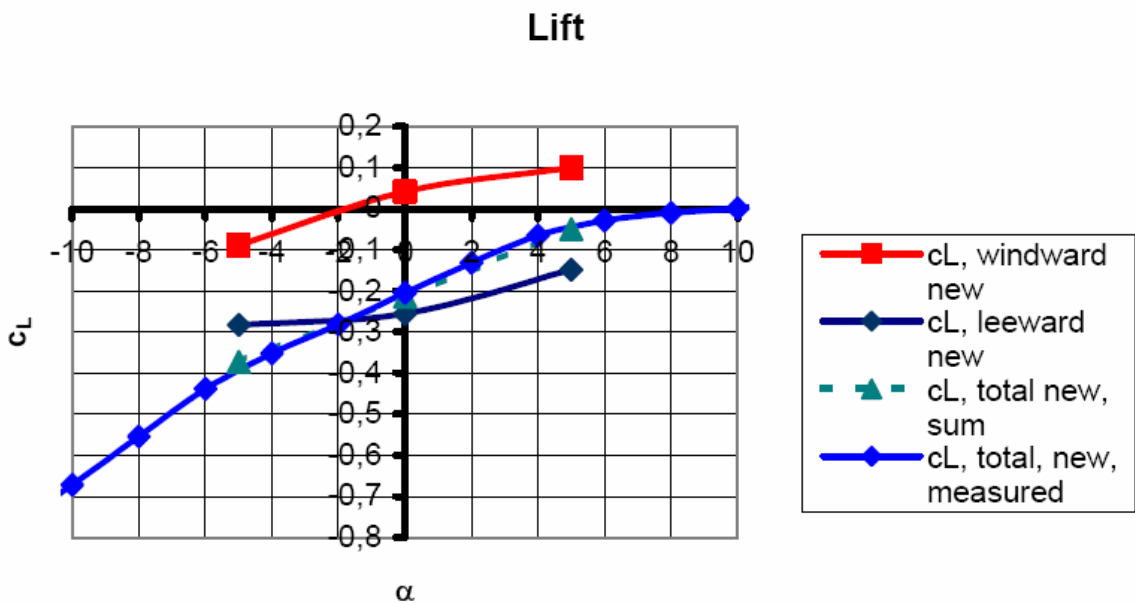


Figure 2.20 Lift coefficients for the entire cross section and each girder separately versus the onflow angle α .

For an approximate evaluation of the drag coefficient of the arch the hypothesis of a two-dimensional problem is made, considering the planar section of the arch immersed in a

uniform flow. This assumption is unrealizable in the reality but it can be considered acceptable when the structural element is long enough, as in the case of the arch, or when it is limited by two parallel walls perpendicular to its axis.

Generally the aerodynamic coefficients depend in very complex way on many parameters such as Reynolds number, the profile of the transversal section and its orientation in respect to the flow, the roughness of the surface and the intensity of turbulence).

The reference case for the rectangular section of the bridge arch is the flow regime around a rectangular cylinder; the separation of the wake occurs at the corners of the section and practically the physic phenomenon results independent from the Reynolds number. For an average ratio between the width and the height of the transversal section, from the abutments to the crown of the arch, equal to ≈ 1.48 it is possible to evaluate (see Figure 2.21) a drag coefficient for the arch ≈ 2 .

The lift coefficient of the arch instead results equal to zero for the symmetry of the section to the wind direction perpendicular to the bridge axis as assumed in this report.

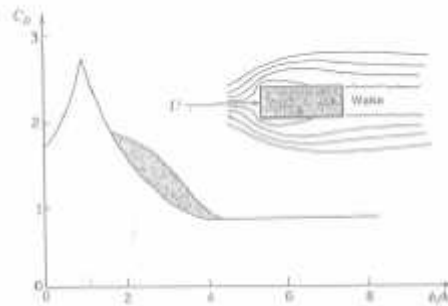


Figure 2.21 Drag coefficient of a rectangular section versus the ratio between the width and the height of the section (ESDU).

Referring to the EC 1 the force coefficient C_f of structural elements of rectangular section with the wind blowing normally to a face :

$$C_f = C_{f0} \psi_r \psi_\lambda \quad (2.40)$$

where:

C_{f0} is the force coefficient of rectangular sections with sharp corners and without free-end flow (EC 1 Figure 7.23).

ψ_r is the reduction factor for square sections with rounded corners (EC 1 Figure 7.24).

ψ_λ is the end-effect factor for elements with free-end flow (EC 1 Figure 7.36).

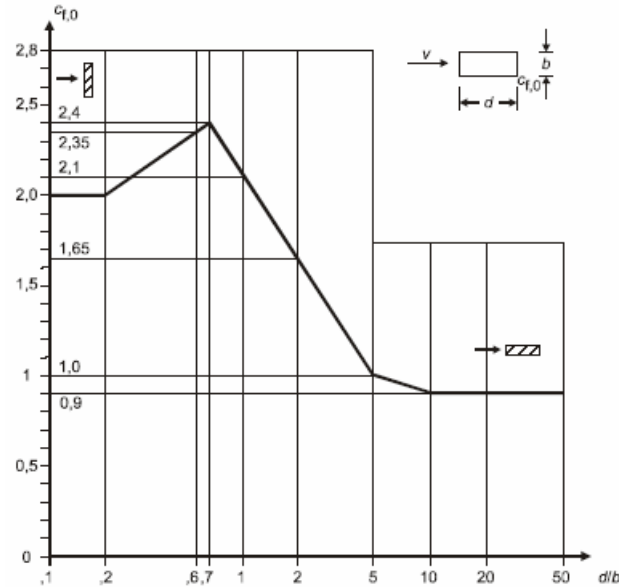


Figure 2.22 Force coefficient C_{f0} of rectangular sections with sharp corners and without free end flow (EC 1).

For an average ratio between the width and the height of the transversal section, from the abutments to the crown of the arch, equal to ≈ 1.48 it is possible to evaluate (Figure 2.22) a force coefficient ≈ 2 . Furthermore for all elements without free-end flow the recommended value is 2 which is assumed to be a safe value (Note 1, page 68).

From the wind tunnel tests for the C_{f0} coefficient a value of 1.9 is given and for the end-effect factor ψ_λ a value equal to 0.91 for a total value $C_f = 1.73$.

2.13 Along-wind forces on the bridge

The wind velocity $V(z, t)$ is modelled as a stationary random normal process defined as:

$$V(z, t) = V_m(z) + u'(z, t) \quad (2.40)$$

The wind velocity is given by the sum of a mean velocity $V_m(z)$, deterministic function of the height above the sea level, and a nil mean fluctuation of the velocity around the mean value $u'(z,t)$, called the longitudinal component of the atmospheric turbulence that is a deterministic function of the height and a random function of the time. The worse condition for the bridge is when the wind direction is perpendicular to the bridge axis and the correspondent along-wind force (or drag force), oriented in the same direction of the wind flow, plays the main role on the wind response of the structure. Applying the quasi-static theory the along-wind forces, for unit of length, are given by:

$$D(z,t) = \frac{1}{2} \rho V^2(z,t) b C_D = \frac{1}{2} \rho (V_m(z) + u'(z,t))^2 b C_D \quad (2.41)$$

This equation can be expressed in two different forms; taking into account the turbulence quadratic term the forces for unit of length, which can be called “completed” forces, are given by:

$$D(z,t) = \frac{1}{2} \rho V_m^2(z) b C_D + \rho V_m(z) u'(z,t) b C_D + \frac{1}{2} \rho u'^2(z,t) b C_D \quad (2.42)$$

The influence of the quadratic turbulence term is often neglected in literature and operating in this way the forces for unit of length, which can be called “reduced” forces, are given by:

$$D(z,t) = \frac{1}{2} \rho V_m^2(z) b C_D + \rho V_m(z) u'(z,t) b C_D \quad (2.43)$$

The forces on each node of the FE model of the bridge can be obtained multiplying the forces for unit of length for the influence length L_i of each node. The completed and reduced forces on the i-th node at z_i height can be expressed respectively as:

$$D(z_i,t) = \frac{1}{2} \rho V_m^2(z_i) b C_D L_i + \rho V_m(z_i) u'(z_i,t) b C_D L_i + \frac{1}{2} \rho u'^2(z_i,t) b C_D L_i \quad (2.44)$$

$$D(z_i, t) = \frac{1}{2} \rho V_m^2(z_i) b C_D L_i + \rho V_m(z_i) u'(z_i, t) b C_D L_i \quad (2.45)$$

Adding to the along-wind force the contribute due to the vertical component of turbulence w' the completed and reduced forces on the i -th node at z_i height can be expressed respectively as:

$$D(z_i, t) = \frac{1}{2} \rho V_m^2(z_i) b C_D L_i + \rho V_m(z_i) u'(z_i, t) b C_D L_i + \frac{1}{2} \rho u'^2(z_i, t) b C_D L_i + \rho V_m(z_i) b (C'_D - C_L) w'(z_i, t) L_i \quad (2.46)$$

$$D(z_i, t) = \frac{1}{2} \rho V_m^2(z_i) b C_D L_i + \rho V_m(z_i) u'(z_i, t) b C_D L_i + \rho V_m(z_i) b (C'_D - C_L) w'(z_i, t) L_i \quad (2.47)$$

The term C'_D represents the first derivate of the drag coefficient at a specified onflow angle.

Usually in structural engineering the wind velocity is assumed to be a Gaussian (or normal) process. As exposed above the along-wind force can be considered as the summation of three terms: the first one corresponding to the mean wind velocity; the second one proportional to the product between the mean and the fluctuating wind velocity; and the third one proportional to the square of the fluctuating wind velocity. Some studies show that this last term can be responsible for the non-Gaussianity of the aerodynamic forces and so both the force and the structural response become non Gaussian processes. Since for many cases ignoring this quadratic term of the fluctuating wind velocity in the aerodynamic force gives acceptable approximations, this term is usually neglected. However the results of some studies show also how neglecting the quadratic term can produce significant errors in the evaluation of the structural response. The parameters that have an influence with their variation on the increasing or decreasing of this error are: the characteristics of the ground surface; the height, the natural frequency and the damping ratio of the structure; finally the reference mean wind velocity. In this work at first both

“completed” and “reduced” aerodynamic forces are considered, discussing the different response observed. Then, having noted not a substantial difference between the two cases, it is decided to retain the quadratic term in the rest of the analyses carried out.

2.14 Fourier analysis

A periodic function $x(t)$, with period T , can be broken into its harmonic components. However the function $x(t)$ can be expressed as an infinite trigonometric series, called Fourier series, of the form:

$$x(t) = a_0 + \sum_{k=1}^{\infty} (a_k \cos \omega_k t + b_k \sin \omega_k t) \quad (2.48)$$

Where a_0 , a_k and b_k are the Fourier coefficients given by:

$$\begin{aligned} a_0 &= \frac{1}{T} \int_{-T/2}^{T/2} x(t) dt \\ a_k &= \frac{2}{T} \int_{-T/2}^{T/2} x(t) \cos(\omega_k t) dt \quad (k \geq 1) \\ b_k &= \frac{2}{T} \int_{-T/2}^{T/2} x(t) \sin(\omega_k t) dt \end{aligned} \quad (2.49)$$

The first coefficient represents the mean value of the $x(t)$ function on the period T . The frequency of the k -th harmonic component is:

$$\omega_k = \frac{2\pi k}{T} \quad (2.50)$$

The spacing between adjacent harmonics is:

$$\Delta\omega = \frac{2\pi}{T} \quad (2.51)$$

The periodic function can also be written as:

$$x(t) = \frac{a_0}{2} + \sum_{k=1}^{\infty} A_k \sin(\omega_k t + \varphi_k) \quad (2.52)$$

The coefficients A_k and φ_k are given by:

$$A_k = \sqrt{a_k^2 + b_k^2} \quad \varphi_k = \arctg\left(\frac{a_k}{b_k}\right) \quad (2.53)$$

They represent respectively the amplitude and the phase angle of the k-th harmonic. A plot of the magnitude versus the frequency is known as the Fourier amplitude spectrum.

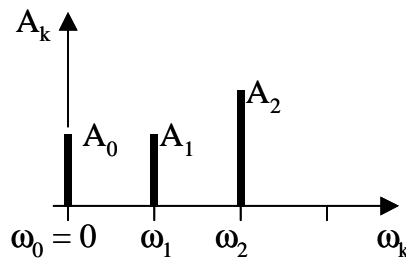


Figure 2.23 Fourier amplitude spectrum.

When the period $T \rightarrow \infty$, $x(t)$ doesn't represent more a periodic phenomenon and it cannot be analysed into discrete frequency components; the Fourier series turns into a Fourier integral and the Fourier coefficients turn into continuous functions of frequency called Fourier transform.

$$X(\omega) = \int_{-\infty}^{\infty} x(t) e^{-i\omega t} dt \quad (2.52)$$

$$x(t) = \int_{-\infty}^{\infty} X(\omega) e^{i\omega t} d\omega$$

The first equation is the (complex) Fourier transform of $x(t)$ and the second is the inverse Fourier transform.

2.15 Power spectral density function (PSD)

If a naturally occurring random process is considered, the time history of a sample function $x(t)$ is not periodic and it cannot be represented by a discrete Fourier series. Even for stationary process, for which $x(t)$ goes on for ever and the condition:

$$\int_{-\infty}^{\infty} |x(t)| dt < \infty \quad (2.53)$$

is not satisfied so that the classical theory of Fourier analysis cannot be applied to a sample function. This difficulty can be overcome by analysing, not sample functions of the process itself, but its autocorrelation functions $R_x(\tau)$.

The logic behind this approach is that the autocorrelation function gives information about the frequencies present in a random process indirectly. $R_x(\tau)$ is a maximum for values of τ for which $x(t)$ and $x(t+\tau)$ are in phase and a minimum for values of τ for which are in antiphase.

When $\tau \rightarrow \infty$ $R_x(\tau) \rightarrow 0$ and it is possible to calculate the Fourier transform of $R_x(\tau)$ and its inverse:

$$S_x(\omega) = \frac{1}{2\pi} \int_{-\infty}^{\infty} R_x(\tau) e^{-i\omega\tau} d\tau$$

$$R_x(\tau) = \int_{-\infty}^{\infty} S_x(\omega) e^{i\omega\tau} d\omega \quad (2.54)$$

Where $S_x(\omega)$ is called the power spectral density of the x process and it is a function of the angular frequency ω .

An important property of $S_x(\omega)$ becomes apparent putting $\tau=0$ in the second equation above.

$$R_x(\tau=0) = E[x^2] = \int_{-\infty}^{\infty} S_x(\omega) d\omega \quad (2.55)$$

The mean square value of a stationary random process x is therefore given by the area under a graph of spectral density $S_x(\omega)$ against ω . The units of the spectral density are accordingly those of $[x^2]/[rad/s]$. Then if the mean value of the process is zero, like for the turbulent component of the wind speed, $E[x^2] = \sigma_x^2$.

The spectral density $S_x(\omega)$ is a real even function of ω and it is never negative.

The mean square value of a stationary random process x in term of the equivalent one-sided spectral density function is:

$$E[x^2] = \int_0^{\infty} W_x(n) dn \quad (2.56)$$

where $n = \omega/2\pi$ is the frequency in Hz. The single-sided spectrum $W_x(n)$ is related to the double-sided spectrum $S_x(\omega)$ by the formula:

$$W_x(n) = 4\pi S_x(\omega) \quad (2.57)$$

If the spectral density function is known, it is possible also to calculate the spectral density of a process which is obtained by differentiating x . In general terms results:

$$\begin{aligned} x^n(t) &= \frac{d^n}{dt^n} x(t) \\ S_{x^n}(\omega) &= \omega^{2n} S_x(\omega) \end{aligned} \quad (2.58)$$

so that the spectral density of the derived process is just ω^{2n} times the spectral density of the original process.

In the same way the cross-spectral density of a pair of random processes x and y is defined as the Fourier transform of the corresponding cross-correlation function for the two processes.

$$S_{xy}(\omega) = \frac{1}{2\pi} \int_{-\infty}^{\infty} R_{xy}(\tau) e^{-i\omega\tau} d\tau \quad (2.59)$$

$$R_{xy}(\tau) = \int_{-\infty}^{\infty} S_{xy}(\omega) e^{i\omega\tau} d\omega$$

While the autocorrelation function is a symmetric function, the cross-correlation function is asymmetric and so the cross-spectral density results a complex function. It can be shown that $S_{xy}(\omega)$ and $S_{yx}(\omega)$ are the same except that the sign of their imaginary parts is reversed. $S_{xy}(\omega)$ is therefore the complex conjugate of $S_{yx}(\omega)$, which is usually written:

$$S_{xy}(\omega) = S_{yx}^*(\omega) \quad (2.60)$$

$$S_{yx}(\omega) = S_{xy}^*(\omega)$$

The normalised cross-spectral density function is a complex function defined as:

$$\gamma_{xy}(\omega) = \frac{S_{xy}(\omega)}{\sqrt{S_{xx}(\omega)S_{yy}(\omega)}} \quad (2.61)$$

where $S_{xx}(\omega)$ and $S_{yy}(\omega)$ are the auto-spectral density functions of the processes x and y ; the coherence of the two random processes can be defined as:

$$|\gamma_{xy}(\omega)|^2 = \frac{|S_{xy}(\omega)|^2}{S_{xx}(\omega)S_{yy}(\omega)} \quad (2.62)$$

It can be shown that:

$$|S_{xy}(\omega)|^2 \leq S_{xx}(\omega)S_{yy}(\omega) \quad \rightarrow \quad |\gamma_{xy}(\omega)| \leq 1$$

If $\gamma_{xy}(\omega) = 1$ for any frequency ω , the two random processes are perfectly correlated.

2.16 N-varied stationary random process

An n-varied stationary random process is a vector $\mathbf{X}(t)$ of n-stationary random processes $x_i(t)$ with $i=1, \dots, n$; it can be used for example to represent the wind forces on a structure with n-degrees of freedom. For the spectral analysis of the vector a correlation matrix can be defined:

$$\mathbf{R}_X(\tau) = E[\mathbf{X}(t)\mathbf{X}^T(t+\tau)] = \begin{pmatrix} R_{x_1x_1}(\tau) & \dots & R_{x_1x_n}(\tau) \\ \vdots & \ddots & \vdots \\ R_{x_nx_1}(\tau) & \dots & R_{x_nx_n}(\tau) \end{pmatrix} \quad (2.63)$$

where the terms on the principal diagonal are the autocorrelation functions and the other terms are the cross-correlation functions of the processes. The matrix is symmetric considering that:

$$\mathbf{R}_X(\tau) = \mathbf{R}_X^T(-\tau) \quad (2.64)$$

A power spectral density matrix can also be defined as:

$$\mathbf{S}_X(\omega) = \frac{1}{2\pi} \int_{-\infty}^{\infty} \mathbf{R}_X(\tau) e^{-i\omega\tau} d\tau = \begin{pmatrix} S_{x_1x_1}(\omega) & \dots & S_{x_1x_n}(\omega) \\ \vdots & \ddots & \vdots \\ S_{x_nx_1}(\omega) & \dots & S_{x_nx_n}(\omega) \end{pmatrix} \quad (2.65)$$

where the terms on the principle diagonal are the spectral density functions and the other terms are cross-spectral density functions of the processes. In the (2.65) the terms above the principal diagonal are the complex conjugate of those below the diagonal: the matrix is called an Hermitian matrix. It can be shown that for any frequency ω , it is a semi-defined positive matrix. The correlation matrix can be obtained by the inverse transform of the power spectral density matrix:

$$\mathbf{R}_X(\tau) = \int_{-\infty}^{\infty} \mathbf{S}_X(\omega) e^{i\omega\tau} d\omega \quad (2.66)$$

2.17 Discrete Fourier Transform (DFT)

Most experimental measurements of random processes are carried out digitally. A typical function $x(t)$ of the process to be measured is fed through an analogue to digital converter. This samples $x(t)$ at a series of regularly spaced times. If the sampling interval is Δt (constant) the length of the registration time T becomes $T = N \Delta t$, where N is the number of the sampling points; the discrete value of $x(t)$ at time $t = n \Delta t$ is written as x_n . Since the continuous function of time is replaced by a discrete time series; the main interest is to determine the frequency composition of the sample function by manipulating the series of discrete numbers obtained and estimate the spectrum of a random process $x(t)$ by analysing the discrete time series obtained by sampling a finite length of a sample function. The continuous function of time $x(t)$ is replaced by the discrete time series $x_n = x(n \Delta t)$ with $n = 0, 1, \dots, N-1$ and the Fourier transform $X(\omega)$ is replaced by the discrete frequency series $X_k = X(2\pi k/T)$ with $k = 0, 1, \dots, N-1$. The discrete Fourier transform of the discrete time series x_n is given by:

$$X_k = \frac{1}{N} \sum_{n=0}^{N-1} x_n e^{-i(2\pi kn/N)} \quad k = 0, 1, \dots, N-1 \quad (2.67)$$

The inverse discrete Fourier transform (IDFT) is given by:

$$x_n = \sum_{k=0}^{N-1} X_k e^{i(2\pi kn/N)} \quad n = 0, 1, \dots, N-1 \quad (2.68)$$

Although the DFT is derived by considering the properties of continuous Fourier series it is important to realize that the discrete Fourier transform (2.67) has the exact inverse defined by (2.68) and that the properties of DFT's are exact properties rather than approximate properties based on the corresponding results for continuous Fourier transform.

2.18 Aliasing

Trying to calculate values of X_k for k greater than N , like $k = N + j$, results $X_{N+j} = X_j$. This means that coefficients X_k just repeat themselves for $k > N$, so that the graph of magnitudes $|X_k|$ along a frequency axis $\omega_k = 2\pi k / N \Delta t$ repeats itself periodically; furthermore this graph is symmetrical about the zero frequency position, cause terms in the time series x_n are real and it follows that:

$$\begin{aligned} X_{-j} &= X_j^* \\ |X_{-j}| &= |X_j| \end{aligned} \quad (2.69)$$

The unique part of the graph occupies the frequency range $|\omega| \leq \pi / \Delta t$ [rad/s]. Higher frequencies just show Fourier coefficients which are repetitions of those which apply at frequencies below $\pi / \Delta t$. It is possible to say that the coefficients calculated by the DFT are only correct Fourier coefficients for frequencies up to:

$$\omega_k = \frac{2\pi k}{N \Delta t} = \frac{\pi}{\Delta t} \quad k = 0, 1, \dots, N/2 \quad (2.70)$$

Moreover if there are frequencies above $\pi / \Delta t$ present in the original signal, these introduce a distortion of the graph called aliasing. The high frequency components contribute to the x_n series and falsely distort the Fourier coefficients calculated by the DFT for frequencies below $\pi / \Delta t$. If ω_0 is the maximum frequency component present in $x(t)$, then aliasing can be avoided by ensuring that the sampling interval Δt is small enough that:

$$\frac{\pi}{\Delta t} > \omega_0 \quad (2.71)$$

or if $f_0 = \omega_0 / 2\pi$ by ensuring that:

$$\frac{1}{2\Delta t} > f_0 \quad (2.72)$$

The frequency is called the Nyquist frequency and it represents the maximum frequency that can be detected from data sampled at time spacing Δt [s]. Since the sampling frequency $1/2\Delta t$ must be high enough to cover the full frequency range of the continuous time series. Otherwise the spectrum from equally spaced samples will differ from the true spectrum because of aliasing. In some cases a way to avoid this phenomenon is to filter the time series to remove all frequency components higher than $1/2\Delta t$ before beginning the analysis.

2.19 Fast Fourier Transform

In order to estimate spectra from measured data, the obvious method is to estimate the appropriate correlation function first and then to Fourier transform this function to obtain the required spectrum. Until the late 1960s, this approach was the basis of practical calculation procedures which followed the formal mathematical route by which spectra are defined as Fourier transforms of correlation functions. However the position was changed by the advent of the fast Fourier transform (FFT).

Instead of estimating spectra by first determining correlation functions and then calculating their Fourier transforms, spectra are estimated directly from the original time series through this quicker and more accurate technique. As it is exposed before the DFT of a finite sequence x_n , with $n = 0, 1, \dots, N-1$ is a new finite sequence X_k , with $k = 0, 1, \dots, N-1$. If the X_k values are obtained by a direct approach it is necessary to make N multiplications of the form $x_n \times \left(e^{i(2\pi kn/N)} \right)$ for each of N values of X_k and so the total work of calculating the full sequence X_k would require N^2 multiplications. The FFT reduces this work to a number of operations of the order $N \log_2 N$. For example if $N = 2^{15}$, $N^2 \approx 10^9$ whereas $N \log_2 N = 4 \cdot 9 \cdot 10^5$, which is only about 1/2000th of the number of operations.

The FFT therefore offers an enormous reduction in computer processing time. Moreover there is also an increase in accuracy; since fewer operations have to be performed by the computer, round-off errors due to the truncation of products by limited number of available digits of the computer are reduced and accuracy is accordingly increased. The FFT works

by partitioning the full sequence x_n into a number of shorter sequences. Instead of calculating the DFT of the original sequence, only the DFT of the shorter sequences are calculated; then the FFT combines these together in a particular way to yield the full DFT of x_n .

Chapter 3 FE model of the bridge

3.1 Creating a model in ABAQUS/CAE

The finite element model of a structure can be created in Abaqus/cae which provides a graphical user interface that makes it easier to build the model than typing the input file. Abaqus/cae is divided into different modules where each module represents a logical aspect of the modelling process; for example defining the geometry, material properties, boundary conditions, loads and generating the mesh. After built the model, Abaqus/cae generates an input file to be submitted to the Abaqus/Standard or Abaqus/Explicit solver. The solver performs the analysis and generates an output database; using the Visualization module it's possible to read the output database and the results of the analysis.

3.1.1 Modules

Now it's illustrated briefly the modelling process moving from module to module. There is not a rigid order to follow and although it is possible to move forth and back between the modules the best way to build the model is by following a logical sequence. Generally different parts of the model are created separately in the Part module and then assembled in the Assembly module. In the Property module Abaqus provides a wide range of material behaviours like elastic, plastic, thermal and acoustic; in the same module the properties of the section are defined. In the Step module the problem history is divided in a sequence of one or more analysis steps; the step concept is a fundamental concept in the process modelling. There are two kinds of steps: general analysis steps, which can be used to analyse linear or non linear response, and linear perturbation steps, which can be used only to analyse linear problems. For each step an analysis procedure can be chosen that defines the type of analysis to be performed during the step. A fundamental division of the analysis procedures is static or dynamic analysis; dynamic problems are those in which inertia effects are significant. Abaqus offers a large flexibility in making this distinction so the

user can change the analysis type from step to step and the same analysis can contain several static and dynamic phases. The rest of the step definition consists of load, boundary and output request specifications. The loads and the boundary conditions acting on the model are defined in the Load module and can be defined to vary over the time as well as over different steps. Then the whole model built can be meshed in the Mesh module; there are different meshing techniques available which vary with the element type and the geometry of the model. Different meshing techniques can be applied to the same part partitioning it. Finally in the Job module the model is submitted to the analysis.

3.1.2 Analysis type

Abaqus provides two different approaches to study the response of the model: a general and a linear perturbation analysis. Loading conditions are defined differently for the two cases, time measures are different and the results should be interpreted differently. The state at the end of a general step provides the initial conditions for the next general step, this allows to simulate consecutive loadings of a model. Linear perturbation analysis provides the linear response about the state reached at the end of the last general analysis prior to the linear perturbation step. If the first step of the analysis is a general or a perturbation step the base state of reference is determined from the initial conditions.

3.1.2.1 General static analysis

The general static analysis can include the effect of nonlinearities present in the model. Nonlinearities can arise from large displacement effects, material nonlinearity and boundary nonlinearities such as contact and friction. If geometrically nonlinear behaviour is expected the “NLGEOM” option should be used. Abaqus uses Newton’s method to solve the nonlinear equilibrium equations. If the problem involves history dependent response the solution is obtained as a series of increments, with iterations to obtain equilibrium within each increment. The choice of increment size is a matter of computational efficiency and if the increments are too large more iterations will be required. Abaqus has two measures of time: step time and total time. The step time of each

general step begins at zero and accumulates into the total time. If the analysis procedure for the step has a physical time scale, as in a dynamic analysis, step time must correspond to that physical time. Otherwise step time is any convenient time scale. If a time period is not specified, the default time varies from 0.0 to 1.0 over the step and time increments represent simply fractions of the total period of the step.

In the dynamic step of the analysis a step time of 600 seconds is assumed, corresponding to the 10-minute observation period of the wind velocity.

3.1.2.2 Linear Eigenvalue Analysis

The linear perturbation analysis is used in the Linear Eigenvalue Analysis to calculate the natural frequencies and the correspondent mode shapes of the model. The extraction of natural frequencies is fundamental to study the dynamic behaviour of our system and the presence of negative eigenvalues normally indicates instability. The linear perturbation analysis can be performed also during a nonlinear analysis and has no effect on the general analysis. The step time of linear perturbation steps is taken generally very small and is not accumulated into the total time. The eigenvalue extraction can be performed using two different eigensolver algorithms: Lanczos and Subspace. The first is faster when a large number of eigenvalues is required and the second can be faster for small systems. It needs only to specify the number of eigenvalues required or alternatively the maximum frequency of interest.

3.1.2.3 Implicit dynamic analysis

Abaqus provides dynamic analysis for both linear and nonlinear problems. In the case of linear problems methods based on the eigenmodes of the system are used to predict the response. In these cases the necessary modes and frequencies must be calculated before in a frequency extraction step. When nonlinear dynamic problems are studied a direct time integration method must be used. The modal methods used in linear dynamic analysis are less expensive computationally than the direct integration methods, where the global equations of motion are integrated through the time, although the eigenmode extraction can become computationally intensive if many modes are required for a large model. The

direct integration method provided in Abaqus/Standard called the Hilbert-Huges-Taylor operator is an extension of the trapezoidal rule. The Hilbert-Huges-Taylor operator is an implicit operator and obtains values for dynamic quantities at $t + \Delta t$. This nonlinear equation solving process is expensive and if the equations are very nonlinear it may be difficult to obtain a solution. However it's easier to handle the nonlinearities in the dynamic procedures than in the static because the inertia terms provide mathematical stability to the problem; thus the implicit method is applicable with success in the most cases expect those of extremely nonlinearities. The most important advantage of the Hilbert-Huges-Taylor operator is that it is unconditionally stable; it means that there is not mathematical limit on the size of time increment that can be used to integrate the equations of motion. In Abaqus/Standard the time step for implicit integration can be controlled by the "half-step residual" introduced by Hibbit and Karlsson (1979). The half-step residual is the equilibrium residual error halfway through a time increment at $t + \Delta t/2$ once the solution at $t + \Delta t$ has been obtained; monitoring its values the accuracy of the solution can assessed and the step time adjusted appropriately. If the half-step residual is small, it indicates that the accuracy of the solution is high and the time step can be increased safely; if the half-step residual is large the time step used in the solution should be reduced. This automatic time increment is convenient especially when the dynamic response can be expected to change significantly during the solution. It's possible also to control the time increment directly through the step specifying a fixed time increment but normally this approach is recommended only in special cases when the problem is well understood or when convergence is not achieved with automatic time increment. The automatic time increment is defined specifying an initial, minimum and maximum increment sizes. If the convergence is not reached with the initial increment is necessary to decrease it, otherwise if the convergence is found it should be used an attempt with a larger one. The algorithm described is purely empirical and based on the experience.

3.1.2.4 Explicit dynamic analysis

The explicit dynamic analysis procedure is available only in Abaqus/Explicit and uses the central difference rule to integrate the equations of motion. The explicit procedure obtains values for dynamic quantities at $t + \Delta t$ based entirely on available values at time t The

central difference operator is conditionally stable and the stability increment limit for the operator is given in terms of the highest eigenvalue of the system as: $\Delta t \leq 2/\omega_{\max}$. Introducing damping in the system the stable time increment is given by:

$$\Delta t \leq \frac{2}{\omega_{\max}} \left(\sqrt{1 + \xi^2} - \xi \right) \quad (3.1)$$

where ξ is the fraction of the critical damping in the mode with the highest frequency. The stability limit of the time increment is related to the time required for a stress wave to cross the smallest element dimension in the mesh; thus the time increment can be very small if the mesh elements are very small or if the stress wave speed is very high. An approximation of the stability limit can be written as $\Delta t = L_{\min}/C_d$ where L_{\min} is the smallest element dimension and C_d the dilatational wave speed of the material. The explicit dynamic analysis is to be used with short dynamic response time and specially to solve extremely discontinuous events or processes. It permits also to solve three dimensional contact problems with deformable bodies. The choice between an implicit and an explicit approach to a nonlinear problem depends on details of the specific case and in most problems only the experience can guide to choose an approach.

Between the two dynamic approaches it is chosen to use an implicit dynamic analysis with a fixed time increment, tested through different analysis running, essentially for the major facility to find a convergence solution.

3.1.3 Elements

Abaqus has a large element library that provides a complete geometric modelling capability. It is possible to choose between different element categories based on the space modelling: 3D, 2D and asymmetric space elements. The element shapes available are: beam, shell and solid element. All the elements use numerical integration to allow complete generality in material behaviour; shell and beam element properties can be defined as general section behaviours or each cross section of the element can be integrated

numerically, so the eventual nonlinear response can be treated accurately. All the elements are defined in a global Cartesian system except the asymmetric elements which are formulated in terms of r-z coordinates. In almost all elements vector quantities like displacements and rotations are defined in terms of nodal values with scalar interpolation functions.

3.1.3.1 Beam elements

In the FE model of the bridge a 3D beam element is used for the permanent part such as the arch, the bridge deck, the piers and the hangers. Using a beam element results in reduction of the mathematical problem to one dimension: the primary solution variables are functions only of the position along the beam axis. It is reasonable to use a beam element only if the length along the axis is large compared with the dimensions of the cross section. There are two fundamental beam theories: the Euler-Bernoulli theory and the Timoshenko theory. The Euler-Bernoulli theory assumes that plane cross-sections initially normal to the beam axis remain plain, normal to the beam axis and undistorted. The elements that use cubic interpolation all use this assumption. The beam elements that use linear and quadratic interpolation, like the element type “B31” used in the FE model, are based on the Euler-Bernoulli formulation but they also allow a transverse shear strain that is the cross-section may not necessarily remain normal to the beam axis. This extension leads to the Timoshenko theory that is generally more useful for thicker beams.

A “BEAM GENERAL SECTION” option is used to define the section properties for each beam element of the bridge. Using this option the following cross-sectional properties are given explicitly for each element: cross-sectional area, moments of inertia, torsion rigidity, eccentricity of the neutral axis, eccentricity of the shear centre, Young’s and Shear modulus.

3.1.3.2 Material Damping

In direct dynamic analyses energy dissipation mechanisms such as dashpots, inelastic material behaviour and other dissipation sources are usually defined; in these cases it is not necessary to introduce in the model a structural damping because its effect is unimportant

compared to the other dissipative effects. However in the models which are without dissipation sources it becomes important to introduce this structural damping.

Abaqus provides the Rayleigh damping and it is defined by the “DAMPING” option in the beam section properties definition. The Rayleigh method, as exposed in the previous chapter, assumes that the element damping matrix can be expressed as a linear combination of the mass and stiffness matrices :

$$\mathbf{C} = a_0 \mathbf{M} + a_1 \mathbf{K} \quad (3.2)$$

The two Rayleigh damping factors a_0 and a_1 are introduced by the “DAMPING” option and represent respectively: the first factor gives the damping contribution proportional to the mass matrix and introduces damping forces caused by the absolute velocities of the model simulating the idea of the model that moves through a viscous ether; the second factor gives the damping contribution proportional to the material stiffness. These two factors can be calculated applying the expression (2.30).

In addition to the Rayleigh damping in an implicit direct time integration analysis it is defined an “artificial damping” using the “ALPHA” parameter in the “DYNAMIC” option. This damping has a different nature from the Rayleigh damping, it grows with frequency and with the ratio of the time increment to the period of vibration of a mode. It results never very substantial for realistic time increment. In the analysis for this parameter the default value is left.

3.2 FE model of the New Svinesund Bridge

The finite element model of the Svinesund Bridge is based on the structural model produced by the bridge contractor Bilfinger Berger (2004). Extra nodes, elements and constraints were added in order to model the supports for the carriageways on the top of the piers and the rigid connections between parts of the carriageways. A large number of element sets was used to couple the elements to the right element properties; the beam elements used have constant cross-sectional properties while the properties in the Bilfinger Berger model varied linearly along the element. In the arch and pier elements, where the

cross-sections vary, the mean values of the cross-sectional properties at the element ends were used as constant cross-sectional properties. Nevertheless for the elements of the carriageways the properties in the first node were used as constant cross-sectional properties. The model was developed also for the analysis of the bridge arch launching but in this report only the model of the bridge in its final configuration is considered without the temporary structures used during the construction process. The analysis starts first with the eigenfrequencies extraction, then the static step with the application of the gravity load and finally the dynamic analysis under the wind loads. The input file was typed using a text editor and it was submitted to the analysis by the Abaqus Command Line. Generally an input file has a basic structure constituted of two main parts: model data and history data part.

- Model data contains the definition of the model: nodes, elements, materials, boundary conditions and initial conditions.
- History data defines the analysis type, loads and output requests. This section is divided in different steps and there is no limit on the number of the steps in an analysis.

3.2.1 General description

The model considered in the report, as it was mentioned before, consists only of the permanent parts of the bridge: the arch, the hangers, the piers and the superstructure. The model is defined in the 3D right-handed Cartesian coordinate system and the origin of the axes is at the sea level under the mid-point of the arch. The x-axis is pointing along the longitudinal axis of the bridge, in approximately northern direction towards Norway; the y-axis is pointing in transversal direction, in approximately eastern direction; the vertical z-axis is pointing downwards, towards the water. SI units are used in the model definition and in the analysis.

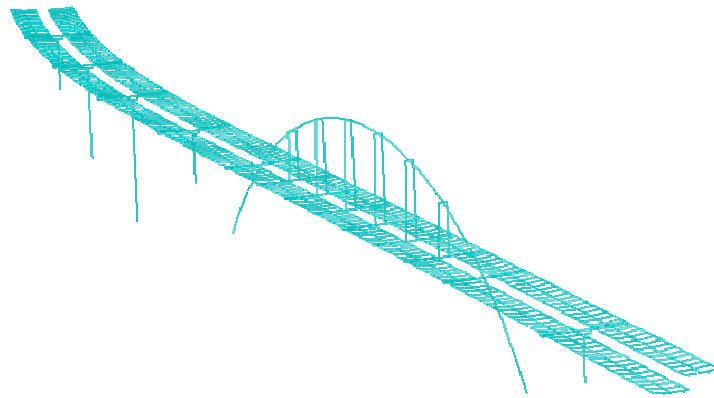


Figure 3.1 Perspective view of the bridge's model.

3.2.2 Different parts of the model

The concrete arch is modelled by beam elements positioned along its neutral axis; the beam elements have a rectangular hollow box cross section.

The hangers that support the carriageways are also modelled with beam elements. The hangers are connected to the arch by stiff beam elements.

The piers that support the carriageways are modelled by beam elements positioned along their neutral axes. Additional stiff beam elements, with the same properties of those used for the arch, connect the supports of the carriageways with the pier top.

One-node spring elements are used to model the support stiffness for the piers and the arch where it is not modelled as fixed or free. For each spring the degree of freedom is given together with the corresponding linear translational or rotational stiffness, taken from the Bilfinger Berger model (2004).

The carriageways are modelled as beam grid structures to represent their box sections. For each double-celled box section three longitudinal beams are defined representing the longitudinal walls with interacting parts of the top and bottom flange. Transversal stiffeners, one approximately every four meter, represent the internal transversal stiffening walls with interacting parts of the top and bottom flange. At each of the support points, over the pier and under the hangers from the arch, there are transversal beams connecting the two parallel carriageways. The transversal beams are integrated into each carriageway

and are supported between the carriageways. The transversal beams are connected to the carriageway elements and the top nodes of the pier bearings through stiff beam elements. At the end supports, stiff beam elements are also used to connect the carriageway elements to the support nodes.

3.2.3 Boundary conditions and constrains

The following assumptions were made regarding the boundary conditions of the bridge:

The arch was assumed to have a fixed foundation for all degrees of freedom (DOF) except for the rotation around the bridge transverse axis. The support for this degree of freedom was modelled by rotational springs. The stiffness values were taken from Bilfinger Berger (2002, 2003).

The piers founded on the rock were assumed to have a fixed foundation for all translational DOF, and for the torsion around the pier axis. The supports for the rotations around the bridge transverse and longitudinal axes were modelled by rotational spring. The stiffnesses according to the indata files of Bilfinger Berger (2004) were used. The stiffnesses for the rotations around the transverse axis correspond to those calculated in Bilfinger Berger (2003). The stiffnesses for the rotations around the longitudinal axis were approximated to be ten times greater.

The supports of the pier founded on steel core piles were modelled by rotational and translational springs for all DOF. The stiffnesses calculated in Bilfinger Berger (2003) were used.

At the end abutments, on both the Swedish and Norwegian side, each carriageway is supported by two bearings. Here all support nodes were fixed for displacement in the vertical direction. The support nodes closest to the centre-line of the bridge were fixed also for displacement in the transversal direction. All other DOF were free.

The assumptions that follow were made regarding the internal connections between the different parts of the structure.

The carriageways were rigidly connected to the arch, with all degree of freedom equal at the connection.

The hangers were rigidly connected to the arch as well as to the transversal beams of the carriageways. However, due to the low bending stiffness, the moments transferred through the hangers, will be negligible. (The stresses in the hangers, however, may become large due to the bending effect).

On the top of the piers the transversal beams connecting the two carriageways are supported by two bearings.

3.3 Model of the wind forces

The wind forces are modelled as concentrated loads by the “CLOAD” option in the last dynamic step of the analysis. These forces are applied on the central part of the bridge: on the arch and on the part of the bridge deck between the piers closest to the arch. An increasing number of nodes, at which the wind forces are applied, is considered through the different analyses carried out.

At first a total number of 22 nodes is considered (Figure 3.2); the positions chosen correspond to the midpoints of the parts of the structure between two consecutive hangers both for the arch and the bridge deck for a total number of 14 nodes. For the arch other 2 more nodes are added between the abutments and the bridge deck. The remaining 6 nodes are uniformly distributed on the parts of the bridge deck included between the arch-bridge deck connections and the piers closest to the arch (numbered in the model as pier 5 on the Swedish side and 8 on the Norwegian side). The nodes on the bridge deck are all at the same height of 60 m and those on the arch vary their heights from the abutments to the crown.

To obtain the resultant concentrated forces the drag forces, which are defined for unit of length, are to be multiplied for a dimension that represents the influence length of each node; for the nodes on the arch the average length is of 28 m and for those on the bridge deck is of 25.5 m.

To define the time-history of the applied load the “AMPLITUDE” option is used and it is included in the model definition portion of the input file. This option allows defining an arbitrary time (or frequency) variations of loads, displacements and other prescribed variables. By default the values of the loads change linearly with time throughout the step. Each amplitude curve must be named by using the “NAME” parameter and then this name

is referred to in the definition of the concentrated load in the dynamic step by using the “AMPLITUDE” parameter.

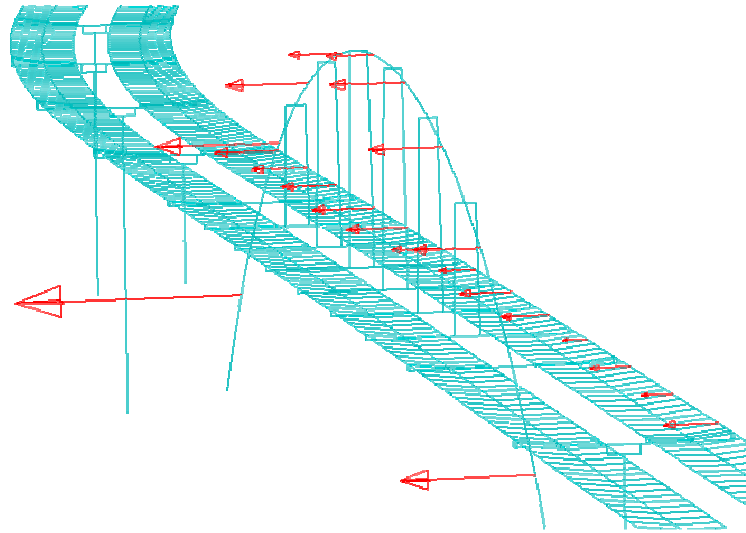


Figure 3.2 Model of wind forces applied on twenty two nodes.

The second step in the increasing number of nodes was to pass to 98 nodes, 58 on the arch and the remaining 40 on the bridge deck; this means an average influence length for the nodes on the arch of 5 m and for the nodes on the bridge deck of 8.3 m. As it will be seen in the next chapter this model will become the reference model for the study of the wind response of the bridge.

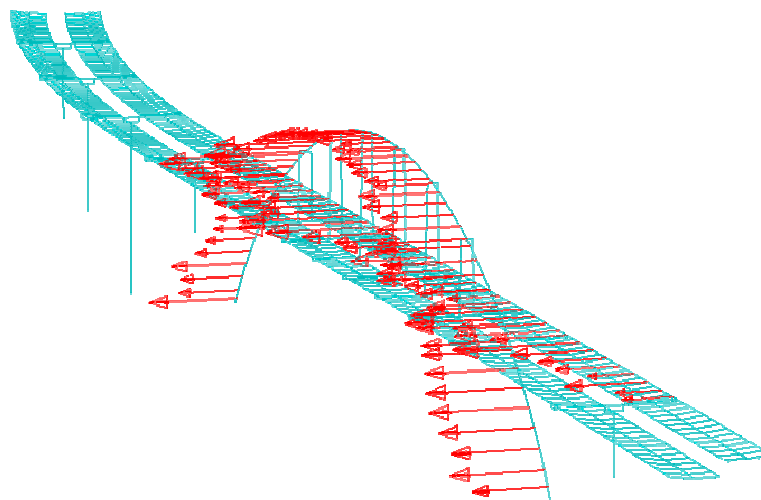


Figure 3.3 Model of wind forces applied on ninth nine nodes.

The last model studied was that with wind forces applied on each node for a total number of 194 nodes, 115 on the arch and 79 on the bridge deck. The average influence length for the nodes on the arch results 2.5 m and for those on the bridge deck 4.15 m. This model was then left having shown substantially the same response of the previous model but taking more computational effort.

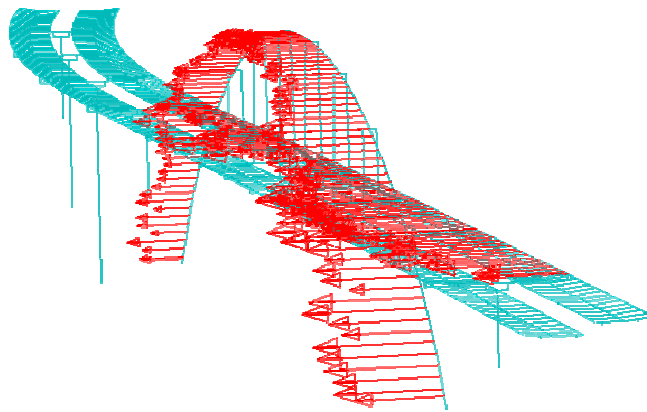


Figure 3.4 Model of wind forces applied on one hundred ninth four nodes.

3.4 Analysis steps

The FE analysis of the bridge is made up of three steps:

- The first step: the gravity load is applied.
- The second step: the natural frequencies of the structure are extracted.
- The third step: the wind forces are applied.

In the next chapter the results about the last two dynamic steps will be analysed and discussed.

Chapter 4 Simulations and analysis of the results

4.1 Dynamic identification of civil structures

The parameter identification through dynamic measurements was originally developed in more advanced mechanical and aerospace engineering fields. The transfer of this technology to civil engineering applications meant to deal with problems which have a completely different scale compared with mechanical and aerospace engineering counterparts. Experimental modal parameter identifications of civil engineering structures mean the extraction of modal parameters (frequencies, damping ratios and mode shapes) from dynamic measurements. In this work at first the frequencies of the bridge are identified from the measurements and the values obtained are compared with those extracted from the FE model. Then taking into account the identified frequencies, the positions of the accelerometers and the results from the FE eigenvalue analysis, the modes of the bridge can be identified. The experimental measurements permit also to estimate a value of the damping ratio through which update the FE model for the simulation.

Three main different types of structural dynamic testings can be recognized:

- Forced vibration testing
- Free vibration testing
- Ambient vibration testing

In the first method the structure is excited by artificial devices such as shakers or drop weights. A condition of free vibrations is induced by suddenly dropping a load on the structure. The disadvantage of artificial excitation methods is that the traffic load has to be shut down for a rather long period of time. This can be a serious problem for the infrastructures intensively used. In contrast, ambient vibration testing is not affected by the disturbances on the structures because it uses the disturbances induced by traffic and wind as natural or environmental excitation; it represents a real operating condition of the structure during its daily use cause the traffic does not have to be interrupted by using this technique.

Basically the modal parameter identification is carried out based both on the input and output measurements data through the frequency response functions in the frequency domain and impulse response functions in the time domain. For civil engineering structures the dynamic responses are the direct records of the sensors installed at several locations. Usually it is difficult to measure the excitation forces acting on a real large structure. The ambient vibration testing has the advantage of being inexpensive since no equipment is needed to excite the structure and only response data are measured; thus the identification techniques based on this dynamic testing were largely used in civil engineering field and successfully applied to many large scale bridges.

These identification techniques need to deal with very small magnitudes of ambient vibration contaminated by noise without the knowledge of loading conditions. Over the past decades several different identification techniques were developed, the identification method used in this work is represented by the peak-picking method which is probably the most widely used method in civil engineering applications because of its simplicity. Other more advanced techniques exist like the stochastic subspace identification method in time domain that it is more time consuming than the peak-picking but permits to yield more accurate results.

4.1.1 Peak-picking method

The peak-picking method, as mentioned before, is the simplest known method for identifying the dynamic parameters of civil engineering structures subjected to ambient vibration loading. The method is initially based on the fact that the frequency response function goes through extreme values around the natural frequencies. The frequency at which this extreme value occurs is a good estimate for the frequency of the system. In the context of ambient vibration measurements the frequency response function is only replaced by the spectra of the ambient response. In such a way the natural frequencies are simply determined from the observation of the peaks on the graphs of the power spectral density functions (Figure 4.1); these functions are basically obtained by converting the measured accelerations to the frequency domain by a Fast Fourier Transform (FFT).

The peak-picking is a technique in the frequency domain; frequency domain algorithms are most used due to their simplicity and processing speed. These algorithms, however, have a theoretical drawback because they involve averaged temporal information, thus losing

most of their details. Nevertheless, having few acceleration data, it seems not necessary to apply more refined methods.

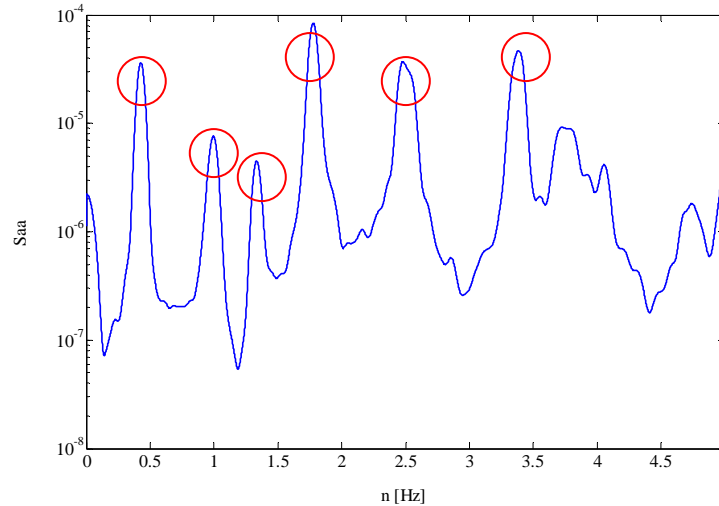


Figure 4.1 Peak-picking method.

4.2 Identification of the natural frequencies

The identification of the natural frequencies of the bridge, as exposed above, can be obtained analysing the power spectral density functions (PSD) of the measured accelerations where high values of the PSD functions indicate probable positions of frequencies. The accelerometers are installed at the midpoint and at the quarter point on the Swedish half of the arch and at the corresponding sections on the west side of the bridge deck. The first seven natural frequencies until a frequency of about 2 [Hz] result well visible analysing the graphs of the PSD of the measured accelerations, labelled as S_{aa} in the graphs, versus the natural frequencies n [Hz]; at higher frequencies the peaks become less clear and consequently it is more difficult to identify the related frequencies; furthermore modes at higher frequencies show to interest the lateral parts of the structure in the direction of the abutments, out of the central part of the bridge where the measurements are taken. Now it follows a summary of the identified natural frequencies with first considerations on the type of the identified modes based on the symmetric or anti-symmetric positions of the accelerometers about the central section of the structure. For each identified frequency the PSD functions of the accelerations, measured at the four mentioned sections, are represented together allowing a comparison between the resultant

amplitudes of vibration of all the sections. The first identified natural frequency occurs at 0.43 Hz.

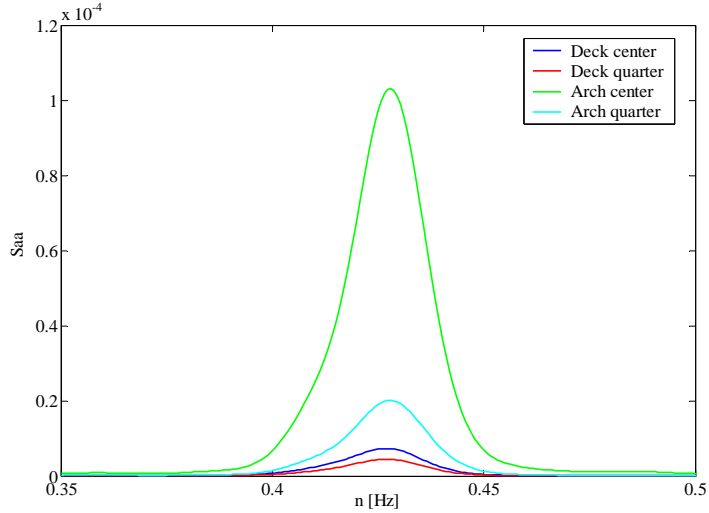


Figure 4.2 First natural frequency.

It can be noted that the arch is more excited than the bridge deck by the first mode of vibration and in particular at its central section; this mode can be recognized as a symmetric mode.

The second identified natural frequency occurs at 0.85 Hz.

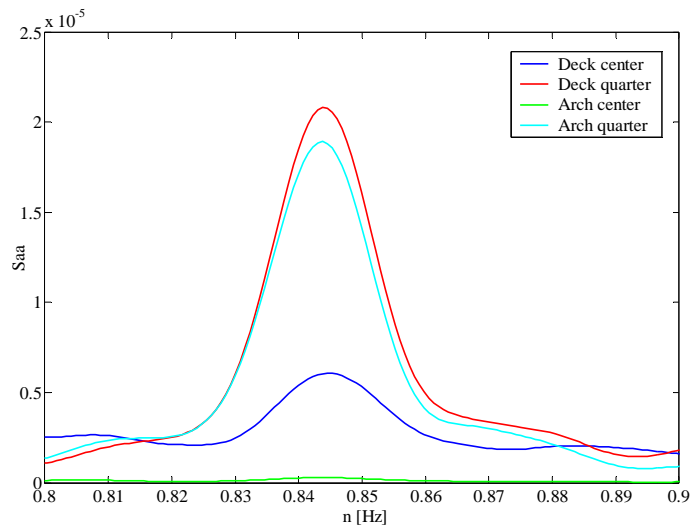


Figure 4.3 Second natural frequency.

The second mode of vibration shows to equally excite the arch and the bridge deck and in particular their quarter sections; this mode can be recognized as an anti-symmetric mode.

The third identified natural frequency occurs at 0.95 Hz.

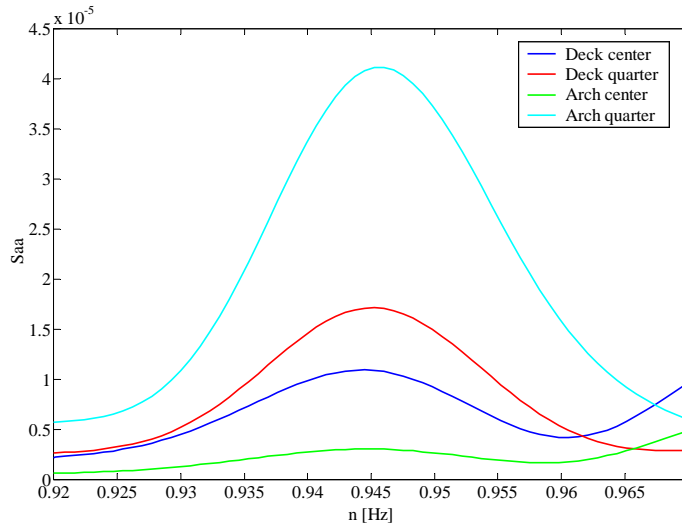


Figure 4.4 Third natural frequency.

The arch results more excited than the bridge deck by the third mode of vibration and in particular at its quarter section. Also this mode can be recognized as an anti-symmetric mode.

The fourth identified natural frequency occurs at 1.01 Hz.

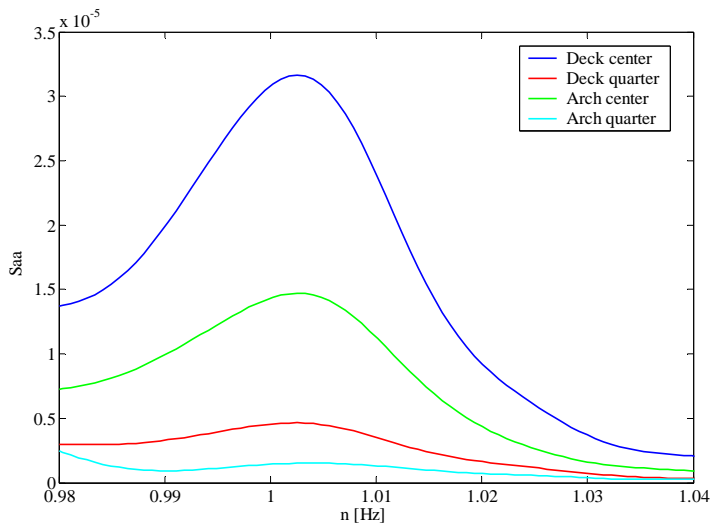


Figure 4.5 Fourth natural frequency.

The bridge deck results more excited than the arch by the fourth mode of vibration and in particular at its central section; this mode can be recognized as a symmetric mode.

The fifth identified natural frequency occurs at 1.33 Hz.

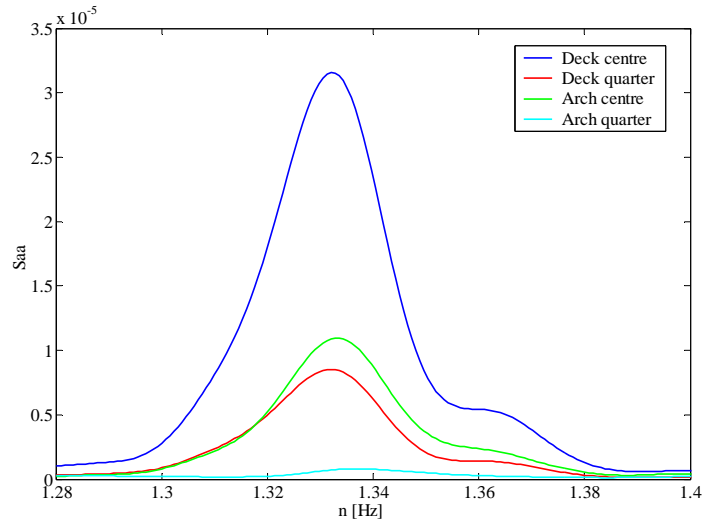


Figure 4.6 Fifth natural frequency.

The fifth mode of vibration excites principally the central section of the bridge deck and it can be recognized as a symmetric mode.

The sixth identified natural frequency results at 1.46 Hz.

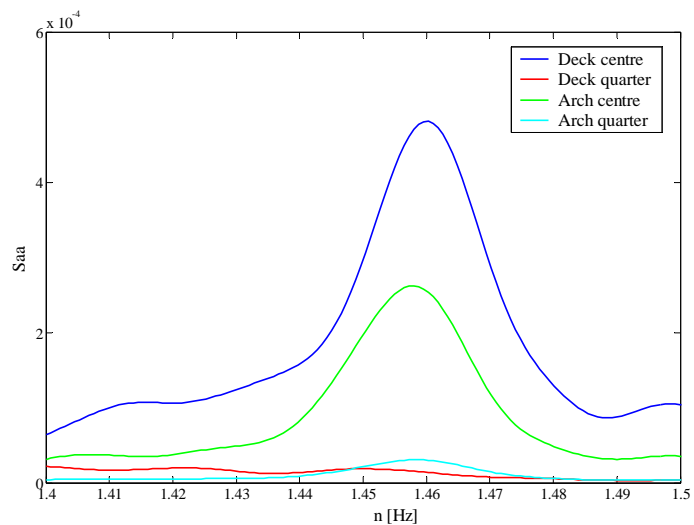


Figure 4.7 Sixth natural frequency.

The sixth mode of vibration excites only the central sections of arch and bridge deck and it can be recognized as a symmetric mode.

The seventh identified natural frequency occurs at 1.78 Hz.

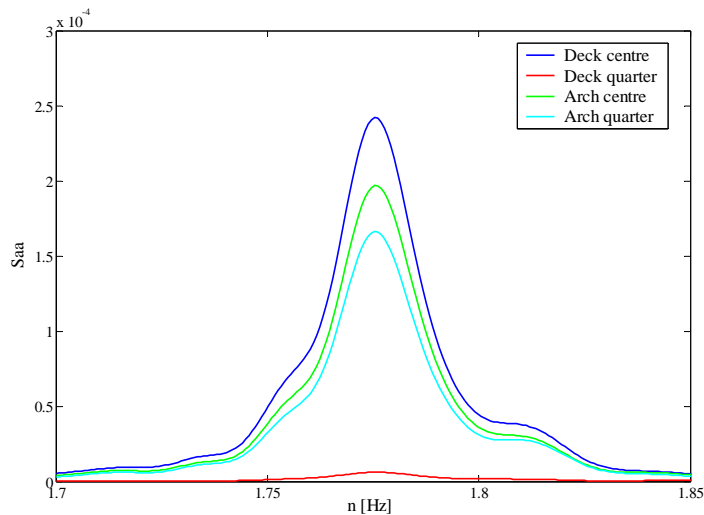


Figure 4.8 Seventh natural frequency.

This represents the last identified natural frequency; the related mode of vibration excites approximately in the same way the arch and the central section of the bridge deck and it can be recognized as a torsion mode.

4.2.1 Numerical results

The previous identified frequencies and the preliminary considerations made on the modes can be compared with the eigenvalue output from the FE analysis, considering the same frequency range until about 2 [Hz]; the results reported in the Table 4.1 point out the first twelve eigenvalues and eigenfrequencies extracted together with the generalize masses; these last terms represent the mass of a single degree of freedom system associated with each mode. It can be noted as the maximum value of the generalized mass is connected to the second mode.

Eigenvalue Output				
Mode Number	Eigenvalue	Frequency		Generalized Mass [Kg]
		ω [rad/s]	n [Hz]	
1	6.5798	2.5651	0.40825	1.51E+06
2	8.3478	2.8893	0.45984	8.18E+06
3	36.073	6.0061	0.9559	2.29E+06
4	41.011	6.404	1.0192	1.87E+06
5	48.378	6.9554	1.107	2.20E+06
6	56.266	7.501	1.1938	3.74E+06
7	67.9	8.2401	1.3115	4.65E+05
8	82.105	9.0612	1.4421	9.35E+05
9	88.373	9.4007	1.4962	9.90E+05
10	119.43	10.929	1.7393	2.01E+05
11	125.47	11.202	1.7828	8.18E+05
12	127.9	11.309	1.8	2.13E+06

Table 4.1 Eigenvalues, natural frequencies and generalized masses.

The participation factors are obtained by the same eigenvalue output; these values are reported in the Table 4.2 and indicate the predominant degrees of freedom in which the modes act.

Participation Factors			
Mode Number	X-Component	Y-Component	Z-Component
1	-0.03	1.69	0.01
2	0.97	0.05	0.00
3	0.01	-0.11	0.00
4	-0.03	0.80	0.00
5	0.43	1.35	0.01
6	-0.88	0.39	0.02
7	0.05	-0.56	0.13
8	0.05	0.04	0.69
9	-0.16	0.00	-0.05
10	-0.37	0.05	0.89
11	0.16	0.15	0.21
12	0.01	0.34	-0.07

Participation Factors			
Mode Number	X-Rotation	Y-Rotation	Z-Rotation
1	131.59	0.70	7.25
2	3.35	-21.98	-11.43
3	-6.16	-0.99	78.79
4	40.76	1.54	96.60
5	78.30	-21.38	-302.25
6	22.51	45.13	-94.02
7	-16.25	-2.90	42.44
8	1.08	7.03	-8.53
9	-3.46	41.54	-1.42
10	8.02	-134.35	13.30
11	-0.78	66.52	64.67
12	19.73	-38.02	54.98

Table 4.2 Participation factors.

Finally the effective masses are extracted; these values indicate the amount of mass active in each degree of freedom for any one mode and together with the participation factors aid to identify the modes of the bridge.

Effective Mass [Kg]			
Mode Number	X-Component	Y-Component	Z-Component
1	1415.7	4.32E+06	38.158
2	7.67E+06	22690	21.536
3	98.002	27120	5.9908
4	1973.3	1.20E+06	39.789
5	4.14E+05	4.03E+06	139.93
6	2.92E+06	5.60E+05	2103.9
7	1361.6	1.45E+05	7313.1
8	2212.2	1455.8	4.41E+05
9	24005	7.1501	2364.1
10	27736	460.01	1.60E+05
11	21938	19410	37447
12	343.72	2.51E+05	9041.6
Total	1.11E+07	1.06E+07	6.59E+05

Effective Mass [Kg]			
Mode Number	X-Rotation	Y-Rotation	Z-Rotation
1	2.62E+10	7.49E+05	7.95E+07
2	9.19E+07	3.95E+09	1.07E+09
3	8.69E+07	2.24E+06	1.42E+10
4	3.10E+09	4.45E+06	1.74E+10
5	1.35E+10	1.01E+09	2.01E+11
6	1.90E+09	7.63E+09	3.31E+10
7	1.23E+08	3.91E+06	8.38E+08
8	1.10E+06	4.63E+07	6.81E+07
9	1.18E+07	1.71E+09	1.99E+06
10	1.29E+07	3.63E+09	3.55E+07
11	5.04E+05	3.62E+09	3.42E+09
12	8.31E+08	3.09E+09	6.45E+09
Total	4.58E+10	2.47E+10	2.78E+01

Table 4.3 Effective masses.

4.2.2 Identification of the modes

The last step in order to complete with major accuracy the identification of the modes is to consider the visualization of the modes given by the eigenvalue output of the FE analysis, taking into account the numerical results exposed above. The first identified mode occurs at 0.43 [Hz] and it is a symmetric horizontal mode.

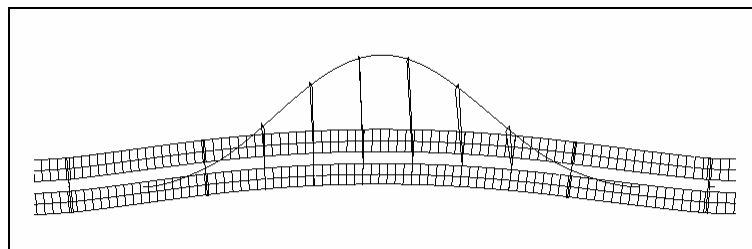


Figure 4.9 View from above of the first horizontal mode.

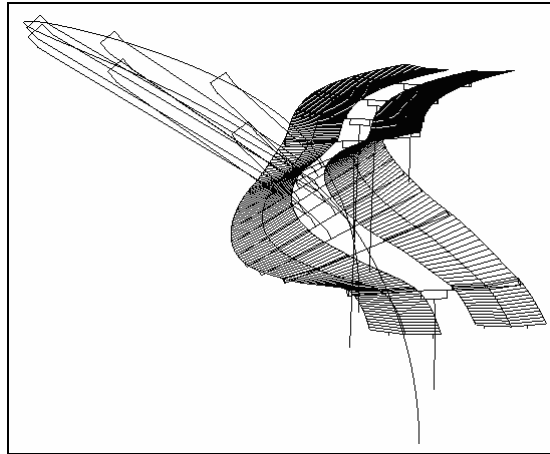


Figure 4.10 Frontal view of the first horizontal mode.

The second identified mode occurs at 0.85 [Hz] and it is an anti-symmetric vertical mode.

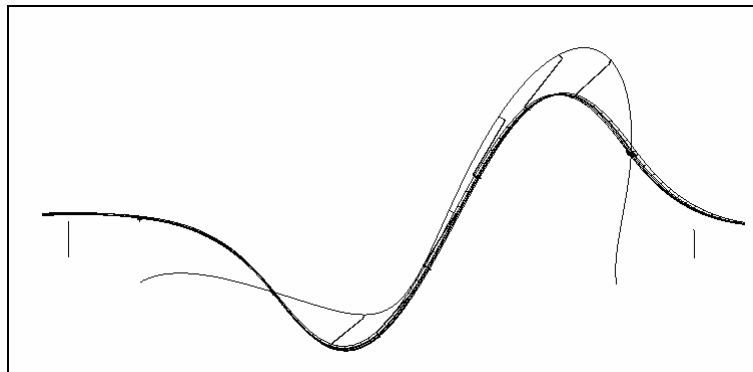


Figure 4.11 Lateral view of the first vertical mode.

The third identified mode occurs at 0.95 [Hz] and it is an anti-symmetric horizontal mode.

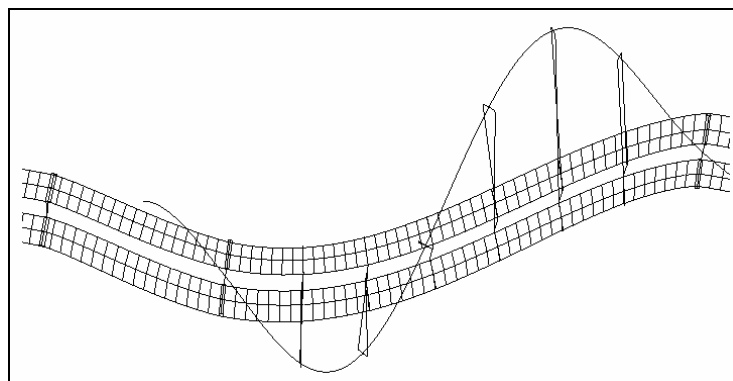


Figure 4.12 View from above of the second horizontal mode.

The fourth identified mode occurs at 1.01 [Hz] and it is a symmetric horizontal mode.

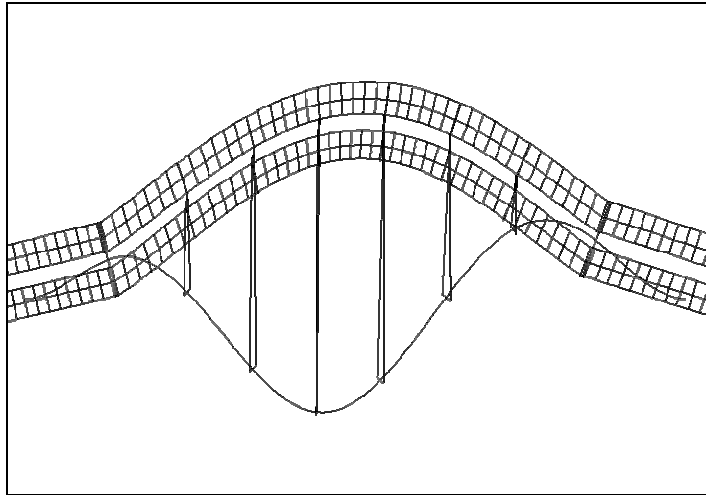


Figure 4.13 View from above of the third horizontal mode.

The fifth identified mode occurs at 1.33 [Hz] and it is a torsion-bending mode.

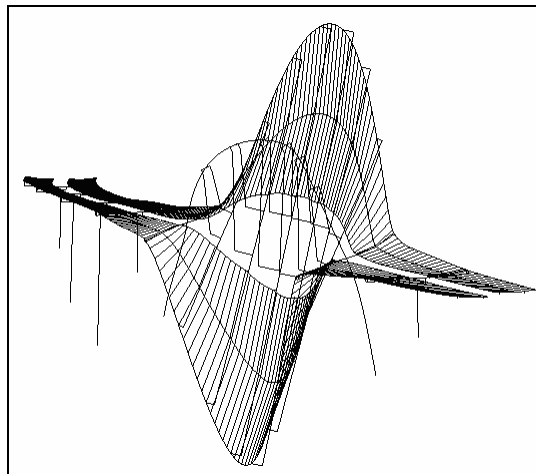


Figure 4.14 View of the first torsion-bending mode.

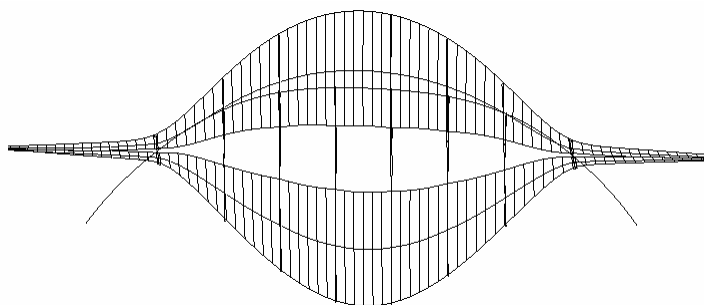


Figure 4.15 Lateral view of the first torsion-bending mode.

The sixth identified mode occurs at 1.46 [Hz] and it is a symmetric vertical mode.

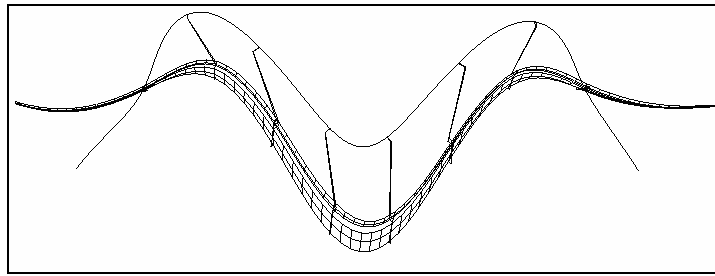


Figure 4.16 Lateral view of the second vertical mode.

The seventh identified mode occurs at 1.78 [Hz] and it is a torsion-bending mode.

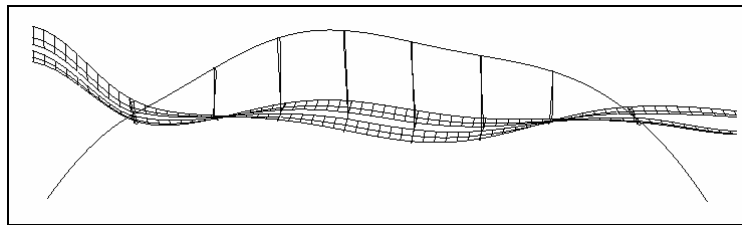


Figure 4.17 Lateral view of the second torsion-bending mode.

From the identified modes it is possible to observe that the first modes of vibration considered excite basically the central part of the bridge on which the wind actions will be applied.

4.2.3 Comparison between numerical and measured results

It has to be noted that not all the natural frequencies and the corresponding modes extracted from the FE analysis find a direct correspondence with the measured values; this fact can be explained considering two main reasons: on one hand not all the natural frequencies and corresponding modes obtained from the FE model represent real modes of vibration of the structure cause the boundary conditions and constraints assumed in the model cannot reproduce exactly the real conditions of the structure; on the other, having few accelerometers placed on the structure, it possible that some modes, which maybe are

correctly obtained from the model, are not picked through the measurements. For the modes which find a correspondence, the Table 4.4 presents a summary of the comparison between numerical and measured results.

Mode Number	Numerical Frequency [Hz]	Measured Frequency [Hz]	Description of the Mode
1	0.41	0.43	Symmetric bending horizontal
2	0.46	0.85	Anti-symmetric bending vertical
3	0.95	0.95	Anti-symmetric bending horizontal
4	1.02	1.01	Symmetric bending horizontal
5	1.31	1.33	Torsion Bending
6	1.44	1.46	Symmetric bending vertical
7	1.78	1.78	Torsion Bending

Table 4.4 Numerical and measured natural frequencies and description of the associated shape modes.

Generally a good agreement is found between numerical and measured results. The numerical and measured horizontal natural frequencies are very close, showing a difference of only 5% for the first, no difference for the second and a difference of only 1% for the third horizontal mode. However, this agreement is not observed for the first vertical mode of vibration, where the numerical natural frequency is 0.46 Hz while the measured is 0.85 Hz. This represents a difference of 46%. The reason of this fact can be searched considering that the joints between the transverse beams, the bridge decks, the top of the columns and abutments on grid lines 1, 2, 5, 8 and 9 are free to move in the longitudinal direction of the bridge (Figure 4.18). The friction between the bearings at the

top of the columns is not considered in the FE model, however this can increase the stiffness of the bridge; this is believed to be the reason for the difference between natural frequency and measured result. Also the prestressing tendons, which prevent the uplift of the bridge deck at the connection of the columns with the transverse beams, have the effect of increasing the friction at the bearings. This friction in the bearings can restrict the longitudinal movement of the bridge deck, at least for the small induced vibrations and it is possible that when the structure is subjected to larger vibrations, for which the frictional forces in the bearings are overcome, the natural vertical frequency of the structure could be that predicted by the FE model.

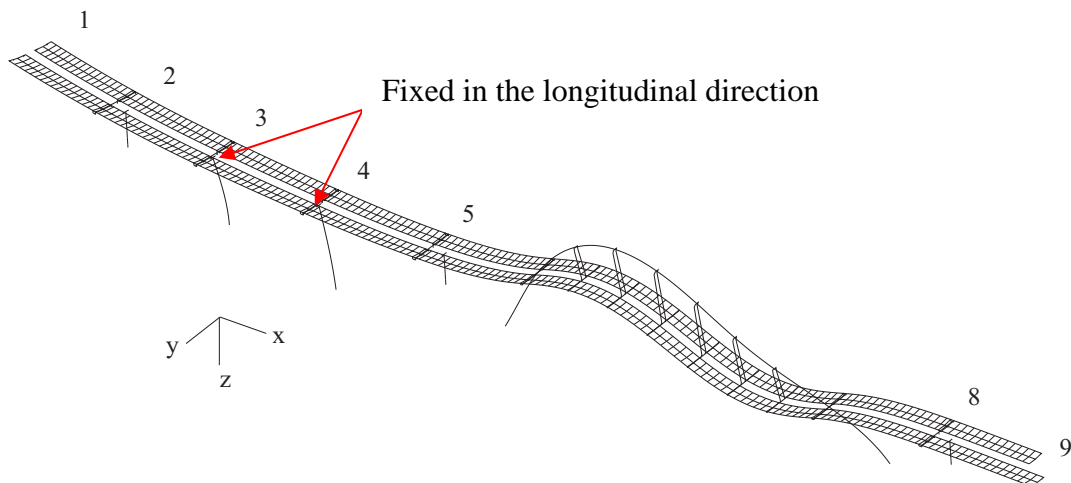


Figure 4.18 The first vertical shape mode with a frequency of 0.46 Hz from the FE model. The bridge deck is free to move in the longitudinal direction at the top of the columns and at the abutments (grid lines 1, 2, 5, 8 and 9).

The good agreement found in terms of measured and numerical natural frequencies indicates that the characteristics of mass and stiffness of the FE model reproduce with accuracy those of the real structure.

Once identified frequencies and modes of the structure, the damping ratio represents the remaining modal parameter which has to be determined; its evaluation will be exposed later describing the simulations carried out; however before starting to consider them it is necessary to introduce the basic concepts of the simulations of random stationary normal processes and the spectral models assumed for the turbulence components.

4.3 Simulation of random stationary normal processes

The knowledge of a suitable set of the sample functions of a random process allows to derive its power spectral density using the principles concerning the temporal averages. On the other hand, the knowledge of a suitable model of the power spectral density of a random process allows to derive artificially its sample functions. This operation is known as simulation of a random process and falls into the broad family of the Monte Carlo methods.

Monte Carlo methods to simulate a random process may be classified into two main families: 1) the methods based on the superposition of harmonic waves with random phase angles (random phase method); 2) ARMA methods based on the filtering of uncorrelated white noises (Auto-Regressive or Mobile-Average methods). Both these methods may be applied to simulate stationary and non-stationary random processes, as well as normal and non-normal random processes. In this work the random phase method is applied to simulate random stationary normal processes with nil mean, representing turbulence histories; this method is briefly described below first for the mono-variate processes and then for multi-variate processes.

4.3.1 Mono-variate processes

If $x(t)$ is a random stationary normal process with zero mean and $S_{xx}(\omega)$ is its power spectral density function, using the random phase method, a generic sample function of $x(t)$ is given by:

$$x(t) = 2 \sum_{j=1}^N \sqrt{S_{xx}(\omega_j) \Delta\omega_j} \sin(\omega_j t + \varphi_j) \quad (4.1)$$

where $\Delta\omega_j$ with $j=1, \dots, N$ is the amplitude of the frequency steps into which the harmonic content of the process is sub-divided (with $\omega \geq 0$); ω_j with $j=1, \dots, N$ is the central value of each step (Figure 4.19-4.20); φ_j is the j -th occurrence of the random phase Φ uniformly distributed between 0 and 2π (Figure 4.19):

$$p_{\phi}(\phi) = \begin{cases} 1/2\pi & 0 < \phi < 2\pi \\ 0 & \text{elsewhere} \end{cases} \quad (4.2)$$

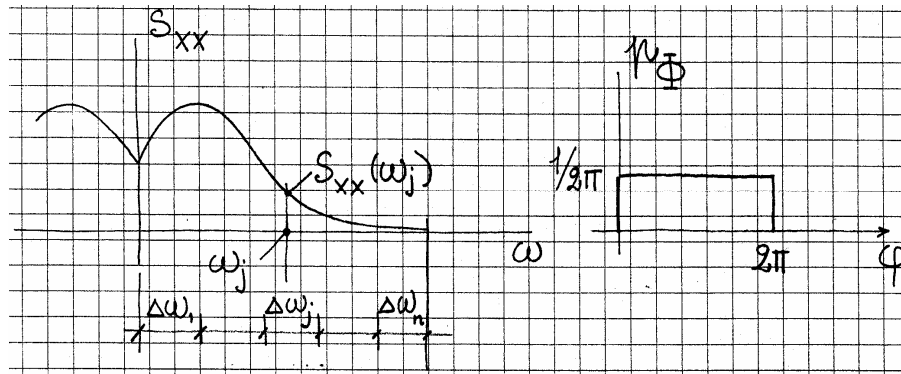


Figure 4.19 PSD of the random process and distribution of the random phase.

considering the j -th term of the sum (4.1):

$$x_j(t) = 2\sqrt{S_{xx}(\omega_j)\Delta\omega_j} \sin(\omega_j t + \phi_j) \quad (4.3)$$

evaluating its variance it follows that:

$$\sigma_{x_j}^2 = 4S_{xx}(\omega_j)\Delta\omega_j \frac{1}{2} = 2S_{xx}(\omega_j)\Delta\omega_j \quad (4.4)$$

Since the harmonics that constitute the sample function defined by (4.1) are uncorrelated with each other, having different circular frequencies, the variance of $x(t)$ is the sum of the variances of its components. Thus it results (Figure 4.20):

$$\sigma_x^2 = \sum_{j=1}^N \sigma_{x_j}^2 = 2 \sum_{j=1}^N S_{xx}(\omega_j)\Delta\omega_j \quad (4.5)$$

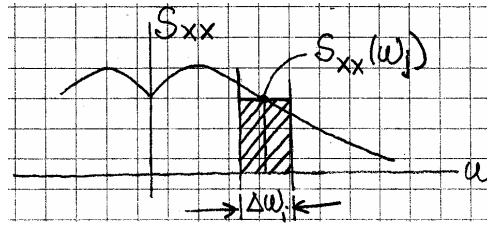


Figure 4.20 Calculation of the variance of the process.

Moreover, the amplitude of each harmonic defines the power content and distribution of the sample function and of the process.

4.3.2 Multi-variate processes

If $\mathbf{X}(t)$ is a n-variate random stationary normal process with zero mean and $\mathbf{S}_{xx}(\omega)$ is the power spectral density matrix of $\mathbf{X}(t)$, the random phase method allows to simulate any number of sample vectors of $\mathbf{X}(t)$. Figure 4.21 shows the basic concept of the simulation of a 3-variate process.

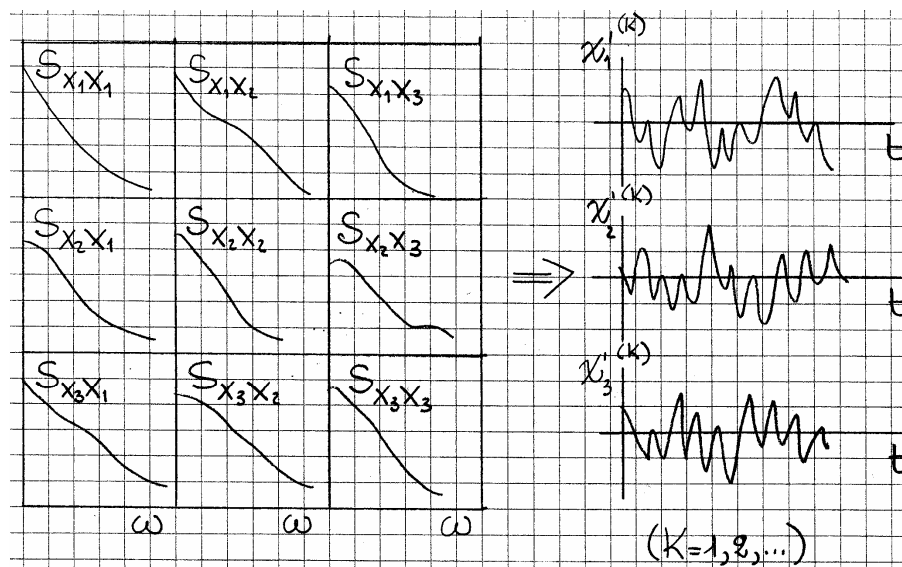


Figure 4.21 Simulation of a 3-variate process.

It is possible to demonstrate that the i -th component of the sample vector of $\mathbf{X}(t)$ is given by:

$$x_i(t) = 2 \sum_{j=1}^N \sum_{k=1}^n D_{ik}(\omega_j) \sqrt{\Delta\omega_j} \sin(\omega_j t + \varphi_{jk}) \quad i = 1, \dots, n \quad (4.6)$$

where $\Delta\omega_j$ with $j = 1, \dots, N$ is the amplitude of the frequency steps into which the harmonic content of the process is sub-divided (with $\omega \geq 0$); ω_j ($j = 1, \dots, N$) is the central value of each frequency step (Figure 4.19); φ_{jk} is the j,k -th occurrence of the random phase Φ uniformly distributed between 0 and 2π .

Equation 4.6 may be rewritten in the following matrix form:

$$\mathbf{X}(t) = 2 \sum_{j=1}^N \mathbf{D}(\omega_j) \sqrt{\Delta\omega_j} \sin(\omega_j \mathbf{I} t + \varphi_j) \quad (4.7)$$

where $\mathbf{I} = (11\dots1)^T$ is a vector of n unit components, $\varphi_j = (\varphi_{j1} \varphi_{j2} \dots \varphi_{jn})^T$, \mathbf{D} is a matrix provided by the relationship:

$$\mathbf{D}(\omega) \mathbf{D}(\omega)^T = \mathbf{S}_x(\omega) \quad (4.8)$$

Equation 4.8 is referred to as matrix decomposition. There are infinite possible matrices $\mathbf{D}(\omega)$ that satisfy equation 4.8 and several methods to determine such matrices. The most well-known methods are referred to as the Cholesky decomposition and the spectral decomposition.

4.3.3 Spectral turbulence model

The horizontal and vertical components of turbulence u and w are modelled as random stationary normal processes, function of the time and space. Considering the number n of nodes of the discretised model on which the wind forces will be applied, the turbulence

components can be modelled as n-variate random processes. In order to carry out the simulation of the processes using the random phase method exposed in the previous paragraph it is necessary to define the power spectral density matrixes $\mathbf{S}_{uu}(\omega)$ and $\mathbf{S}_{ww}(\omega)$ of the longitudinal and vertical component of turbulence.

The power spectral density matrix $\mathbf{S}_{\varepsilon\varepsilon}(\omega)$ ($\varepsilon = u, w$) has on the principal diagonal the power spectral density functions of the turbulence component $\varepsilon(t)$ defined by the (4.10) and for the terms out of diagonal $(\mathbf{S}_{\varepsilon\varepsilon}(\omega))_{ij}$ the cross power spectral density functions of the turbulence component $\varepsilon(t)$ between points M_i and M_j . These last terms are given by:

$$S_{\varepsilon\varepsilon}(\omega, M_i, M_j) = \sqrt{S_{\varepsilon}(\omega, M_i) S_{\varepsilon}(\omega, M_j)} \text{Coh}_{\varepsilon\varepsilon}(\omega, M_i, M_j) \quad (4.9)$$

where $S_{\varepsilon}(\omega, M_i)$ and $S_{\varepsilon}(\omega, M_j)$ are the power spectral density functions of the turbulence component ε at points M_i and M_j and the term $\text{Coh}_{\varepsilon\varepsilon}(\omega, M_i, M_j)$ is the coherence function between points M_i, M_j .

The power spectral density functions can be defined on the base of the Eurocode expression as:

$$S_{\varepsilon}(\omega, M_i) = \frac{1}{4\pi} \frac{d_{\varepsilon} \frac{L_{\varepsilon}(M_i)}{V_{mi}} \sigma_{\varepsilon}^2(M_i)}{\left[1 + 1.5 d_{\varepsilon} \left(\frac{|\omega| L_{\varepsilon}(M_i)}{2\pi V_{mi}} \right) \right]^{\frac{5}{3}}} \quad \varepsilon = u, w \quad (4.10)$$

where $d_u = 6.868$ and $d_w = 9.434$.

L_{ε} are the integral length scales and they can be calculated by the expressions:

$$L_u(z) = 300 \left(\frac{z}{200} \right)^{\nu}, \quad L_w(z) = 0.10 L_u(z) \quad (4.11)$$

where:

$$\nu = 0.67 + 0.05 \ln(z_0) \quad (4.12)$$

The term σ_ε^2 represents the variance of the turbulence component ε with the standard deviation which can be obtained by:

$$\sigma_\varepsilon = V_m I_\varepsilon \quad \varepsilon = u, w \quad (4.13)$$

with I_ε representing the intensity of the turbulence component ε . For the longitudinal turbulence component is given by:

$$I_u(z) = \frac{1}{\ln\left(\frac{z}{z_0}\right)} \quad (4.14)$$

The intensity of the vertical turbulence component can be obtained using the expression proposed by Solari and Piccardo (2001):

$$I_w(z) = 0.50 I_u(z) \quad (4.15)$$

The coherence function can be modelled by an exponential decay law as:

$$Coh_{\varepsilon\varepsilon}(\omega, M_i, M_j) = \exp\left\{-\frac{|\omega| \sqrt{\sum_r C_{r\varepsilon}^2 |r - r'|^2}}{\pi (V_{mi} + V_{mj})}\right\} \quad \begin{array}{l} \varepsilon = u, w \\ r = y, z \end{array} \quad (4.16)$$

where $C_{r\varepsilon}$ is a decay coefficient of the component turbulence ε along the r direction connecting the points M_i and M_j .

Cxu	Cyu	Czu	Cxw	Cyw	Czw
3	10	10	0.5	3	6.5

Table 4.5 Average values of the decay coefficients.

The transversal turbulence component along the bridge axis is not taken into account in this study; it should be considered studying the vortex excited cross vibrations of the arch for wind directions parallel to the bridge axis; however the measurements from the wind tunnel tests show no indications for a sensitivity of the arch against this phenomenon.

4.3.4 Spectral models, models errors and parameter uncertainties

Some considerations have to be made about the spectral equations which provide a model of the atmospheric turbulence; these models involve unavoidable errors and uncertainties which it is difficult to quantify.

The only thing that can be said is that these errors are mainly due, on one hand, to the impossibility of schematizing the atmospheric turbulence in a simple and at the same time physically suitable way and, on the other, to some persistent lacks of knowledge in this field. Relevant errors can occur in the low frequency range and in presence of large separations between the points considered where it could be necessary to consider the dependence of the decay exponential factor on $|r - r'|$.

In the high frequency range the spectral model overestimates the spectral turbulence content. On the other hand in the inertial subrange and for usual separation distances model errors seem to be quite limited. It follows that usually the model errors are less influent on the gust-excited response of structures than the parameter uncertainties which involve the turbulence variances, the integral length scales and the exponential decay coefficients. The uncertainties concerning these parameters are primarily caused by the enormous dispersion of the available data. These three types of parameters can be characterised statistically by mean values (see Table 4.5), coefficients of variation and cross-correlation coefficients.

Finally it must be considered that these spectral models are limited to flat homogenous terrains and near-neutral atmospheric conditions established when wind takes on high intensity.

4.4 Wind velocity history

In the Figure 4.22 the wind velocity history taken as reference is represented. The registration is made on ten minutes and the mean velocity results equal to 4.5 [m/s].

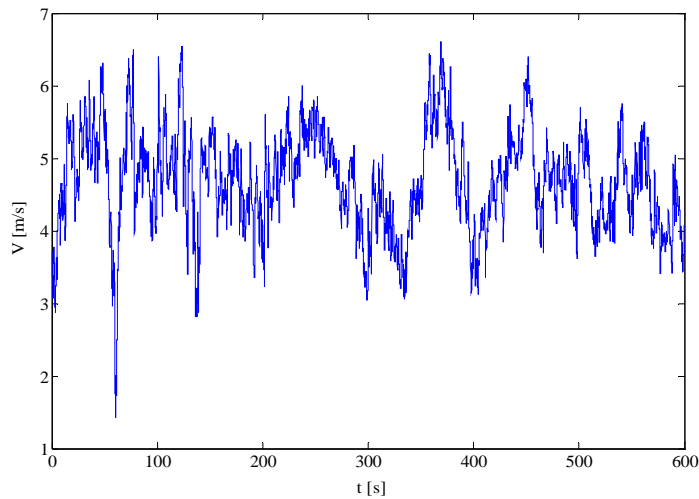


Figure 4.22 Measured wind velocity

The values of the aerodynamic coefficients considered are those for a wind flow horizontal and perpendicular to the bridge axis (nil onflow angle); this represents also the worse condition for the structure. So from the measured wind velocity V the perpendicular component to the bridge axis V_N is calculated as showed in Figure 4.23.

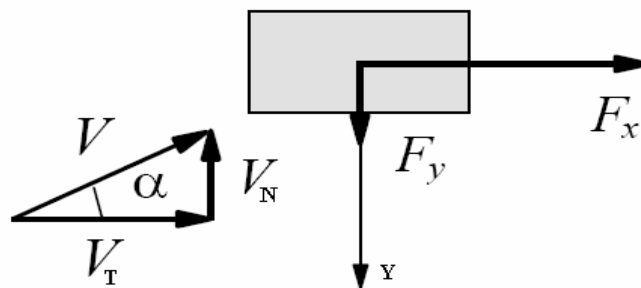


Figure 4.23 Normal component of the wind velocity.

The measured wind velocity together with the calculated normal component are represented in Figure 4.24.

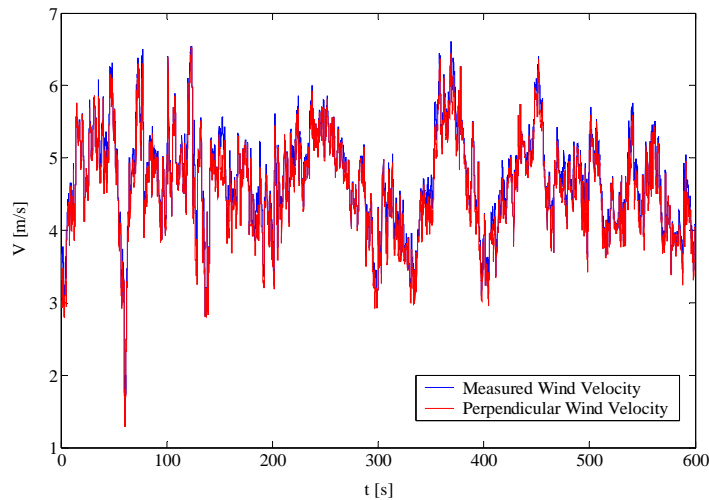


Figure 4.24 Perpendicular and measured wind velocity.

The wind data from in situ measurements concerns easterly and westerly winds; the westerly winds represent the prevalent winds measured at the bridge site and simply comparing one of their wind velocity histories with that taken as reference from the opposite direction a relevant difference between their fluctuations around the mean values can be observed (Figure 4.25). The mentioned difference and the choice to take as reference an easterly wind velocity history can be explained considering the position of the anemometer and the problems connected with it. The anemometer is placed on east side of the bridge deck close to the structure and in correspondence of the pier, on the Swedish side of the bridge, closest to the arch (Figure 4.27). The measurements are certainly affected by the presence of the structure for both the mentioned directions but it is reasonable suppose that the easterly winds can be measured with less disturbances. A westerly wind has to cross the whole section of the bridge and can separate a turbulent wake from the windward side of the structure with a consequent increasing disturbance on the measurements; the different turbulence content of the two wind velocity histories can be appreciated also observing their PSD functions. The direction of the wind forces applied on the model is from west to east and this choice reflects the provenience of the prevalent winds; anyway the application of the actions from the opposite side couldn't give a

different response of the structure due to its symmetry. Finally it has to be noted the anomaly in the position of the accelerometers placed on the west side of the bridge deck compared with the mentioned position of the anemometer on the opposite side.

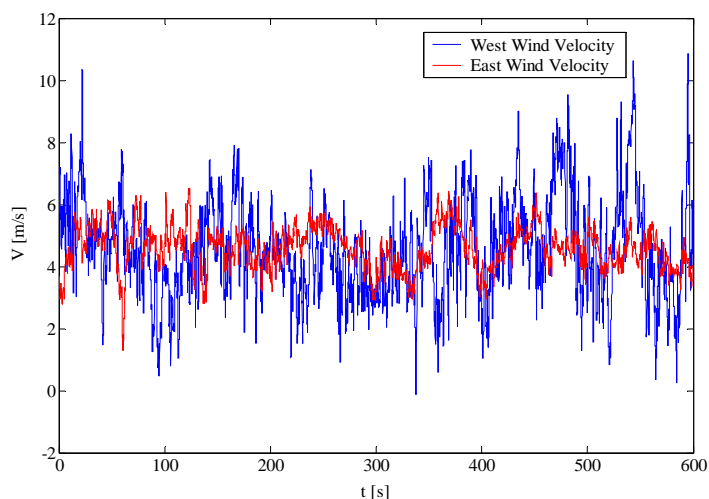


Figure 4.25 West and east wind velocity histories.

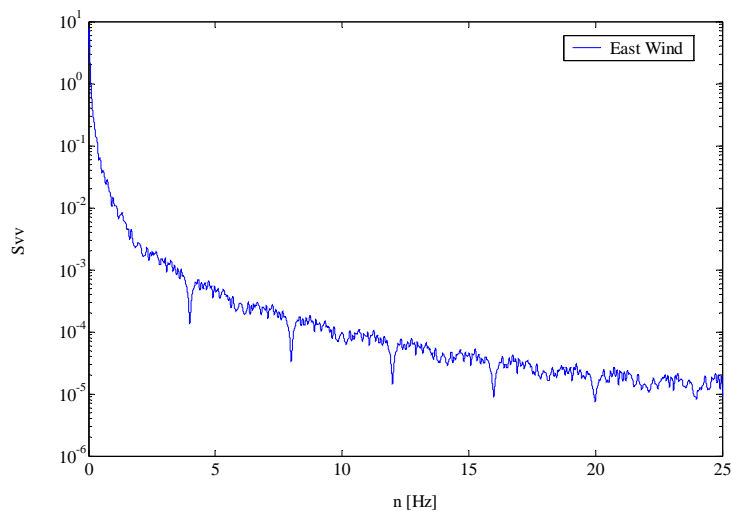


Figure 4.26 PSD of the measured east wind velocity.

Some pointing down peaks can be noted in the PSD of the measured wind velocity; it is believed that they could be related with the modes of vibration of the mast on which the anemometer is installed (Figure 4.26).

In the Figure 4.28 the PSD of the east and west velocity histories are compared and the mentioned relevant difference in the turbulent content of the two registrations can be pointed out.

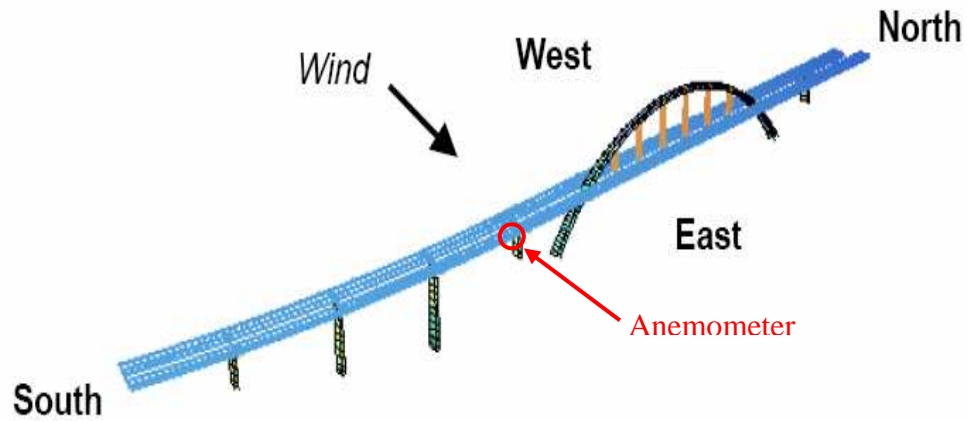


Figure 4 27 Direction of the prevalent winds and position of the anemometer.

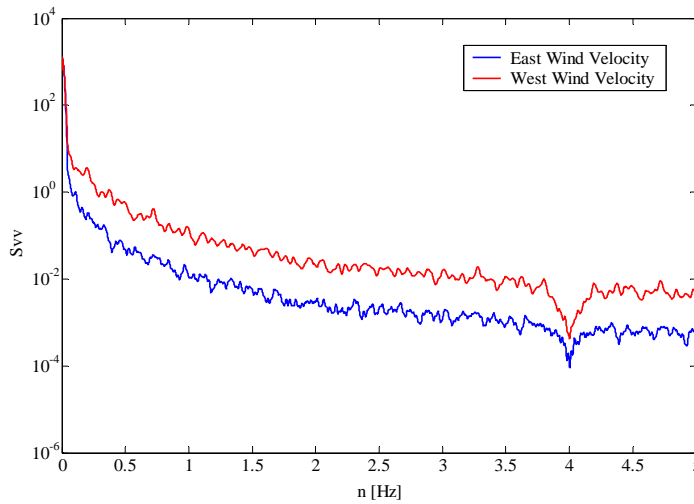


Figure 4.28 Comparison between the PSD of westerly and easterly wind velocities.

Before begin to consider in detail the analyses carried out and the related results it is necessary to go back to a simplification assumed in all the simulations carried out; the wind forces are applied only on the arch and the central part of the bridge deck included between the first two piers from the arch. This assumption can be regarded as suitable and

reliable considering that the response of the structure to the along-wind actions is concentrated on the first horizontal mode of vibration. As it will be seen studying the influence on the resultant response of the number of nodes at which the wind actions are applied, it can be supposed that still the second horizontal mode of vibration has a weight on the response of the structure. The same conclusion can be made analysing the PSD of the horizontal measured accelerations. However both the first two horizontal modes interest only the central part of the bridge on which the wind actions are applied. Moreover it has to be noted as this simplification aids to decrease the computational effort taken by the analysis and allows obtaining a response comparable to the measurements.

4.5 Analysis with correlated forces

For the first analyses the measured wind velocity is transferred by the along-wind forces on the whole structure in such a way that the peaks of velocity and the related pressures at difference points are simultaneously and so the forces result completely correlated. This kind of analysis can be considered as a first step in the study of the dynamic response of the bridge to wind actions; the expected response will be certainly not comparable and much bigger than the measured, however it permits a first quality evaluation of the structural response.

The forces are applied on a total number of 22 nodes, distributed 9 on the arch and 13 on the bridge deck. The average influence length for the points on the arch is 28 m and for the points on the bridge deck 25.5 m. The drag coefficient of the arch is assumed equal to 2 and for the bridge deck a value equal to 0.15 is deduced from the wind tunnel tests and it will be used in all the analyses which follow. The damping ratio is now evaluated by the Eurocode expression (4.17), adapted to the structure in the form exposed below. In this case both forces which take into account the quadric turbulence term (labelled as completed) and forces without this term (labelled as reduced) are calculated; this permits an evaluation of the difference between the two cases and it will follow the choice of retain this quadratic turbulence term.

4.5.1 Damping ratio from the Eurocode

The total damping ratio of the structure consists of a structural part ξ_s and an aerodynamic part ξ_a . For the structural damping ratio ξ_s a value of 1 % is chosen. The correspondent Rayleigh damping factors are evaluated by the expression (2.30) with frequencies $\omega_m = 2.7 [rad/s]$, $\omega_n = 12.5 [rad/s]$ and a structural damping ratio $\xi = 1\%$. The resultant coefficients are $a_0 = 0.044 [s^{-1}]$ and $a_1 = 0.0013 [s]$.

The aerodynamic damping ratio ξ_a is obtained from the formula proposed by the Eurocode, adapted to the bridge. The value is based on the first mode of vibration of the bridge along the wind direction.

$$\xi_a = \frac{C_{fd} l_d V_m(z_d) + C_{fa} l_a V_m(\bar{z}_a)}{2 n_1 m} = \frac{0.15 b_d l_d V_m(z_d) + 2 \bar{h}_a l_a V_m(\bar{z}_a)}{2 n_1 m} \quad (4.17)$$

where the terms of the expression are respectively:

$V_m(z_d)$, $V_m(\bar{z}_a)$ are the mean wind velocities at the bridge deck high of 60 [m] equal to 4.4 [m/s] and at a mean high of the arch of 69.5 [m] equal to 4.5 [m/s].

l_d , l_a are the length of the part of the bridge deck between the first two piers from the arch equal to 325 [m] and the length of the arch of about 300 [m].

b_d , \bar{h}_a are the width of the bridge deck equal to 28 [m] and the mean high, from the abutments to the crown, of the rectangular section of the arch equal to 3.45 [m].

n_1 is the frequency of the first mode of vibration of 0.4 [Hz].

m is the participant mass to the first mode of vibration equal to 4.32348E+06 [Kg] (see Table 4.3)

The estimated value for the aerodynamic damping is equal to 0.44%. Considering the two different contributes, a total value of 1.44% can be assumed in the analysis. The two Rayleigh damping factors a_0 and a_1 can be calculated by the expression (2.30) with frequencies $\omega_m = 2.7 [rad/s]$, $\omega_n = 12.5 [rad/s]$ and a total damping ratio $\xi = 1.44\%$. The resultant coefficients are $a_0 = 0.064 [s^{-1}]$ and $a_1 = 0.0019 [s]$.

In the table 4.6 there is a summary of the Rayleigh damping factors obtained assuming a structural and a structural plus aerodynamic damping ratio; in Figure 4.29 then the corresponding Rayleigh damping curves are compared.

Damping	$a_0 [s^{-1}]$	$a_1 [s]$
Structural	0.044	0.0013
Structural + Aerodynamic	0.064	0.0019

Table 4.6 Summary of the Rayleigh damping factors estimated.

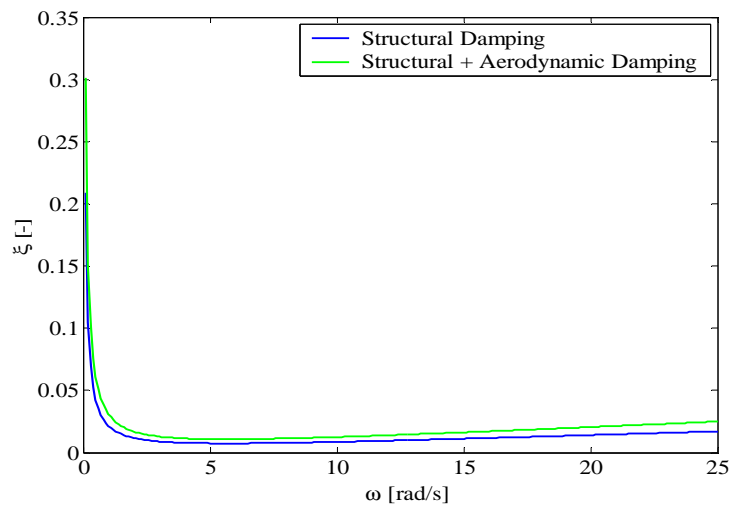


Figure 4.29 Rayleigh damping curves.

4.5.2 Filtering

Filtering is often used to minimize high frequency signals (noise) in order to make the primary pulse more readable. Filtering can attenuate the unimportant parts of the signal, but it can also be misapplied if the signal is over-filtered. This will lead to a distortion of the data, which normally reduces the signal peak amplitude. To prevent over filtering, the filter frequency should be at least five times greater than the highest frequency of interest. The most common type of filter is a low-pass filter, which attenuates the high frequency signals while the low frequency signals are unmodified. Another common type of filter is a

band-pass filter which attenuates signals with frequencies that are not within a specified interval. Filters can be either mechanical or applied digitally. Mechanical (analogue) filters are used when measuring the signal, while digital filtering only is possible when the signal has been digitalised, such as with PC-based instrumentation systems.

Digital filtering is accomplished in three main steps. First the signal has to be Fourier transformed and then the signals amplitude in frequency domain should be multiplied by the desired frequency response function. Finally the transferred signal must be inversely Fourier transformed back into time domain. The advantage with a digital filter is that it does not introduce any phase errors and that the original unfiltered signal can be stored. It was decided to filter the measured acceleration signals in the frequency domain by a low-pass filter in order to cancel the high frequency contents, which could be associated for example with the traffic vehicle, and so compare the measured filtered response with numerical results.

The filter used is represented by a co-sinusoidal function applied to the FFT of the measured acceleration signal; this filter operates retaining the frequency content below the 5 [Hz] and cancelling the higher frequency content as showed in the Figure 4.30-4.31 for the horizontal acceleration measured at the midpoint of the arch. The choice of this filter frequency seems to be reasonable permitting to keep the principal frequency content of the signal; furthermore the deleted components show to have not a relevant effect on the measured displacement (Figure 4.33). This last signal can be extracted from the measured acceleration working in the frequency domain dividing two times for $i\omega$ the FFT of the acceleration and obtaining respectively the FFT of the velocity and the FFT of the displacement. The last step is to apply the IFFT to the FFT of the displacement getting the displacement in the time domain.

The same procedure exposed will be carried out to extract the displacements from the accelerations obtained through the simulation which will follow.

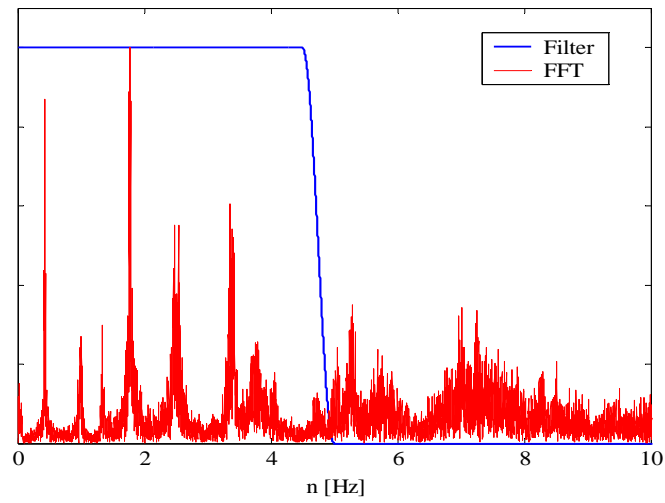


Figure 4.30 Filter applied to the FFT of the measured acceleration.

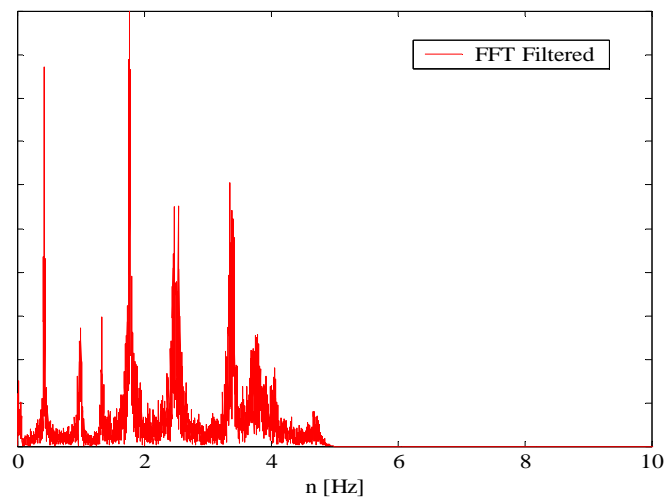


Figure 4.31 FFT after filtering.

Comparing the measured and filtered horizontal acceleration at the midpoint of the arch in the time domain the effect of the applied filtering can be clearly appreciated.

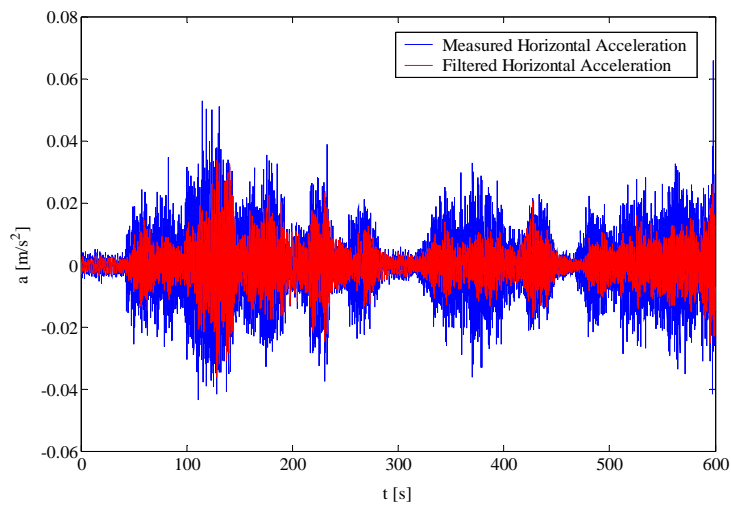


Figure 4.32 Measured and filtered acceleration time histories.

Looking the Figure 4.32 it possible to see the significant difference in the measured acceleration response after filtering; this can be explained considering that the measurement is carried out during the operating time of the structure when it results excited by other relevant sources. The same difference cannot be appreciated by the displacement time history, even if the mean maximum value extracted from its fluctuating component will show a not negligible difference compared with that extracted from the original measured signal.; the procedure in order to extract this value will be exposed laer.

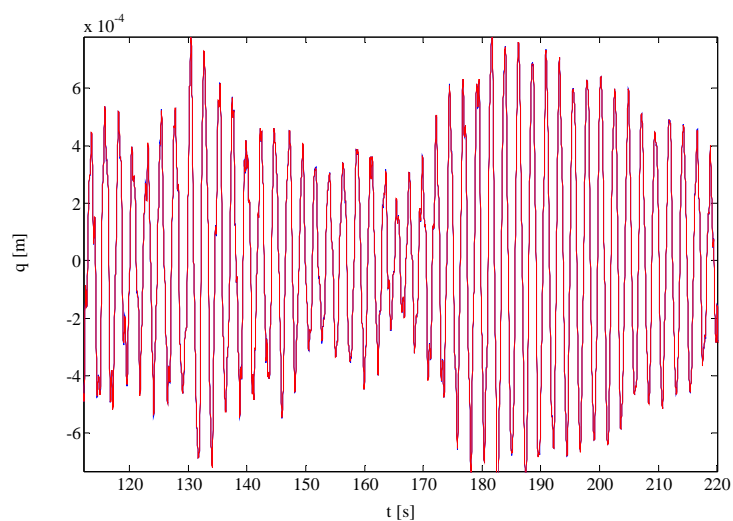


Figure 4.33 Measured and filtered displacement time histories.

In the Table 4.7 the mean maximum values of the measured displacement before and after filtering are shown.

	Center Arch	Quarter Arch	Center Deck	Quarter Deck
Measured [mm]	2.07	1.01	0.75	0.57
Filtered [mm]	1.46	0.71	0.53	0.4

Table 4.7 Mean maximum displacement measured and filtered.

4.5.3 Determination of the roughness length

The roughness length can be approximated by a fitting procedure. This parameter is certainly affected by a large uncertainty which propagates on the one hand on the mean wind velocity and on the other on the turbulence intensity (4.14). The PSD of the measured wind velocity is compared with the spectral model proposed by the Eurocode for the longitudinal turbulence (4.10) and the value estimated for the roughness length is that makes the best fitting between the two spectra; this value results equal to 0.1 [m] and it is taken as the reference value for the rest of the analysis.

However simulations will be made for other two roughness lengths one lower and one higher, respectively equal to 0.05 and 0.15 [m]. The response will show to be not so influenced by the variation of this parameter.

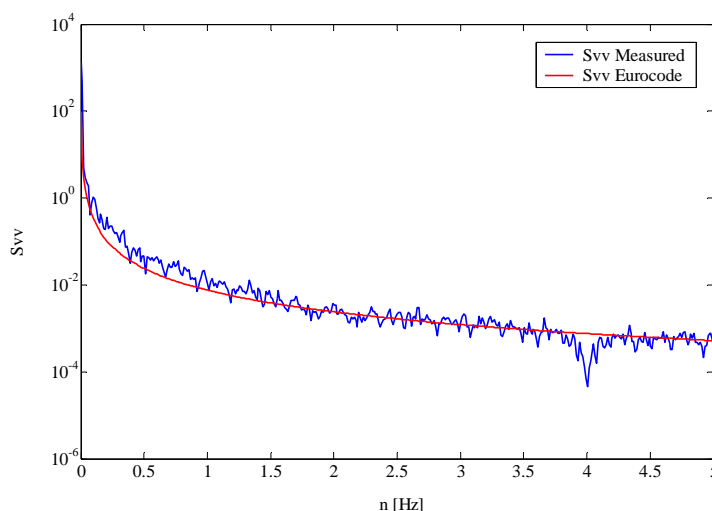


Figure 4.34 Fitting of the PSD of the measured wind velocity.

4.5.4 Results

At first the responses between the analyses with completed and reduced forces are examined. The acceleration and displacement at the central section of the arch are represented in Figure 4.35-4.36.

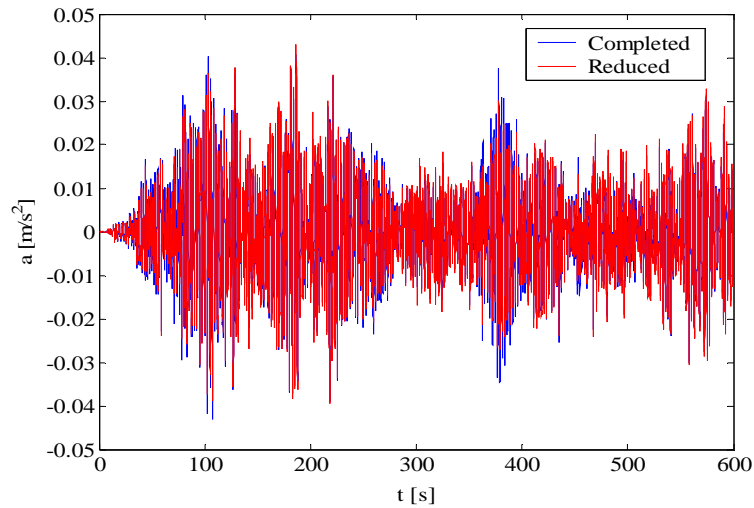


Figure 4.35 Acceleration at the midpoint of the arch.

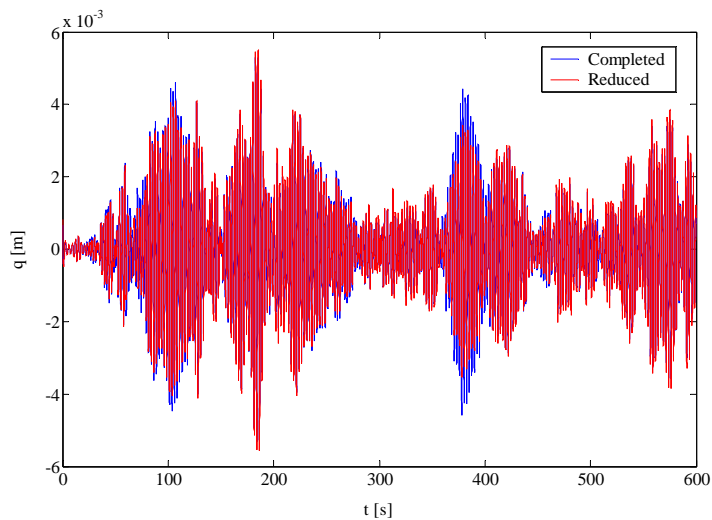


Figure 4.36 Displacement at the midpoint of arch.

It can be noted that the application of the reduced forces, which do not take into account of the quadratic turbulence term, mitigate some evident peaks of the acceleration; anyway the

application of the two different types of forces doesn't give substantial differences on the final results and it is chosen to carry on in the analyses considering the results from the models with completed forces and comparing these results with the measurements. In the following figures the acceleration time histories from the model and from the measurements are represented for all the four section considered.

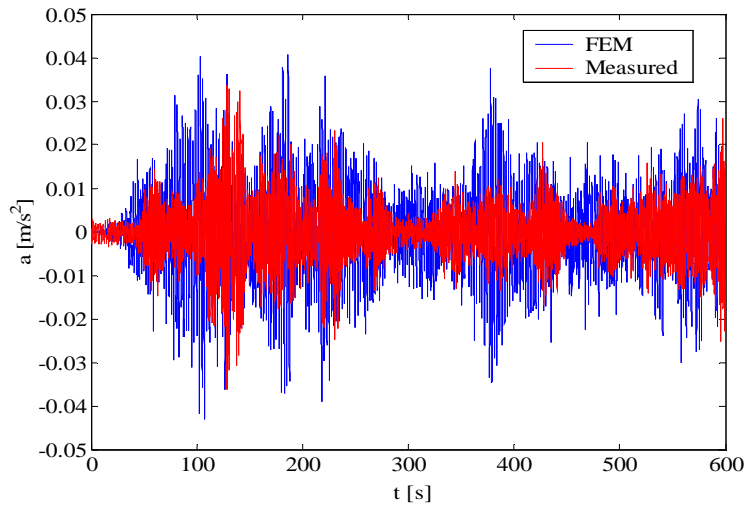


Figure 4.37 Acceleration at the midpoint of the arch.

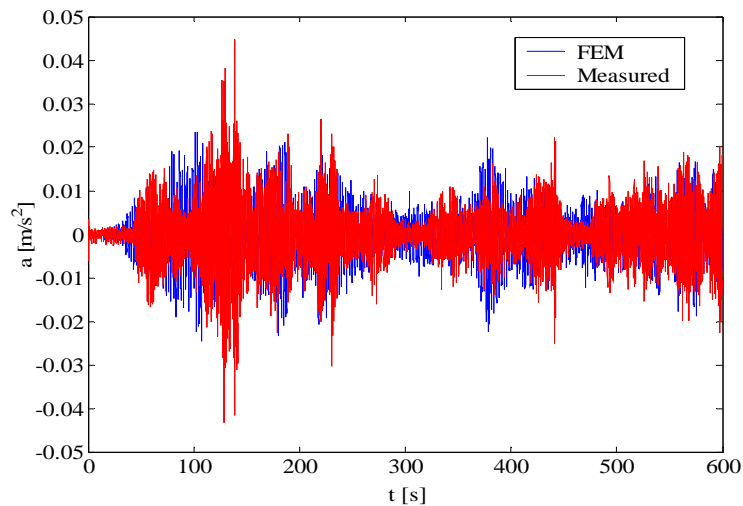


Figure 4.38 Acceleration at the quarter point of the arch.

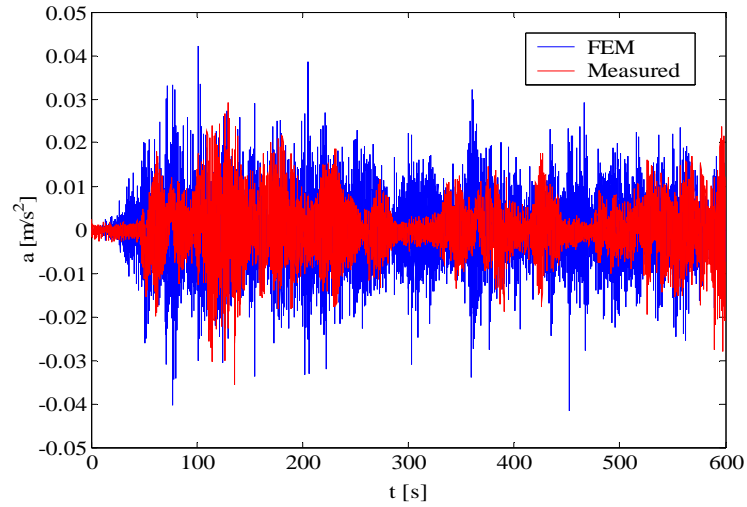


Figure 4.39 Acceleration at the midpoint of the bridge deck.

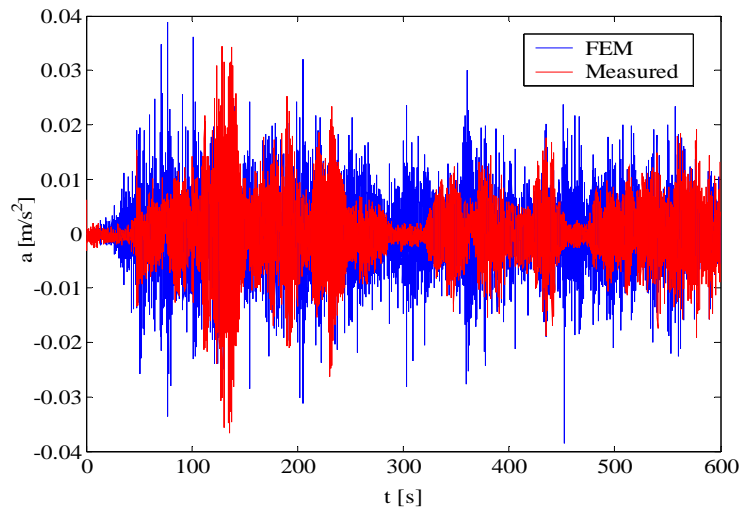


Figure 4.40 Acceleration at the quarter point of the bridge deck.

The same comparison can be made also considering the time history of the displacement for example taking into account the central section of the arch. It can be noted how the difference, between measured and numerical results in terms of displacement, is much larger than for the corresponding accelerations and generally not comparable (Figure 4.41).

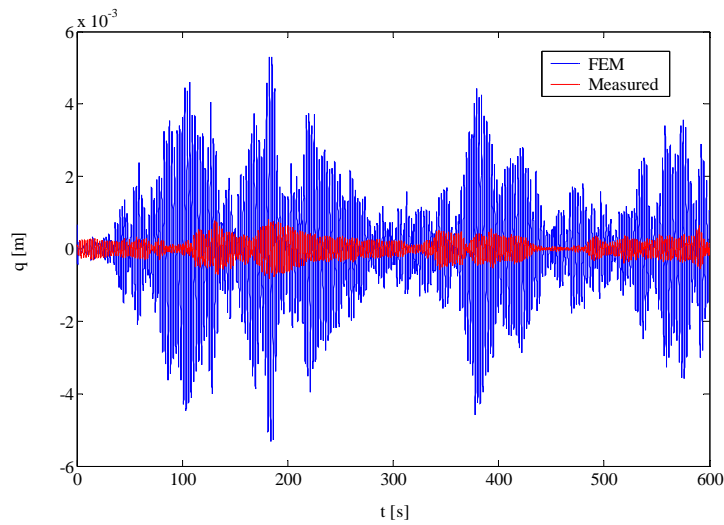


Figure 4.41 Displacement at the midpoint of the arch.

4.6 Numerical simulation of wind velocity histories along the bridge

Simulation of the longitudinal turbulence components consists of some basic steps. At first the reference mean velocity is assumed equal to 4.5 [m/s], which is the mean value of the measured history; the mean wind velocity at the different points of the structure is defined by a logarithmic profile (4.18) assuming the previous reference mean velocity and a roughness length approximated taking into account the characteristics of the bridge site and the result of the fitting procedure described before. The mean wind velocity is defined by a vector of n components with each component V_{mi} representing the mean wind velocity at i -th node of the FE model.

$$V_{mi}(z_i) = \frac{1}{\chi} u_* \ln \left(\frac{z_i}{z_0} \right) \quad (4.18)$$

In the expression above z_i is the height of the i -th node of the FE model and the other terms were specified at (2.32).

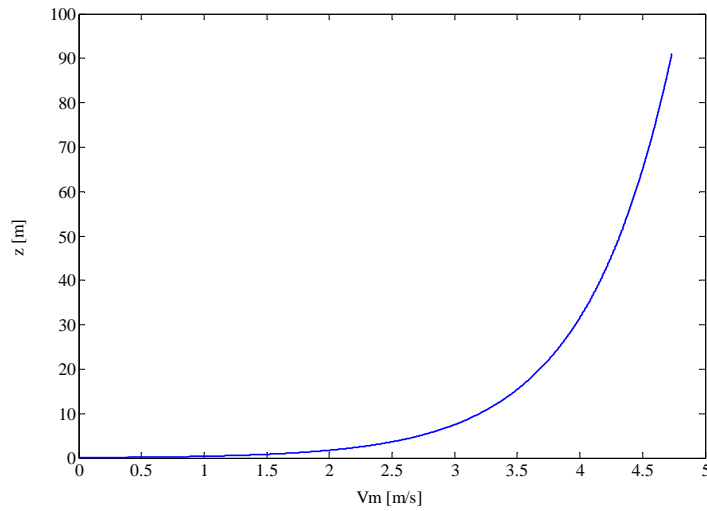


Figure 4.42 The assumed mean wind velocity profile.

The length in the time domain of each simulation is of 600 [s] (ten minutes) with a time increment Δt of 0.2 [s] corresponding to a sample frequency of 50 [Hz]; the number of frequency points at which the spectral functions are calculated is chosen equal to 1000. The cross power density functions are obtained defining the power density functions of the turbulence component at each point (4.10) and the coherence function between turbulence components at different points (4.16). For decay coefficients taken equal to 10 (Table 4.5) and considering the fifth frequency step, the coherence function between the longitudinal turbulence components at ninth eight points assumes the form showed in Figure 4.43.

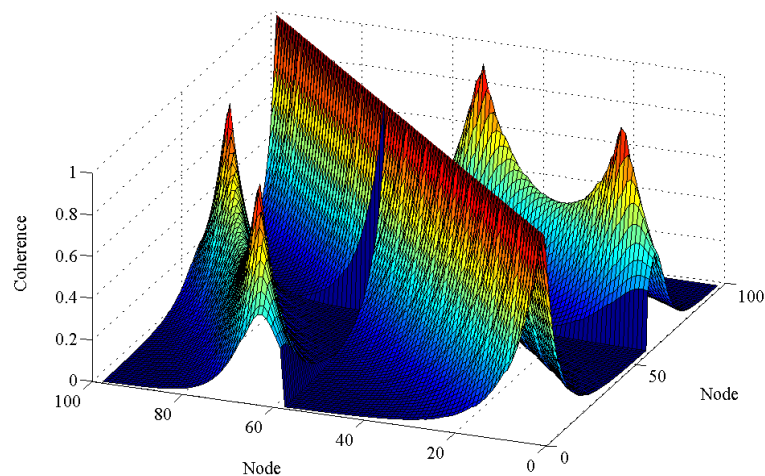


Figure 4.43 Coherence function for 98 nodes and decay coefficients equal to 10.

The power spectral density functions are based on the Eurocode model. Once defined these functions the spectral density matrix can be built and the Cholesky matrix decomposition can be applied on it. The turbulence components at each point are generated by the superimposition of harmonics functions with a random phase.

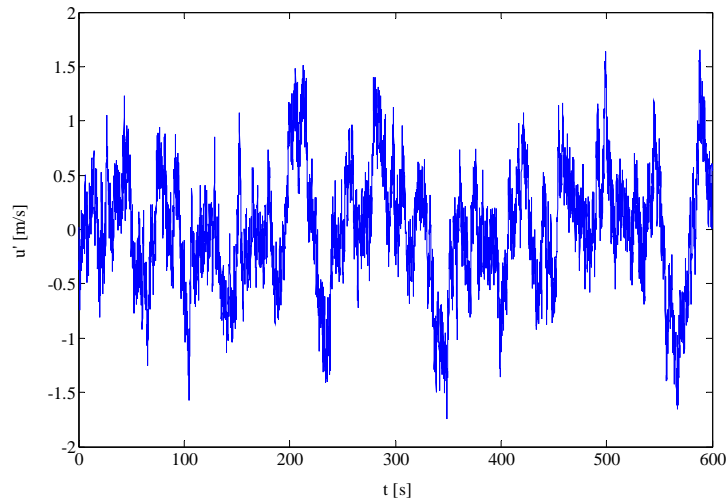


Figure 4.44 Simulated longitudinal turbulence at the midpoint of the arch.

Finally the reference mean wind velocity is added to the turbulence component in order to get the resultant velocity history.

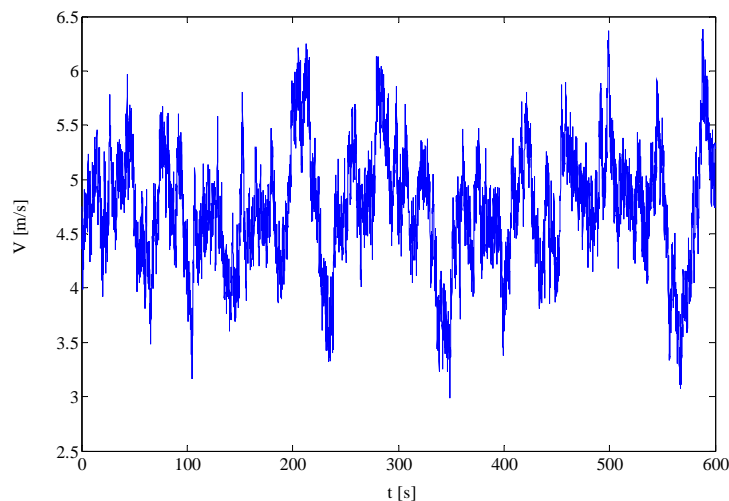


Figure 4.45 Simulated wind velocity at the midpoint of the arch.

The reliability of the simulated wind velocities can be checked comparing their standard deviation with that from the measured velocity and their PSD functions with the spectral model proposed by the Eurocode and the PSD function of the reference wind velocity from the measurements (see Figure 4.46-4.47).

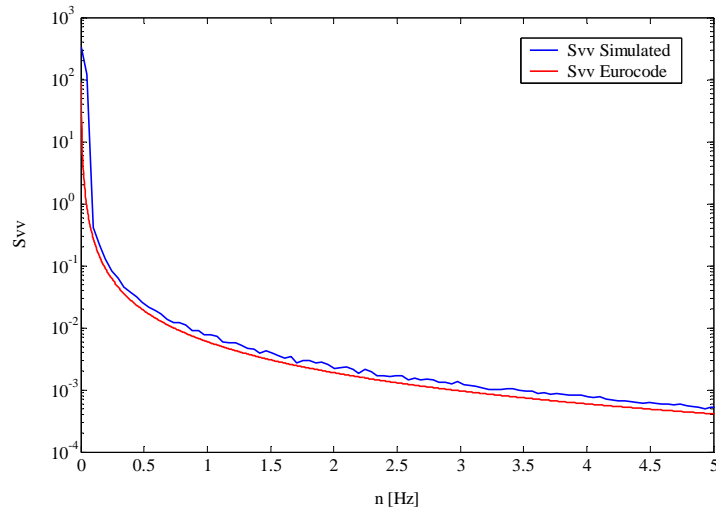


Figure 4.46 Comparison with the Eurocode spectrum.

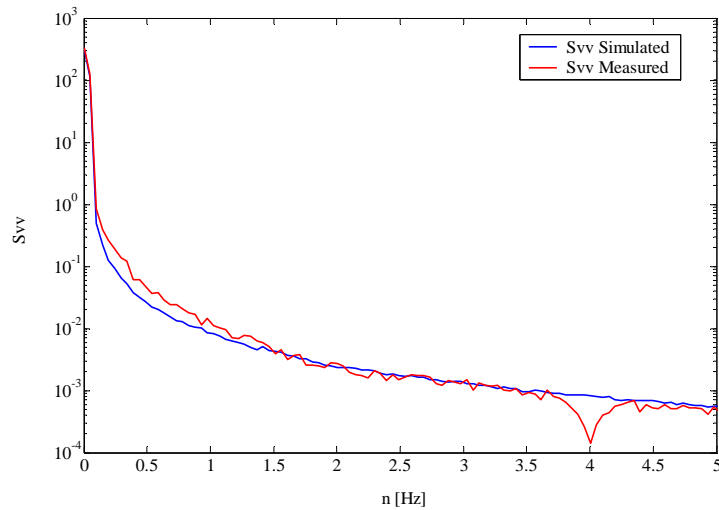


Figure 4.47 Comparison with the measured spectrum.

4.7 Evaluation of the measured damping ratio

The FE model can be now updated by a new value of the damping ratio. The Rayleigh damping parameters a_0 and a_1 are evaluated finding the curve of the damping ratio versus the natural circular frequency ω that better fits the damping ratios in correspondence of five selected frequencies (Figure 4.48). For each frequency the damping ratio is calculated applying the Band-width method at the peaks of the PSD functions of the measured accelerations. The first three frequencies chosen represent the first three horizontal natural frequencies of the structure and the other two represent the fifth and seventh measured natural frequencies, corresponding to torsion-bending modes.

Mode Number	n [Hz]	ω [rad/s]	ξ [-]
1	0.43	2.68	0.0174
3	0.95	5.94	0.0087
4	1.01	6.35	0.0101
5	1.33	8.37	0.00675
7	1.78	11.16	0.0045

Table 4.8 The natural frequencies considered and the corresponding damping ratios estimated.

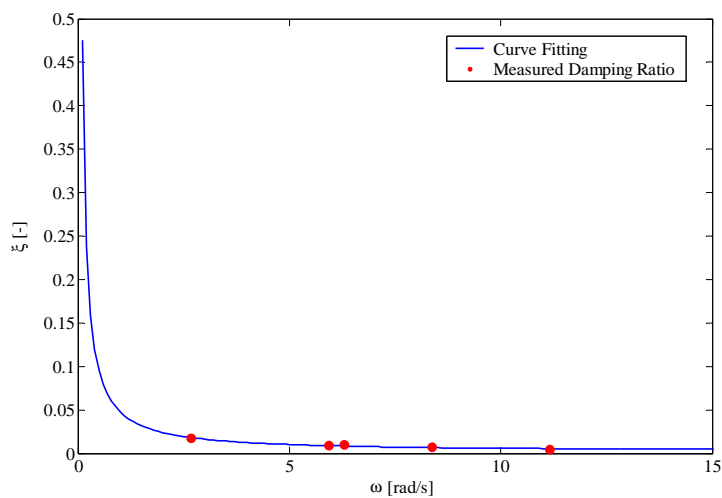


Figure 4.48 Fitting of the measured damping ratios.

The Rayleigh damping factors found by this fitting procedure are $a_0 = 0.095101 [s^{-1}]$, $a_1 = 0.00022334 [s]$.

In Figure 4.49 the Rayleigh damping curve of the measured damping ratio is compared with those correspondent to the structural damping ratio and the structural plus the aerodynamic damping ratio.

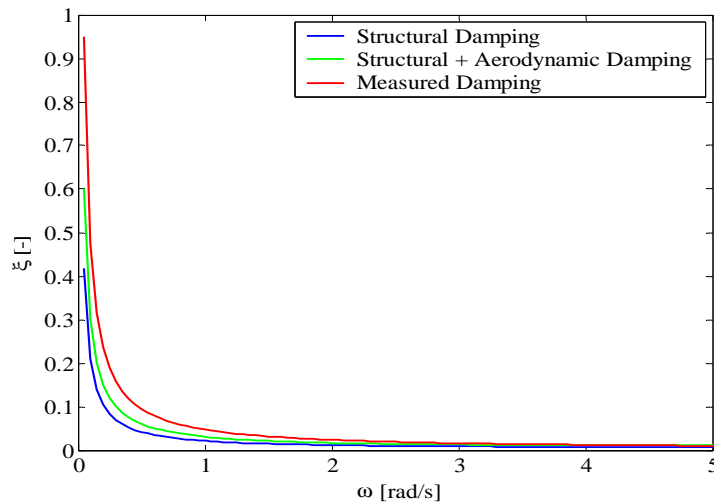


Figure 4.49 Rayleigh damping curves.

Table 4.9 finally shows a summary of the values for all the Rayleigh damping factors obtained.

Damping	$a_0 [s^{-1}]$	$a_1 [s]$
Structural	0.044	0.0013
Structural + Aerodynamic	0.064	0.0019
Measured	0.095	0.00022

Table 4.9 Summary of the Rayleigh damping factors.

4.8 Distribution of the maximum displacement

The results from the numerical simulations and from the measurements have to be compared in statistical terms; so the mean maximum of the fluctuating part of the displacement and its standard deviation are evaluated from the measured and numerical accelerations. In order to extract the fluctuating displacement from the acceleration signals it is necessary to work in the frequency domain following the procedure exposed at 4.5.2. Once obtained the velocity and displacement functions their standard deviations can be calculated through the integration of their spectra.

As the wind action the structural response can be modelled by a Gaussian process and so an expected frequency of the process can be defined as:

$$v_{\dot{\varrho}} = \frac{1}{2\pi} \frac{\sigma_{\dot{\varrho}}}{\sigma_{\varrho}} \quad (4.19)$$

where σ_{ϱ} and $\sigma_{\dot{\varrho}}$ are respectively the standard deviations of the displacement and of the velocity of the structure; this frequency represents the mean number of crossings of the time axis carried out by the displacement function. The mean value of the maximum displacement can be obtained by the closed formula:

$$\mu_{\dot{\varrho}} \cong \sigma_{\varrho} \left[\sqrt{2 \ln(v_{\dot{\varrho}} T)} + \frac{0.5772}{\sqrt{2 \ln(v_{\dot{\varrho}} T)}} \right] \quad (4.20)$$

where the second term of the previous product is a non-dimensional factor known as peak coefficient. The standard deviation of the maximum displacement is given by:

$$\sigma_{\dot{\varrho}} \cong \sigma_{\varrho} \left[\frac{\pi}{\sqrt{6}} \frac{1}{\sqrt{2 \ln(v_{\dot{\varrho}} T)}} \right] \quad (4.21)$$

Once obtained the mean and standard deviation of the maximum displacement its Gaussian distribution results completely defined (see Figure 4.50).

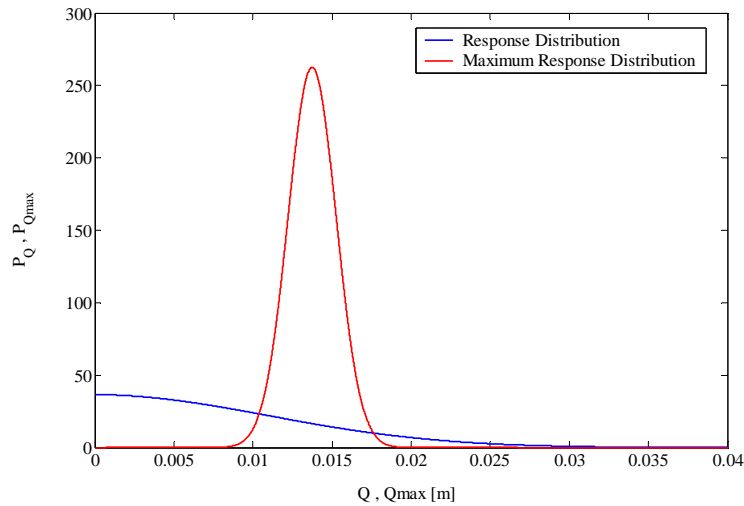


Figure 4.50 Response and maximum Gaussian response distribution.

As $v_Q T$ increases the density function of the maximum tends to translate on the time axis, cause the maximum displacement increases, and the density function becomes progressively more narrow and pointed; so when $v_Q T$ is high, as in the case of wind with an assumed time period T equal to 600 [s], the maximum displacement could be treated in first approximation as a deterministic variable.

4.9 Study of a simplified beam model

A preliminary study of the wind effects induced on a simplified beam model is now introduced in order to point out the influence of some relevant parameters involved in the simulations. This model concerns a beam, double fixed at its ends and subjected to wind forces acting perpendicularly to its longitudinal axis as shown in Figure 4.51. The influence of two parameters on the maximum displacement of the beam is studied: on one hand the number of applied concentrated forces which then coincides for the model considered with its number of degrees of freedom; on the other the coherence of the applied forces that it is the same of the longitudinal simulated turbulence components.

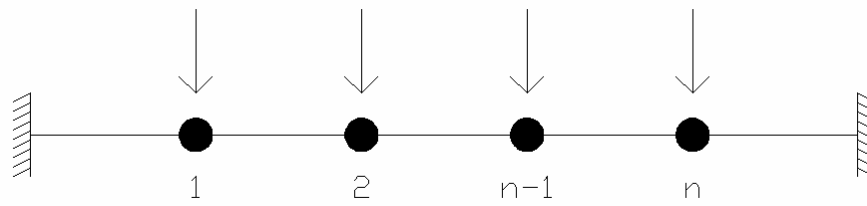


Figure 4.51 Beam model.

These two parameters are chosen cause they show to be together with the aerodynamic static coefficients the most influent on the final structural response. This simulation is carried out through the Matlab simulink and it is made up of the following steps: definition of the model properties and extraction of its eigenfrequencies and eigenvalues; simulation of the longitudinal wind velocities at a varying number of nodes along the structure; application of the aerodynamic forces, integration of the equations of motion and extraction of the results.

The beam is discretised in an increasing number of elements of length L_i and its mass matrix is defined by a real, defined positive, diagonal (or lumped) mass matrix. An easy way to obtain a lumped mass matrix is to replace the distributed mass m of the beam by particles of mass $m_i = \rho A L_i$ at each node, where ρ is the material density and A is the section area of the beam. The rotational inertia can be defined by considering that a uniform slender bar of length L_i and mass $m_i = \rho A L_i$ is attached at each node; the associate inertia moment is $J = (\rho A L_i) L_i^2 / 3$. The advantage of operate through a diagonal matrix is on one hand the less storage space and on the other the less processing time needed, especially taking into account the direct time integration procedure that is applied. The stiffness matrix for each double clamped beam element is given by:

$$k_e = E J \begin{bmatrix} 12/L_i^3 & 6/L_i^2 & -12/L_i^3 & 6/L_i^2 \\ 6/L_i^2 & 4/L_i & -6/L_i^2 & 2/L_i \\ -12/L_i^3 & -6/L_i^2 & 12/L_i^3 & -6/L_i^2 \\ 6/L_i^2 & 2/L_i & -6/L_i^2 & 4/L_i \end{bmatrix} \quad (4.22)$$

The next step is to assembly the stiffness matrices of each element to get the stiffness matrix of the entire beam that it results to be a real, symmetric, defined positive and three-diagonal matrix. Then in order to decrease the number of degrees of freedom of the problem a condensation procedure is carried out by writing the classical eingevalue problem for an n-degrees of system in a portioning form as:

$$\begin{bmatrix} \mathbf{K}_{tt} & \mathbf{K}_{tr} \\ \mathbf{K}_{rt} & \mathbf{K}_{rr} \end{bmatrix} - \omega^2 \begin{bmatrix} \mathbf{M}_{tt} & \mathbf{0} \\ \mathbf{0} & \mathbf{M}_{rr} \end{bmatrix} \begin{Bmatrix} \Psi_t \\ \Psi_r \end{Bmatrix} = \begin{Bmatrix} \mathbf{0} \\ \mathbf{0} \end{Bmatrix} \quad (4.23)$$

where the terms with the index t correspond to translational degrees of freedom and those with index r to rotational degrees of freedom. The rotational inertia moments in the mass matrix usually are very small and can be neglected, so the eigenvalue condensate problem results as:

$$(\mathbf{K}_{tt}^* - \omega^2 \mathbf{M}_{tt}) \Psi_t = \mathbf{0} \quad (4.24)$$

where the dimension of the problem is reduced to the only translational components of the eigenmodes and the matrix \mathbf{K}_{tt}^* is a real symmetric matrix as \mathbf{M}_{tt} given by:

$$\mathbf{K}_{tt}^* = \mathbf{K}_{tt} - \mathbf{K}_{tr} \mathbf{K}_{rr}^{-1} \mathbf{K}_{rt} \quad (4.25)$$

Once defined the mass and the stiffness matrices the eigenvalues and eigenmodes of the beam can be extracted.

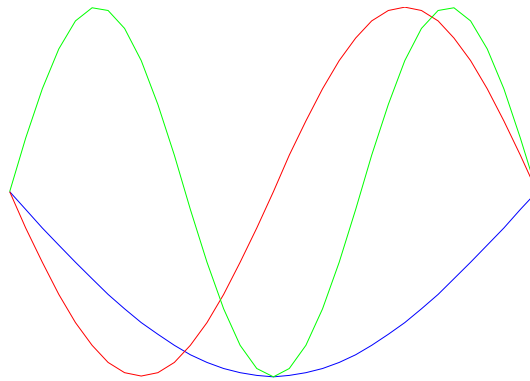


Figure 4.52 The first three eigenmodes of the beam.

The last matrix to determine is the stiffness matrix; this matrix is not derived by the beam discretisation but it can be defined by the Rayleigh damping relation on the base of the mass and stiffness matrices determined. Finally before carry out the integration of the equations of motion it is necessary to transform the equation of motion in the state space:

$$\dot{\mathbf{z}} = \mathbf{G} \mathbf{z} + \mathbf{p} \quad (4.26)$$

The expression above represents a system of $2n$ linear differential equations of the first order with:

$$\mathbf{z} = \begin{Bmatrix} \mathbf{u} \\ \dot{\mathbf{u}} \end{Bmatrix} \quad \mathbf{G} = \begin{bmatrix} \mathbf{0} & \mathbf{I} \\ -\mathbf{M}^{-1} \mathbf{K} & -\mathbf{M}^{-1} \mathbf{C} \end{bmatrix} \quad \mathbf{p} = \begin{Bmatrix} \mathbf{0} \\ \mathbf{M}^{-1} \mathbf{f} \end{Bmatrix} \quad (4.27)$$

and the initial condition:

$$\mathbf{z}(0) = \mathbf{z}_0 = \begin{Bmatrix} \mathbf{u}_0 \\ \dot{\mathbf{u}}_0 \end{Bmatrix} \quad (4.28)$$

Once defined the model and its dynamic characteristics, the longitudinal turbulence components are simulated following the procedure exposed at 4.6 and assuming the defined coherence function and spectral model.

Only one dimension is involved in the coherence function and it is that along the beam axis with the spatial distance between each node given by the length of the elements which discretise the beam. For each step in the increasing number of elements considered the decay coefficient C_{yu} of the coherence function varies from a value close to zero to values much bigger than those proposed in literature (see Table 4.5); this is made in order to get a generalized trend of the response with the variation of this parameter. Once simulated the turbulence histories the mean velocity is added and the resultant wind velocities at each node of the model are obtained. The aerodynamic drag forces along the wind direction are calculated imposing a drag coefficient equal to two for the rectangular section of the beam. For any of the discretisation steps the displacements are calculated varying the coherence between the forces applied on the beam.

The displacement taken as reference is that of the node closer to the midpoint of the beam; finally from the time history of displacement obtained the maximum distribution and the related mean maximum displacement are extracted. The results about the maximum displacements versus the number of degrees of freedom of the system and the values of the decay coefficient C_{yu} assumed for the coherence function are shown in Figure 4.53 by a 3D graph; then some sections of the 3D graph are represented in order to catch better the trend of the results obtained (Figure 4.54-4.55-4.56).

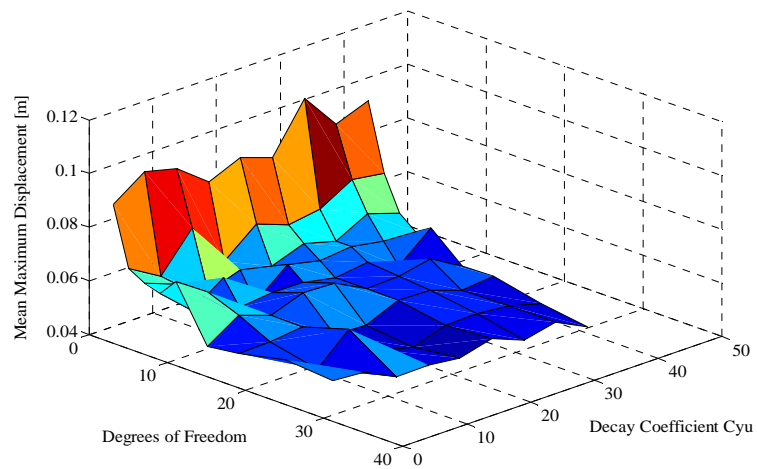


Figure 4.53 Mean maximum response.

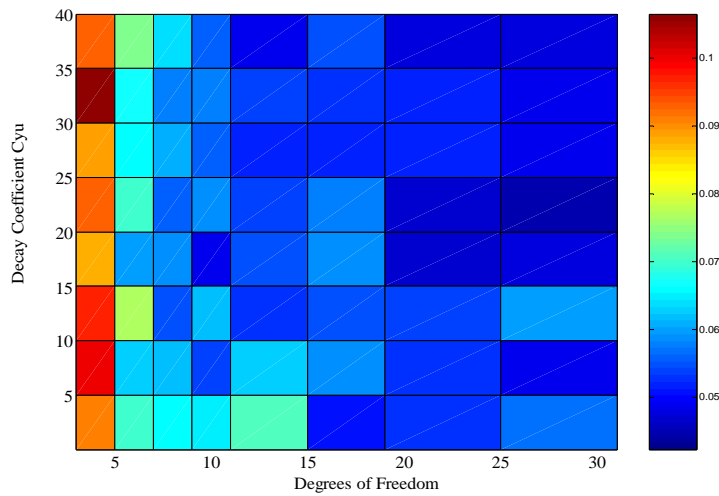


Figure 4.54 Planar view of the mean maximum response.

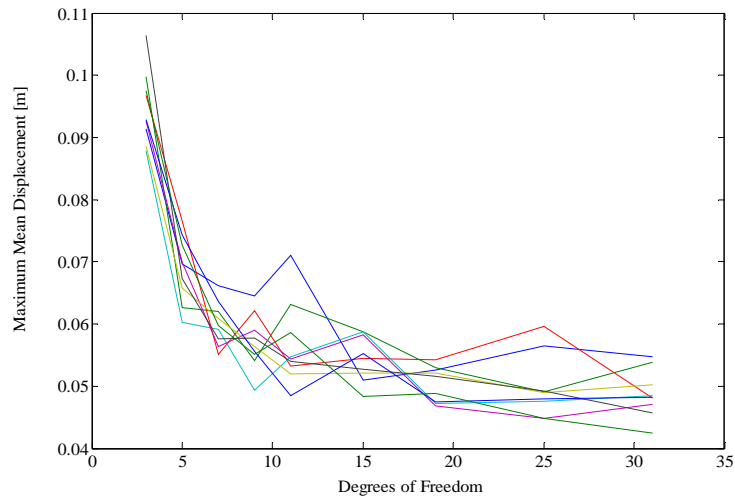


Figure 4.55 Mean maximum displacement varying the number of nodes.

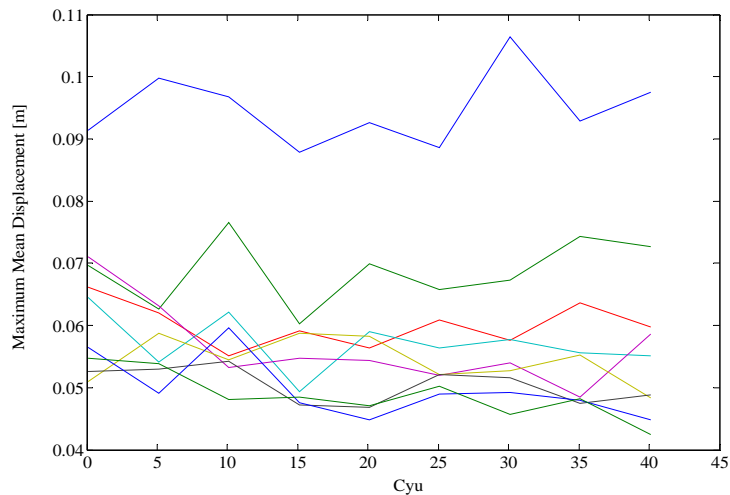


Figure 4.56 Mean maximum displacement varying the decay coefficient.

It can be noted from the results about the maximum displacement at midpoint of the beam that at the increasing number of degrees of freedom there is a convergence of the results. The same thing cannot be observed at the increasing value of the decay coefficient C_{yu} for which the forces become progressively less correlated and the resultant displacement shows a fluctuant trend.

4.10 Analysis of the results from the simulations

The results from the simulations carried out are now analysed. The time history response from the numerical simulation, in term of acceleration or displacement, cannot be directly compared with the time history obtained from the measurements as made before for the first analyses with correlated forces. The reason of this fact is that the measured response and any one simulation represent two processes completely uncorrelated; so the comparison can be made only in statistical terms, evaluating and comparing the mean maximum displacements from the simulations and the measurements. The values shown in the following tables represent, as specified before, the fluctuating part of the displacement evaluated at the four sections considered. The next paragraphs are organized in order to point out the influence of the parameters involved in the analysis showing the values of displacement obtained and the percentage difference from the measured results. The percentage difference is reported as an absolute value but in reality it should be negative cause the numerical response always underestimates the measurements.

4.10.1 Influence of the number of nodes

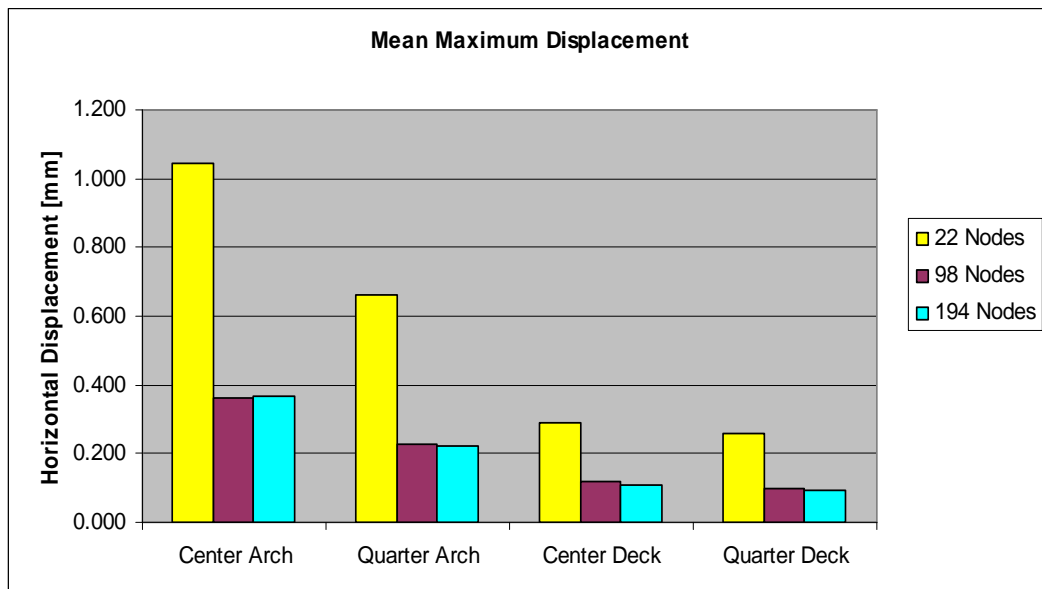


Figure 4.57 Mean maximum displacement varying the number of nodes.

Three configurations are studied respectively with 22, 98 and 194 applied concentrated

forces and the results regard the four considered sections of the structure.

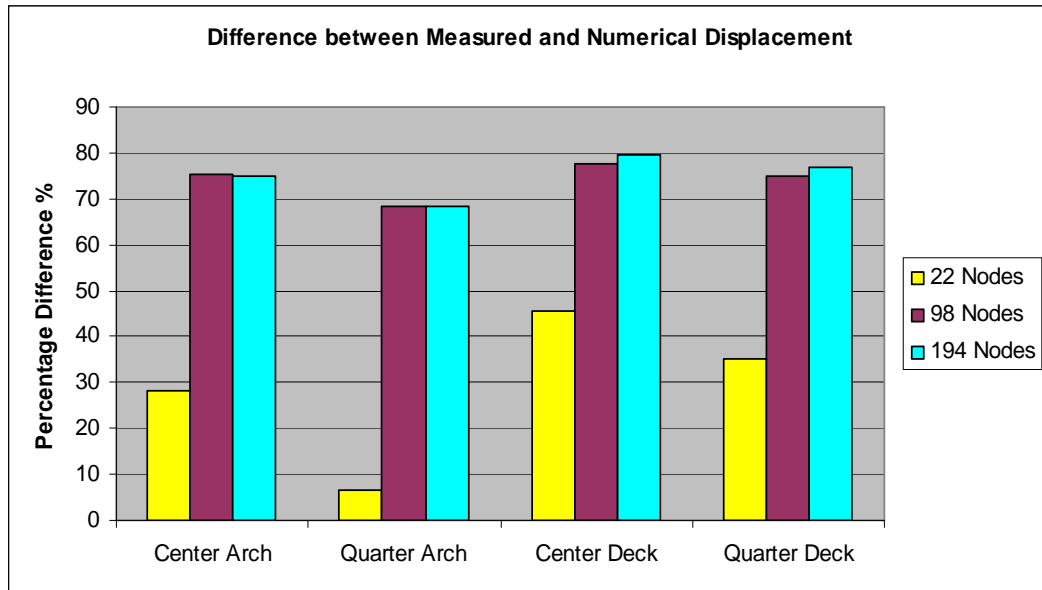


Figure 4.58 Percentage difference from the measurements.

As seen before from the analysis of the simplified beam model the number of nodes at which the forces are applied plays an important role on the final results. The decreasing value of the response at the increasing number of forces applied can be explained considering that for a lower number of forces each force acts on a larger influence length; this fact has the same effect as assuming perfectly correlated forces on this length. It can be noted that there is not a remarkable difference between the results of the models with 98 and 194 applied forces; so it can be considered to have found a convergence of the results at the varying number of nodes; the model with 98 forces will be the reference model in the next paragraphs where the influence of other parameters involved in the simulations will be considered. Moreover this model aids to decrease the CPU time needed for the analysis. The difference from the measurements varies, for the assumed configuration, between 70% and 80%.

4.10.2 Influence of the drag coefficient of the arch

Three different values for the drag coefficient of the arch are considered. The lower value equal to 1.73 results from the multiplication between a force coefficient equal to 1.9 and an

end-flow factor equal to 0.91 checked in the wind tunnel tests by comparing the mean wind response with the response calculated on a numerical model of the physical model. The second value considered equal to 1.86 is only a medium step between the previous value and 2; this last coefficient is an approximate value determined from Eurocode and ESDU.

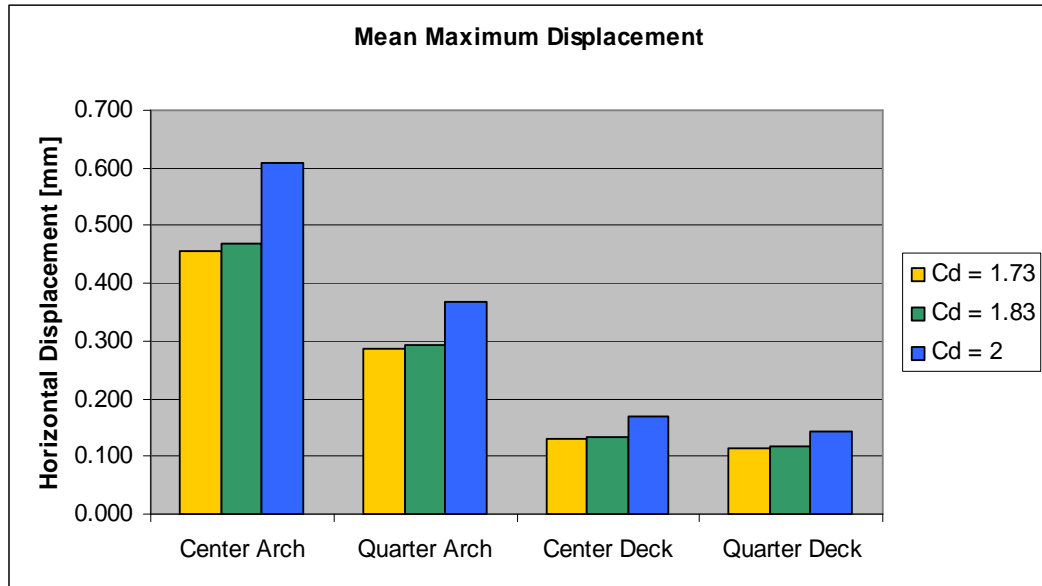


Figure 4.59 Mean maximum displacement varying the drag coefficient of the arch.

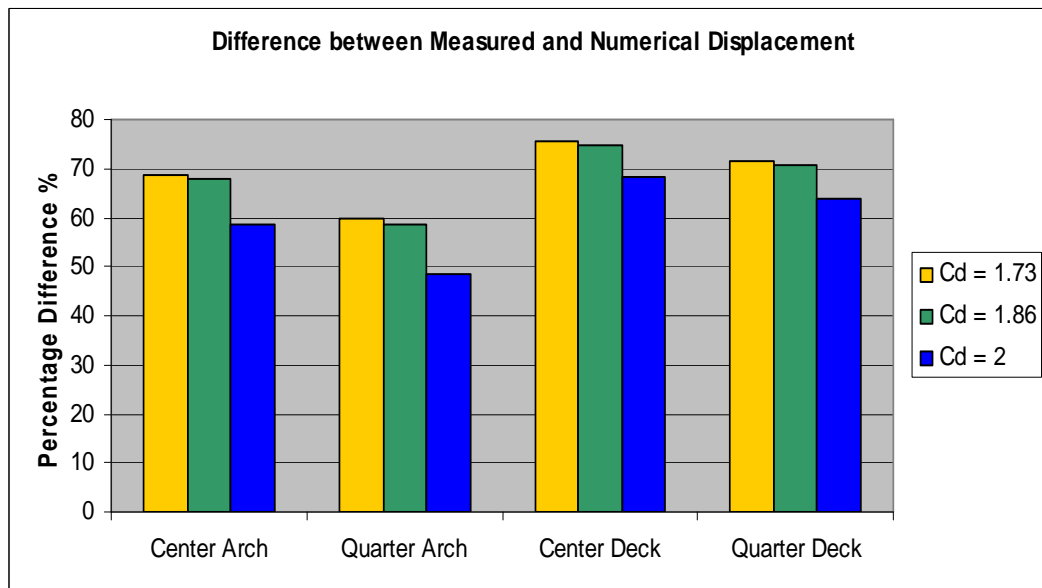


Figure 4.60 Percentage difference from the measurements.

The structural response, especially of the arch, shows to be largely influenced by this coefficient. As mentioned for this coefficient different values should be determined along the arch cause the inclination of each section varies with respect to the assumed horizontal perpendicular wind flow. In order to simplify this problem a constant value has to be assumed for the whole element. For the bridge deck instead the drag coefficient has a more precise value deduced from the wind tunnel tests. The difference from the measurements varies from 50% and to about 70%.

4.10.3 Influence of the coherence

A relevant weight, as seen before in the study of the beam model, has the coherence between the along-wind forces applied on the model. The decay coefficients of the longitudinal turbulence components along the x and z direction are varied, assuming the same values. The values equal to 10 are those proposed by the spectral models in literature (Table 4.5). These values are probably too much conservative considering the large underestimation of the measured response and more reliable values could be considered close to 5; the lowest coefficients, correspondent to 1, are those for which the numerical response results closer to the measurements; these values anyway should be considered not reasonable and they don't find a counterpart between the experimental data.

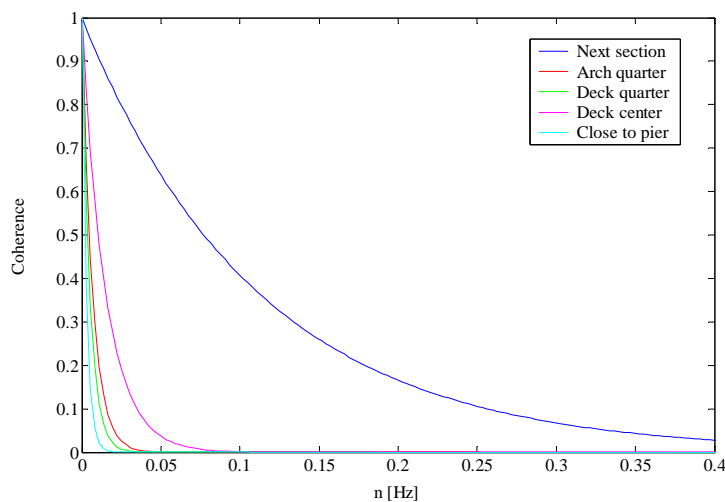


Figure 4.61 Coherence for decay coefficients equal to 10.

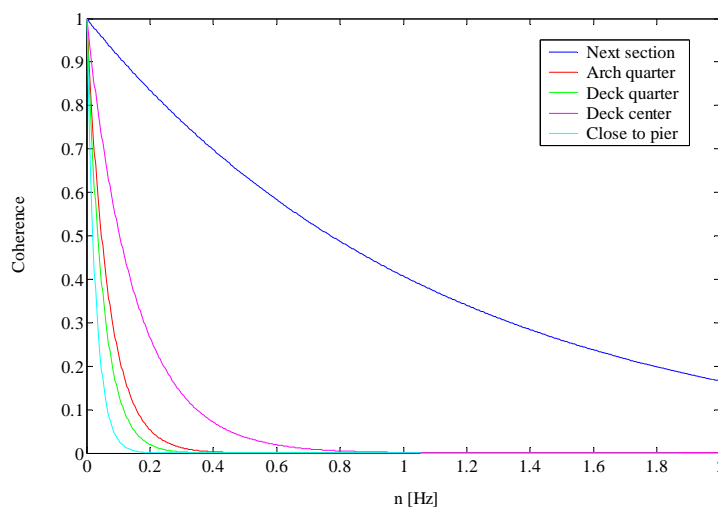


Figure 4.62 Coherence for decay coefficients equal to 1.

In the Figure 4.61-4.62 it is possible to appreciate the different coherence functions assuming decay coefficients equal to 10 and 1. The coherence function, defined by an exponential decay form, decreases at the increasing of the frequency $n [Hz]$ and at the increasing of the spatial distance between the pints considered.

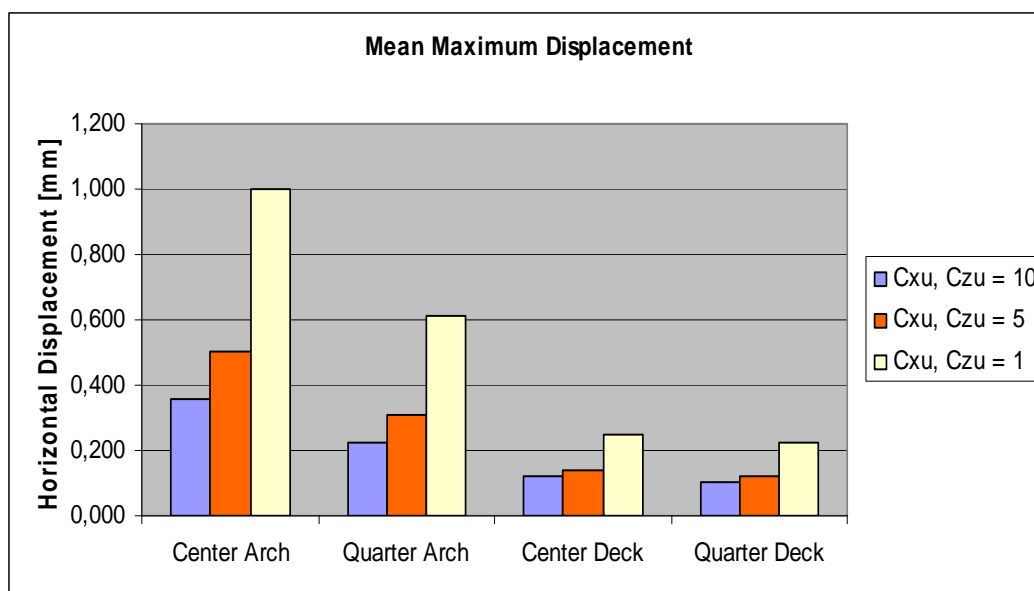


Figure 4.63 Mean maximum displacement varying the decay coefficients.

The difference from the measurements varies between about 10% and 80%.

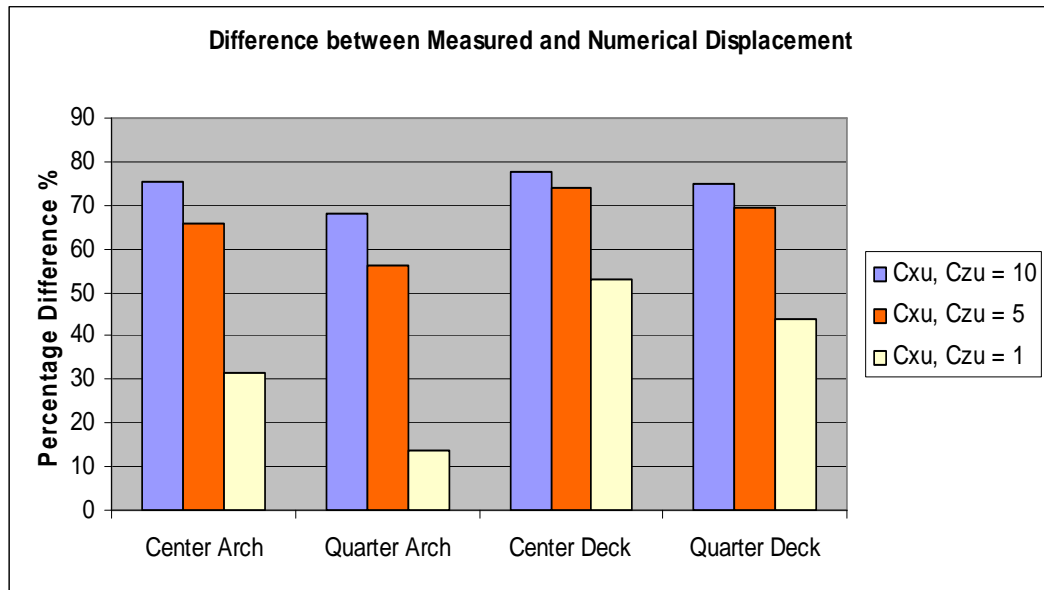


Figure 4.64 Percentage difference from the measurements.

4.10.4 Influence of the roughness length

The roughness length, representing the characteristics of roughness of the bridge site, doesn't show to have a large influence on the final response of the structure. This parameter has a double effect on the wind field: on one hand the mean wind velocity, defined at a specified high by a logarithmic law, decreases at the increasing of the roughness length (Figure 4.65).

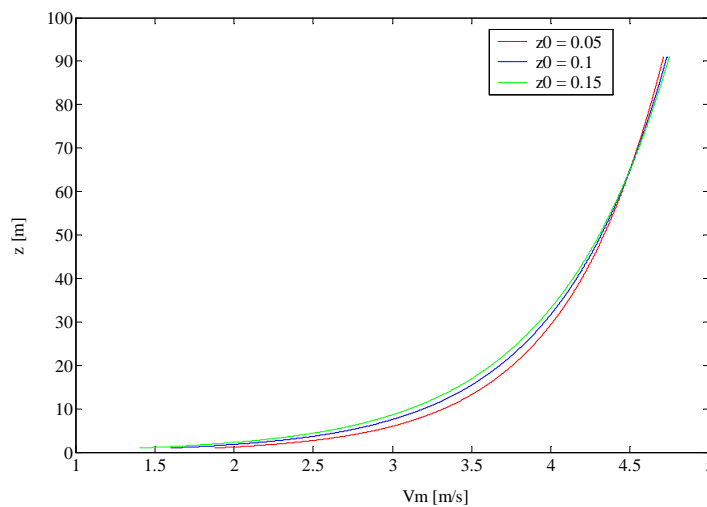


Figure 4.65 Comparison between mean wind velocity profiles.

On the other hand the turbulence intensity increases at the increasing of the roughness length (Figure 4.66).

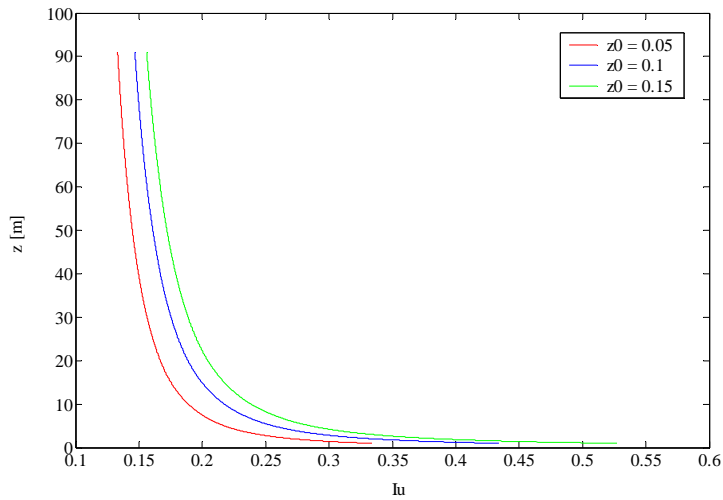


Figure 4.66 Comparison between longitudinal turbulence intensities.

This second effect results predominant on the first and the final response, as shown from the results in Figure 4.67, increases with higher values of the roughness length.

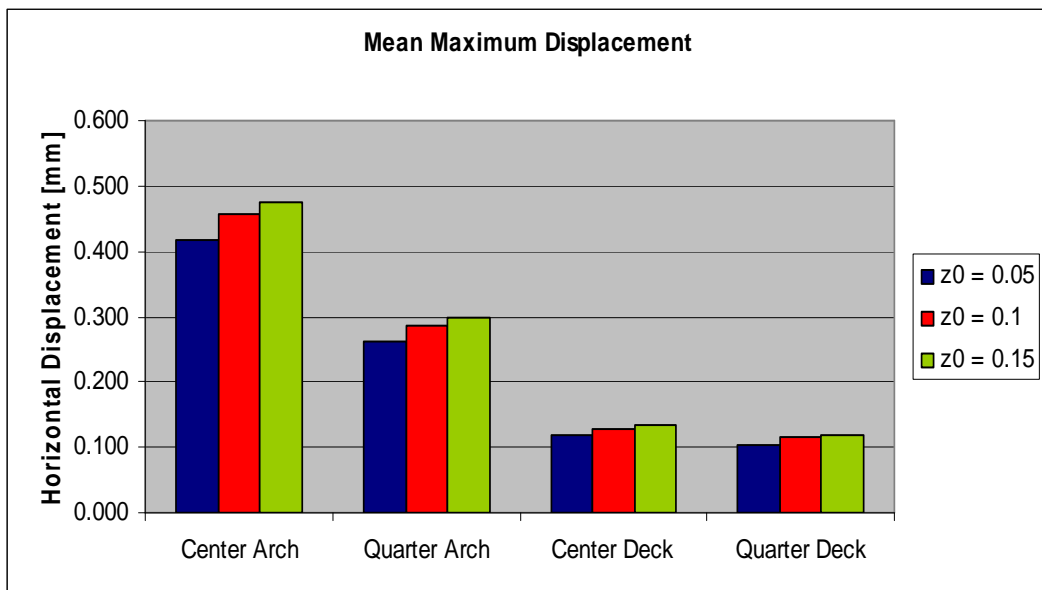


Figure 4.67 Mean maximum displacement varying the roughness length.

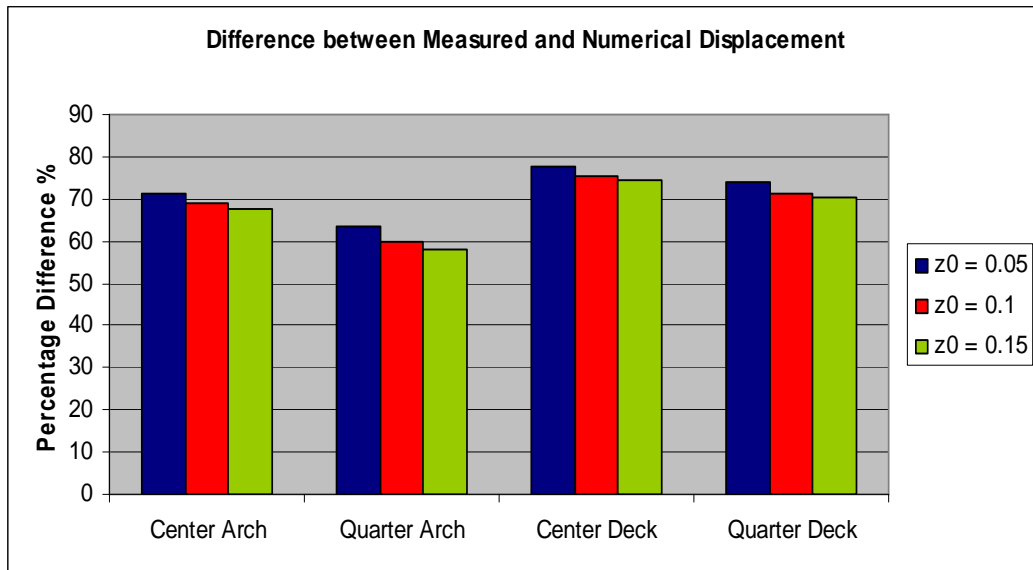


Figure 4.68 Percentage difference from the measurements.

The reference value assumed in this work is equal to 0.1 [m], estimated by the fitting procedure. The simulations are carried out for other two values respectively equal to 0.05 and 0.15 [m]. The difference from the measurements varies between 60% and 80%.

4.10.5 Drag forces divided in equal parts between the two deck girders

The drag forces on the bridge deck are divided in two equal parts and applied symmetrically on the two external longitudinal beams.

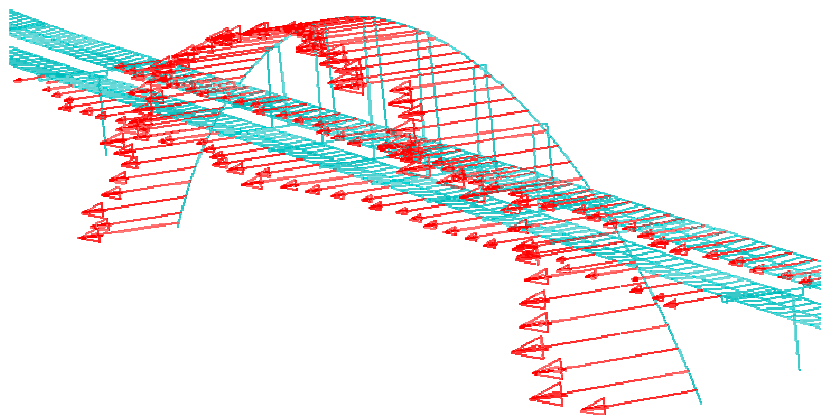


Figure 4.69 Wind forces applied on both carriageways.

The decay coefficients of the coherence function are assumed equal to 10 and the drag coefficient of the arch equal to 2. The closeness of the results obtained with the corresponding configuration where the forces on the bridge deck are applied only on one external longitudinal beam can show the global rigidity of the structural system. The difference between the responses of the two configurations is less than 5%.

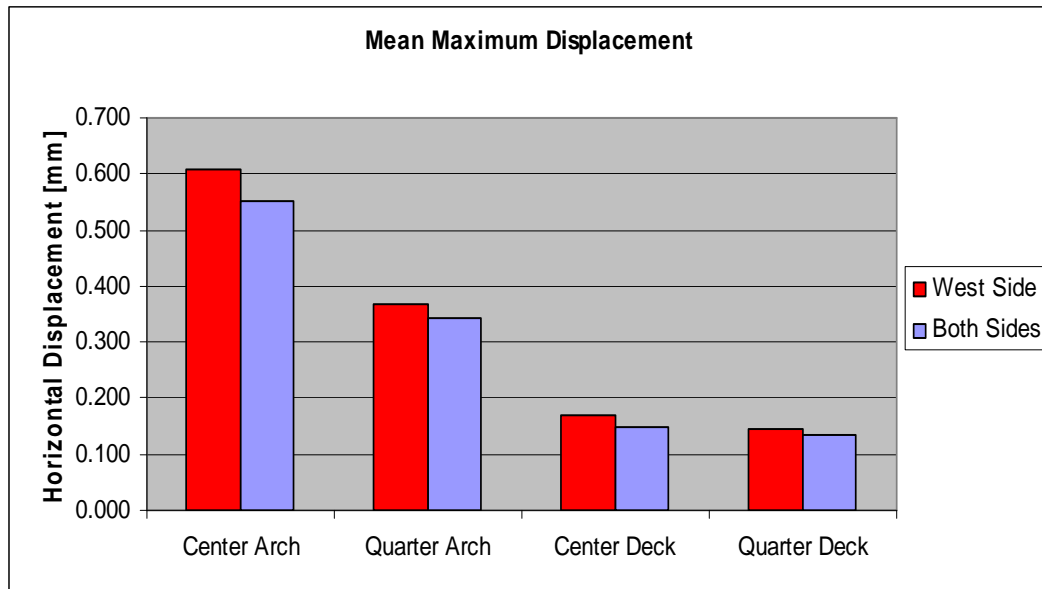


Figure 4.70 Mean maximum displacement dividing the drag forces between the two deck girders.

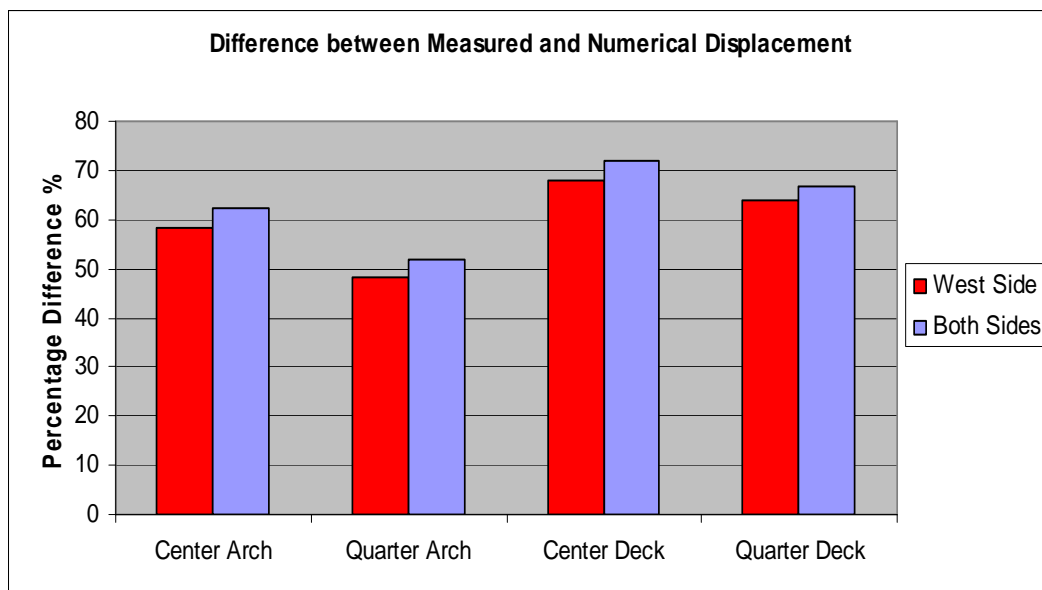


Figure 4.71 Percentage difference from the measurements.

The percentage difference from the measurements varies between 50% and 70%.

4.10.6 Contribution of the vertical turbulence

Adding the contribution due to the vertical turbulence component the drag forces increase their intensity; this component is added only to the forces applied on the bridge deck cause both the first derivative of the drag coefficient and the lift coefficient of the rectangular section of the arch, due to its symmetry about the horizontal wind flow, are zero. In this case the longitudinal and vertical turbulence components are generated by two separated simulations. The spectral equation for the vertical turbulence is the same used for the longitudinal turbulence and the simulation is carried out following the procedure exposed before; the values of the decay coefficients C_{yw} and C_{zw} for the coherence function are those proposed in literature respectively equal for the transversal and vertical direction to 6.5 and 3. The corresponding decay coefficients C_{yu} and C_{zu} for the longitudinal turbulence are both taken equal to 10. The difference between the responses obtained through the two configurations is less than 5% for the arch and of about 8% for the bridge deck.

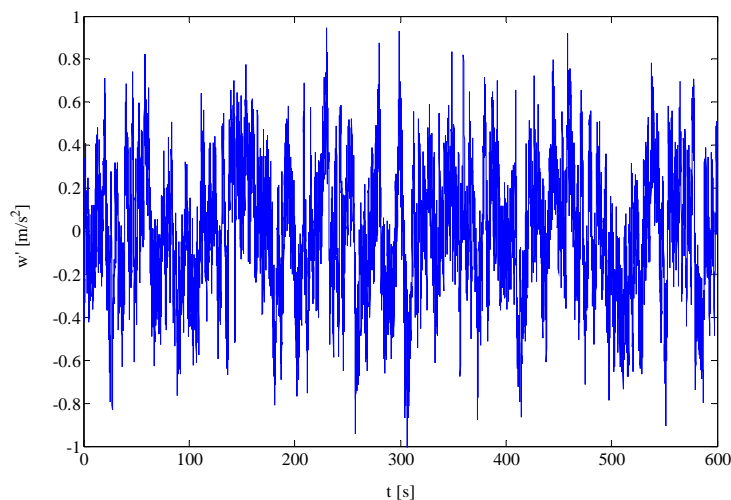


Figure 4.72 Simulated vertical turbulence at the midpoint of the bridge deck.

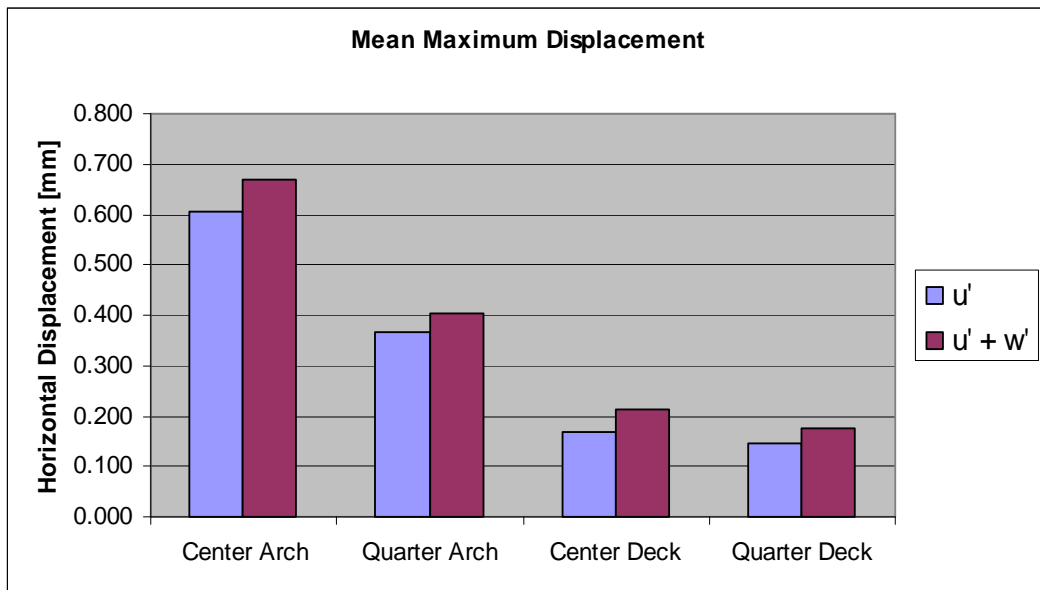


Figure 4.73 Mean maximum displacement adding the vertical turbulence.

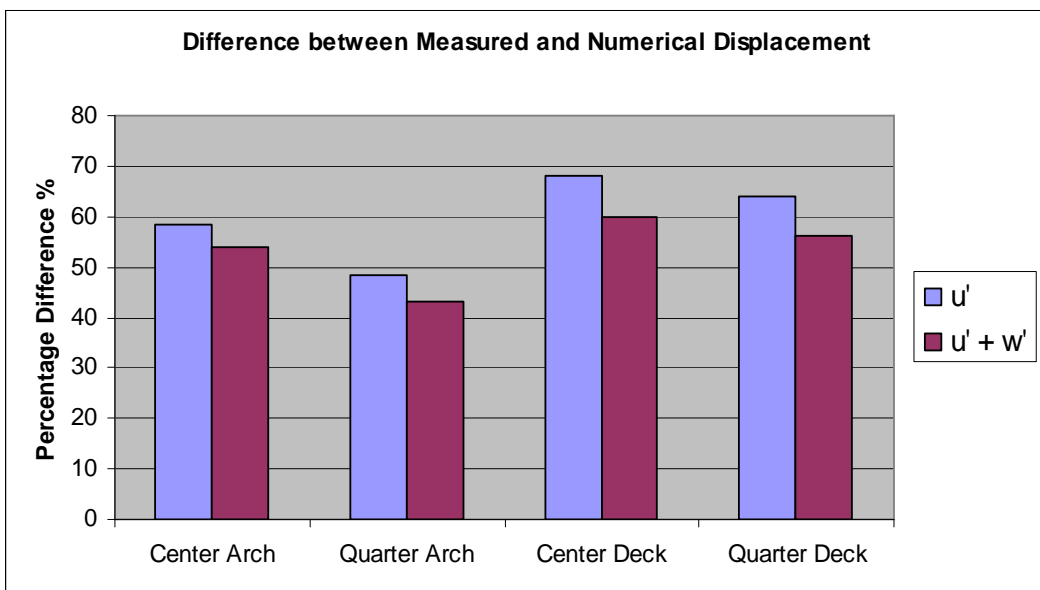


Figure 4.74 Percentage difference from the measurements.

The percentage difference from the measurements varies between 40% and 70%.

4.10.7 Coherence between different turbulence components

In this case longitudinal and vertical turbulence components are generated together during the same simulation. The drag force and the contribution due to the vertical turbulence are both divided between the two bridge deck girders by the drag and lift coefficients measured on each carriageway separately. The drag coefficient of the arch is assumed equal to 2.

	Windward	Leeward
C_D	0.09	0.06
C_L	0.05	-0.25
C'_D	0.007	-0.0075

Table 4.10 Drag, lift coefficient and first derivative of the drag coefficient for each deck girder.

A simplification is introduced in the simulation of the longitudinal turbulence components on the bridge deck assuming that they are completely correlated at both of its sides. The coherence between the longitudinal turbulence components at the arch and the west side of the bridge deck is considered together with the coherence of the vertical turbulence components between the two sides of the bridge deck and the coherence between different turbulence components at the same points. The cross power spectral density function of different turbulence components at different points can be expressed as:

$$S_{\varepsilon\eta}(M, M', n) = \sqrt{S_{\varepsilon}(z, n)S_{\eta}(z', n)} \text{Coh}_{\varepsilon\eta}(M, M', n) \quad (\varepsilon, \eta = u, w) \quad (4.28)$$

where the coherence function between different turbulence components is expressed as:

$$\text{Coh}_{\varepsilon\eta}(M, M', n) = \text{sgn}(\Gamma_{\varepsilon\eta}) \sqrt{\Gamma_{\varepsilon\eta}(z, n)\Gamma_{\varepsilon\eta}(z', n)} \sqrt{\Lambda_{\varepsilon}(M, M', n)\Lambda_{\eta}(M, M', n)} \quad (4.29)$$

The term $\Gamma_{\varepsilon\eta}(z, n)$ is the point coherence function of different turbulence components in the same point:

$$\Gamma_{\varepsilon\eta}(z, n) = \text{Coh}_{\varepsilon\eta}(M, M, n) \quad (\varepsilon \neq \eta) \quad (4.30)$$

The term Λ_ε is the space coherence function of the same turbulence components at different points (4.16); $\text{sgn}(\Gamma_{\varepsilon\eta})$ is the sign function:

$$\Gamma_{\varepsilon\eta} / |\Gamma_{\varepsilon\eta}| \quad (4.31)$$

The atmospheric turbulence is thus described by three types of functions: the power spectral density function $S_\varepsilon(z, n)$ ($\varepsilon = u, w$), the point coherence function $\Gamma_{\varepsilon\eta}(z, n)$ ($\varepsilon \neq \eta$) and the space coherence function $\Lambda_\varepsilon(M, M', n)$ ($\varepsilon = u, w$).

The point coherence function which quantifies the cross-correlation of different turbulence components in the same point of the space is given by:

$$\Gamma_{uw}(z, n) = \frac{1}{k_{uw}} \frac{1}{\sqrt{1 + 0.4 \left[n L_u(z) / V_m(z) \right]^2}} \quad (4.32)$$

where $L_u(z)$ is the integral length scale of the longitudinal component of turbulence and k_{uw} is a non-dimensional coefficient called point coherence scaling factor given by:

$$k_{uw}(z) = A_{uw} \sqrt{\beta_u(z) \beta_w(z)} \quad (4.33)$$

The two terms under root square $\beta_u(z)$ and $\beta_w(z)$ are non-dimensional coefficients defined as the turbulence intensity factors.

The other term $A_{uw}(z)$ can be expressed by the approximate formula:

$$A_{uw}(z) = 1.11 \left[L_w(z) / L_u(z) \right]^{0.21} \quad (4.34)$$

where $L_w(z)$ is the integral length scale of the vertical component of turbulence.

Once determined the cross power spectral density functions of longitudinal and vertical turbulence at different points of the structure a matrix of terms S_{uw} [98x80] can be built; this matrix assembled with the spectral density matrix S_{uu} [98x98] of the longitudinal turbulence components at the fifty eight points along the arch and forty points on the west side of the bridge deck and the spectral density matrix S_{ww} [80x80] of the vertical turbulence components at the forty points on each side of the bridge deck builds the total spectral density matrix S [178x178] (Figure 4.75).

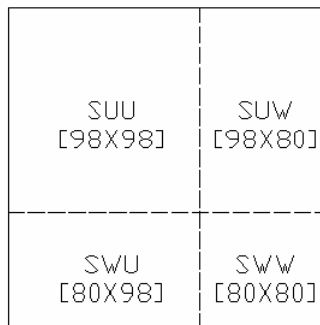


Figure 4.75 Spectral density matrix.

The next step in the generation of the wind velocity histories is to submit this matrix to the Cholesky decomposition and then applying the random phase method to simulate the turbulence components; the total number of generated turbulence histories is equal to 178 divided in such a way: 98 longitudinal turbulence histories at the fifty eight points on the arch and forty points at the west side of the bridge deck; 80 vertical turbulence histories at the two sides of the bridge deck.

The percentage difference from the measurements varies between 40 and 50%. It is reasonable to consider this last model proposed as that closer to the real configuration of the structure; this assumption can be based also on the results obtained which show to be the closest to the measurements. The response of the arch is almost the same of that found by adding the vertical turbulence component to the drag forces applied on the west side of the bridge deck (4.10.6); a increase instead of about 10% can be noted in the response of the bridge deck.

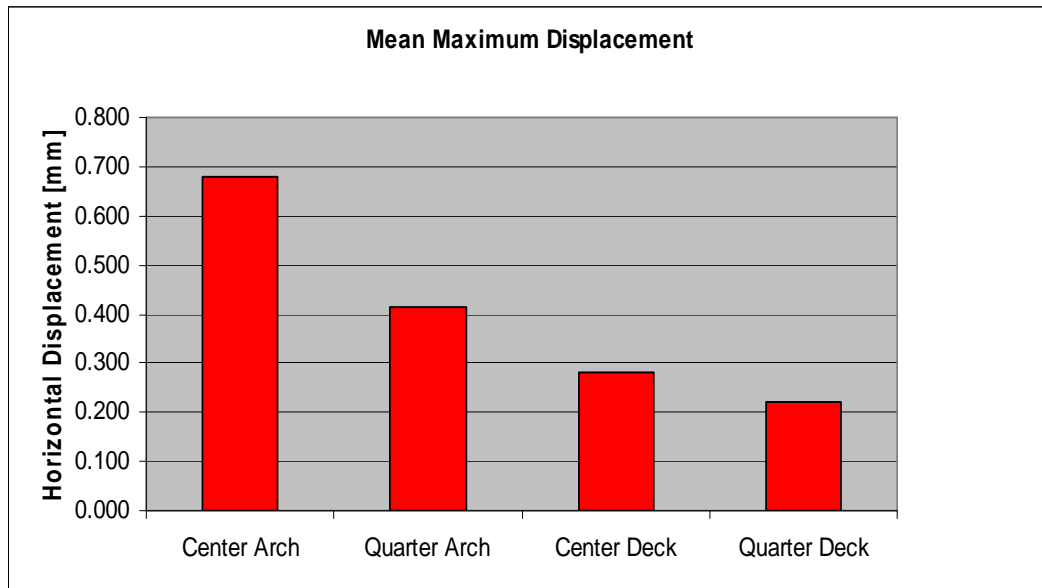


Figure 4.76 Mean maximum displacement.

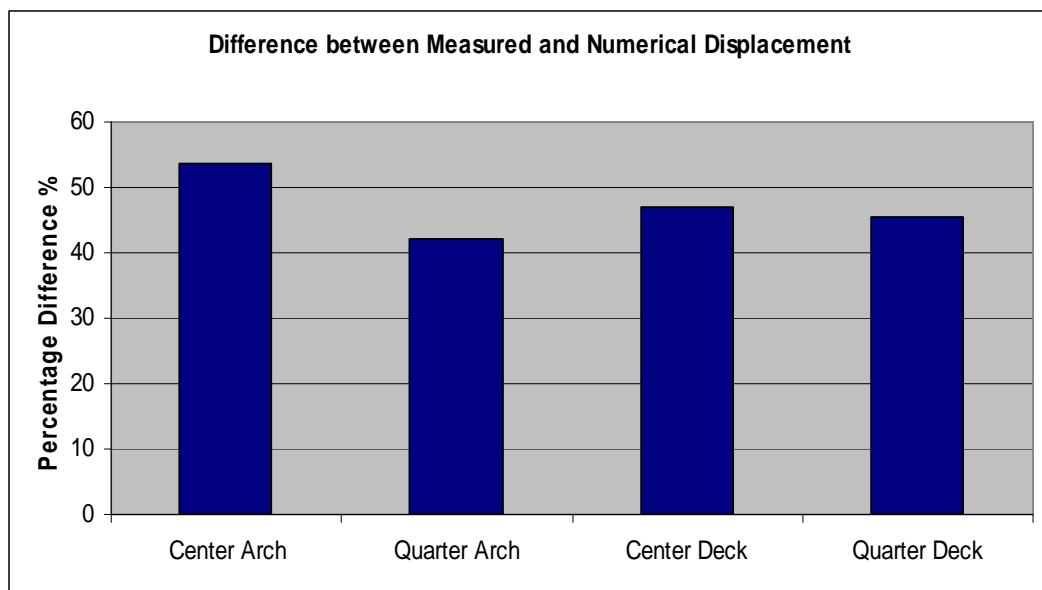


Figure 4.77 Percentage difference from the measurements.

It has to be pointed out that using the aerodynamic coefficients for the entire section and applying the forces only on the windward side of the bridge deck the turbulence effect on the leeward part of the bridge deck due to the separated wake is lost and the response of the system results mitigated. Looking Figure 4.78 the large difference in the turbulence content between the forces applied on the windward and leeward side can be appreciated.

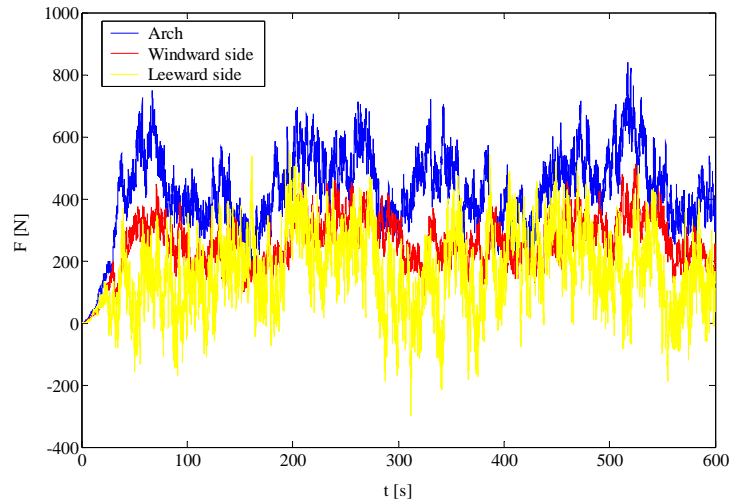


Figure 4.78 Comparison between the forces applied at the central section of the bridge.

4.11 Eurocode method to calculate the static equivalent forces

The following is a brief summary of the recommended method for the evaluation of the static equivalent forces in the Eurocode 1. The Tables and Figures from which obtain the terms of the relations below are referred to the sections and pages of the Eurocode 1.

4.11.1 Basic wind velocity

$$V_b = C_{dir} C_{season} V_{b,0} \quad (4.35)$$

where:

$V_{b,0}$ is the fundamental value of the basic wind velocity, characteristic 10 minutes mean wind velocity, irrespective of wind direction and time of the year, at 10 m above ground level in open country terrain that corresponds to terrain category II (Table 4.1, page 20); this value is taken equal to 25 [m/s].

C_{dir} is the directional factor; the value may be found in the National Annex. The recommended value is 1.0.

C_{season} is the season factor; the value may be found in the National Annex. The recommended value is 1.0. This factor may be used for temporary structures and for all structures in the execution phase.

4.11.2 Mean wind velocity

$$V_m(z) = C_r(z) C_o(z) V_b \quad (4.36)$$

The mean wind velocity at height z above the terrain depends on the terrain roughness, on the orography and on the basic wind velocity. The roughness factor C_r is given by:

$$C_r(z) = k_r \ln\left(\frac{z}{z_0}\right) \quad \text{if } z_{\min} \leq z \leq z_{\max} \quad (4.37)$$

$$C_r(z) = C_r(z_{\min}) \quad \text{if } z \leq z_{\min} \quad (4.38)$$

where:

z_0 , z_{\min} depend on the terrain category (Table 4.1, page 20) and represent respectively the roughness length and the minimum height; z_0 is assumed equal to the roughness length estimated equal to 0.1 [m].

k_r is the terrain factor defined as:

$$k_r = 0.19 \left(\frac{z_0}{z_{0,II}} \right)^{0.07} \quad (4.39)$$

where:

$z_{0,II}$ is equal to 0.05 m (terrain category II, Table 4.1, page 20).

z_{\max} is to be taken as 200 m, unless otherwise specified in the National Annex.

The orography factor C_o is given by:

$$\begin{aligned} C_o &= 1 & \text{if } \phi \leq 0.05 \\ C_o &= 1 + 2s\phi & \text{if } 0.05 < \phi < 0.3 \end{aligned} \quad (4.40)$$

$$C_o = 1 + 0.6 s \phi \quad \text{if } \phi \geq 0.3$$

ϕ is the upwind slope H/L_u in the wind direction; H is the effective height of the feature and L_u is the actual length of the upwind slope in the wind direction.

s is the orography location factor, to be obtained from Figure A.2 or Figure A.3 (Annex A, page 99) scaled to the length of the effective upwind slope length L_e (Table A.2, page 98).

4.11.3 Wind turbulence

The turbulence intensity at height z is defined as the standard deviation of the turbulence divided by the mean wind velocity.

$$I_v(z) = \frac{\sigma_v}{V_m(z)} = \frac{k_I}{C_o(z) \ln(z/z_0)} \quad \text{if } z_{\min} \leq z \leq z_{\max} \quad (4.41)$$

$$I_v(z) = I_v(z_{\min}) \quad \text{if } z < z_{\min} \quad (4.42)$$

with the standard deviation of the turbulence given by:

$$\sigma_v = k_r V_b k_I \quad (4.43)$$

where:

k_r and V_b are the terrain factor and the basic wind velocity defined before.

k_I is the turbulence factor. The value may be given in the National Annex. The recommended value is 1.0.

4.11.4 Peak velocity pressure

The peak velocity pressure at height z should be determined by the expression:

$$q_p(z) = [1 + 7 I_v(z)] \frac{1}{2} \rho V_m^2(z) = C_e(z) q_b \quad (4.44)$$

where $C_e(z)$ is the exposure factor defined as:

$$C_e(z) = C_r^2(z) C_o^2(z) [1 + 7 I_v(z)] \quad (4.45)$$

The value 7 is based on a peak factor equal to 3.5. For flat terrain with $C_o(z) = 1$, the exposure factor can be illustrated as a function of height above terrain and a function of terrain category (Figure 4.2, page 23).

q_b is the basic velocity pressure defined as:

$$q_b = \frac{1}{2} \rho V_b^2 \quad (4.46)$$

4.11.5 Wind pressure on external surfaces

The wind pressure acting on the external surfaces should be obtained by:

$$W_e = q_p(z_e) C_{pe} \quad (4.47)$$

where:

z_e is the reference height for the external pressure (Figure 7.4, page 35).

C_{pe} is the pressure coefficient for the external pressure (Section 7, page 31).

4.11.6 Wind forces

The wind forces for the whole structure or a structural component should be determined:

- Calculating forces using force coefficients.
- Calculating forces from surface pressures.

Following the first method, the wind force acting on a structure or a structural element is given by:

$$F_w = C_s C_d C_f q_p(z_e) A_{ref} \quad (4.48)$$

or by vectorial summation over the individual structural elements:

$$F_w = C_s C_d \sum_{elements} C_f q_p(z_e) A_{ref} \quad (4.49)$$

where:

$C_s C_d$ is the structural factor (Section 6, page 28).

C_f is the force coefficient for the structure or structural element (Section 7 for structures or structural element such as prisms, cylinders, roofs etc; Section 8 for bridges).

$q_p(z_e)$ is the peak velocity pressure at reference height.

A_{ref} is the reference area of the structure or structural element (Section 7 and Section 8).

The wind force acting on a structure or a structural element can be determined, following the second method, by vectorial summation of the forces obtained from the surface pressures. For the external forces:

$$F_{w,e} = C_s C_d \sum_{surfaces} W_e A_{ref} \quad (4.50)$$

where:

W_e is the external pressure on the individual surface at the reference height.

A_{ref} is the reference area of the individual surface.

The frictional forces resulting from the friction of the wind parallel to the external surfaces are given by:

$$F_{fr} = C_{fr} q_p(z_e) A_{fr} \quad (4.51)$$

where:

C_{fr} is the friction coefficient (Table 7.10, page 65).

A_{fr} is the area of the external surface parallel to the wind (Figure 7.22, page 66).

4.11.7 Structural Factor

The detailed procedure for calculating the structural factor is given by:

$$C_s C_d = \frac{1 + 2k_p I_v(z_e) \sqrt{B^2 + R^2}}{1 + 7I_v(z_e)} \quad (4.52)$$

where:

z_e is the reference height (Figure 6.1, page 29)

k_p is the peak factor defined as the ratio of the maximum value of the fluctuating part of the response to its standard deviation.

B^2 is the background factor, allowing for the lack of full correlation of the pressure on the structure surface (Annex B and Annex C).

R^2 is the resonance response factor, allowing for turbulence in resonance with the vibration mode (Annex B and Annex C).

4.11.8 Equivalent static forces on the bridge

The equivalent static forces given by the Eurocode 1 are simplified forces which have a static effect equivalent to the maximum dynamic effect of the wind actions. Using the concepts given by the Eurocode 1 and the aerodynamic coefficients obtained by the wind tunnel tests the equivalent static forces for unit of length are given by:

$$D(z) = \frac{1}{2} \rho V_m^2(z) [1 + 7I_v(z)] C_s C_d B C_D \quad (4.53)$$

where:

ρ is the density of the air equal to 1.25 Kg/m³.

V_m is the mean wind velocity at the height z where the force is applied.

I_v is the intensity of the longitudinal turbulence.

B is a characteristic geometric dimension represented for the bridge deck by the transversal width, equal to 28 m and for the arch by the height of the section exposed to the longitudinal wind flow, varying from 4.2 m at the abutments to 2.7 m at the crown of the arch.

$C_s C_d$ is the structural factor defined at 2.14.7. This factor can be assumed in first approximation equal to the unit, as made in this work. A detailed procedure for determining this factor can be found in the Annex B and C of the Eurocode 1.

C_D is the aerodynamic drag force coefficient for an onflow angle $\alpha = 0^\circ$; for the bridge deck this coefficient is assumed equal to 0.15, determined from the wind tunnel tests and for the arch an approximate value equal to 2 is assumed.

The equivalent static forces on each node of the FE model of the bridge can be obtained multiplying the forces for unit of length obtained at (4.53) for the influence length L_i of each node. The force on the i -th node at z_i height can be expressed as:

$$D(z_i) = \frac{1}{2} \rho V_m^2(z_i) [1 + 7 I_v(z_i)] C_s C_d B L_i C_D \quad (4.54)$$

4.12 Equivalent static forces from the wind tunnel test

The equivalent static forces for unit of length are calculated by a mean component, a background component and a resonant component following the formula:

$$D(z) = \frac{1}{2} \rho V_m^2(z) C_D B G_q \quad (4.55)$$

All the terms were defined before expect G_q that is the gust response factor given by:

$$G_q(z) = 1 + 2 k_q I_u(z) \sqrt{B^2 + R^2} \quad (4.56)$$

Where B^2 and R^2 are the background and resonant response factors and I_u is the intensity of the longitudinal turbulence. The factor k_q is the peak factor which is given by:

$$k_q = \sqrt{2 \ln(v_q T)} + \frac{0.577}{\sqrt{2 \ln(v_q T)}} \quad (4.57)$$

Where T is the time period equal to 600 [s] and v_q is the expected frequency of the gust response.

The value of the gust response factor results equal to 1.99 and 2 respectively for the arch and for the bridge deck.

The force on the i-th node at z_i height can be expressed as:

$$D(z_i) = \frac{1}{2} \rho V_m^2(z_i) C_D B G_q(z_i) L_i \quad (4.58)$$



Figure 4.79 Deformed configuration due to static equivalent forces.

4.13 Analysis with a high mean wind velocity

Finally a simulation based on the model described at 4.10.7 and an analysis with the equivalent static forces introduced at 4.12-4.13 are carried out assuming as reference an high mean wind velocity equal to 25 [m/s]. The results obtained from these two analyses can be compared in order to point out on one hand the validity of the dynamic simulations made and on the other to show the major facility to get results closer to response of the structure for higher wind velocities.

It has to be noted that as expected the analysis with equivalent static forces gives a larger response compared with that from dynamic simulation; the equivalent static forces are conservative forces which give the maximum response of the structure due to dynamic effects and they are usually applied for the design of the structures. The results obtained with the equivalent static forces calculated by the formula from the Eurocode and from the wind tunnel test show to be really close.

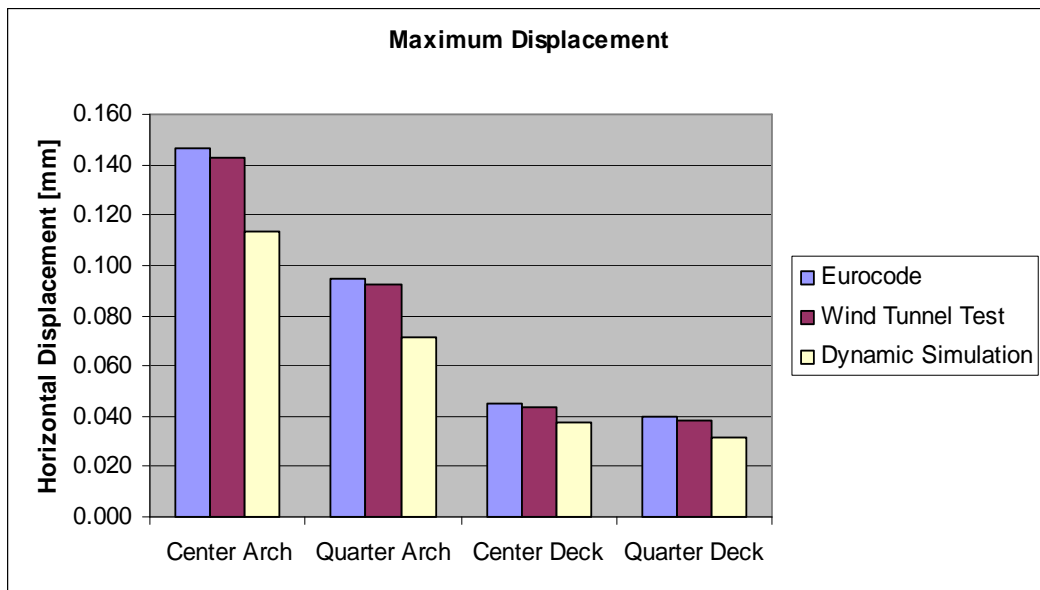


Figure 4.80 Maximum displacement for a high mean wind velocity.

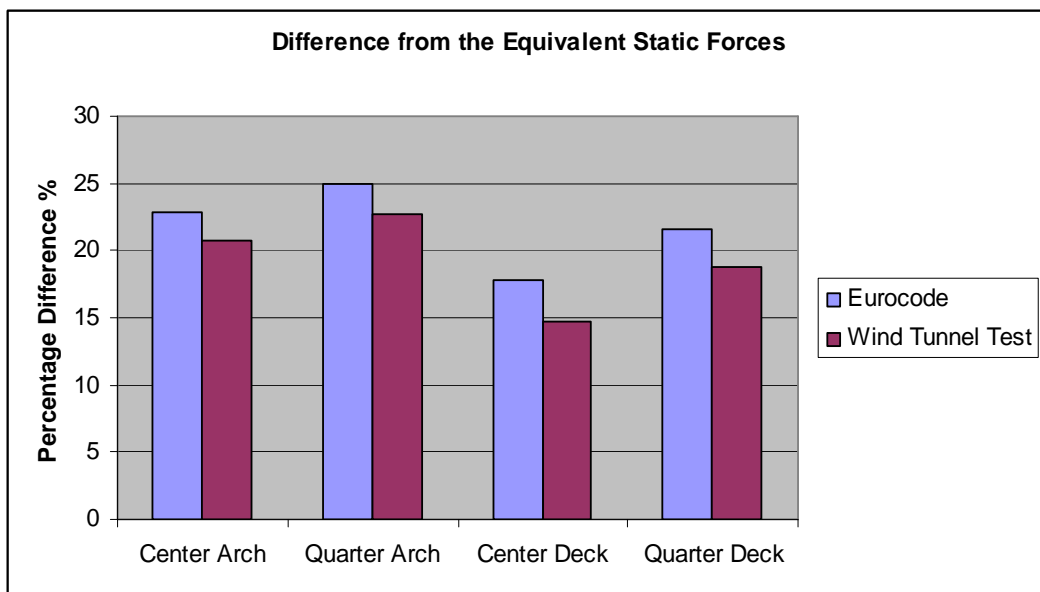


Figure 4.81 Percentage difference from the measurements.

The percentage difference between the results obtained from the dynamic simulation and those from the equivalent static forces is about of 20%.

Chapter 5 Conclusions and suggestion for further research

5.1 Conclusions

The analysis developed doesn't propose the common approach followed in the design of structures where the response due to wind actions is evaluated by the application of conservatives static forces, known as static equivalent forces, which give the maximum response due to dynamic effects on the structure. This work instead follows another way and the analysis starts from response of the structure through the experimental data produced during the monitoring of the bridge and tries to point out the influence of the wind effect on the global measured response. The observed distance which separates numerical and measured results has to be interpreted taking into account on one hand the simplifications assumed in the model and on the other the uncertainties of many parameters involved in the simulation, together with the anomalies found in the wind velocity measurements. For what concerns the FE model of the bridge certainly it can be said that it represents a simplified model which schematizes all the structural elements by beams; however, as found by the comparison between the numerical and measured eigenfrequencies and eigenvalues, it reproduces well the characteristics of mass and stiffness of the real structure. More uncertainties, instead, affect the model of the damping ratio even if the value estimated by the measurements can be considered more reliable than that first estimated from the Eurocode form; anyway this parameter doesn't show to be much influent on the final results. The parameters which characterize the properties of the wind field and the related actions on the structure can be recognized as the most aleatory, and errors and uncertainties affect also the spectral model used in their simulations. The coherence functions show to have a central rule in the calculation of the along-wind forces and consequently in the resultant response of the structure. The definition of this functions passes through the assumption of their decay coefficients; the values proposed in literature are mean values extracted from experimental data and it is necessary to take into account the dispersion of their values and the uncertainties from which they are affected. Furthermore these values show to be not suitable in order to represent the effective coherence of the wind actions in the examined case, and a reduction of their values is necessary in order to get results closer to the measurements. Uncertainties, then, affect the definition of the roughness length which characterizes the properties of roughness of the

bridge site; anyway also this parameter doesn't show to be much influent on the final response. Two other parameters show to have a large influence on the determination of the wind actions and on the final results obtained: on one hand the number of concentrated forces applied on the model and on the other the values of the aerodynamic static coefficients. The results obtained varying the number of forces applied show to get a convergence for the configuration with fifty eight forces on the arch and forty on the west side of the bridge deck; this configuration is that taken as reference in the analyses carried out. The choice of the west side reflects the direction of the prevalent winds and the effects of this choice will be discussed later; anyway the application of the forces on the other side don't give different results due to the symmetry of the structure. It has also to be pointed out the simplification for which the along-wind forces are applied only on the arch and the central part of the bridge deck; this assumption can be considered reasonable taking into account that the first horizontal modes of vibration, principally involved in the response of the structure to the along wind forces, interest only these parts of the structure; moreover the accelerometers were placed on the arch and on the main suspended span of the bridge deck thinking that these are certainly the parts of the structure more sensible to problems of induced vibrations. Considering the aerodynamic static coefficients involved in the definition of the along-wind forces it must be distinguished between the bridge deck and the arch; for the first the values assumed are deduced from the wind tunnel tests; for the second, instead, an approximated constant value is assumed for the whole element. Actually one value for each section considered of the element should be determined varying their inclination respect to the assumed perpendicular horizontal wind flow. Furthermore it has to be noted as it wasn't studied by the wind tunnel tests which could be the value of the drag coefficient of the bridge deck at the passage of a long queue of high vehicles; in such a configuration the aerodynamic of the structure results completely modified. About the experimental data on the wind velocity it can be point out some uncertainties related to the positions of the anemometer. At first due to the closeness of the anemometer to the bridge the measurements are certainly affected by the presence of the structure. The direction of the prevalent winds is from the west side and the anemometer is positioned on the east side of the bridge deck in proximity of the pier closest to the arch on the Swedish part of the bridge. The wind flow arriving from the opposite west direction can separate a turbulent wake with a consequent disturb of the measurements and an

increased contribute given to drag forces which act on the leeward side of the bridge deck. This last effect is pointed out by the simulation carried out separating the along-wind forces through the aerodynamic static coefficients determined on each deck girder separately; this configuration reproduces better the real configuration of the structure and gives the results closer to the measurements. Finally, regarding the position of the anemometer, it has to be noted the anomaly for which it is placed at the opposite side of the accelerometers which are installed along the west side of the bridge deck; this doesn't seem to be a good solution and demonstrates not much consideration given to the study of the wind effect in the monitoring of the structural behaviour. A theoretical drawback, then, affects all the analyses carried out because it has to work assuming a reference wind velocity history with a low mean value. The quasi-steady theory used for the calculation of the along-wind forces works well for sufficiently high values of the wind velocities (>5 m/s) and, probably, in this case the theory used is at the limit of its validity. Moreover with a low mean wind velocity also the values of the aerodynamic static coefficients, determined by the wind tunnel test, should have a larger dispersion. The purpose of the last analyses carried out assuming an high mean wind velocity is to test the validity of the simulations, taken into account of the mentioned limitation. The results from this last dynamic simulation are compared with those obtained applying the equivalent static forces proposed by the Eurocode; the response shows to be less than that from the static analysis, as expected, and the observed percentage difference is about 20%.

5.2 Further research

The analysis of the wind effects on the bridge could be completed considering the lift and moment aerodynamic forces and simulating also these forces; moreover the validation of the study carried out should be completed through the analysis of more stationary wind velocity histories characterised by a high mean value. It will be of interest then, with a more general perspective concerning also other studies of wind effects on structures, to define more reliable coherence functions. Recent experimental results (e.g. Larose) demonstrate as the aerodynamic forces are more coherent than the turbulence components; the knowledge of this larger coherence of the aerodynamic forces is now limited only to the lift forces and it is still not known how quantify this effect in analytical terms through

the coherence functions. However it is reasonable to believe that the same measured effect could concern also the along-wind forces.

Bibliography

- Abaqus Version 6.4 Manual, 2003.
- Battini J.M. Lecture notes in Structural Dynamics, Royal Institute of Technology (KTH), Stockholm, Sweden, 2002.
- Benfratello S., Falsone G., Muscolino G., “Influence of the quadratic term in the alongwind stochastic response of SDOF structures”, Engineering and Structures, Vol. 18, No 9, pp 685-695, 1996.
- CEN “Eurocode 1 – Actions on Structures – General Actions – Part 1.4: Wind Actions”, ENV 1991-1-4, 2004.
- Clough R.W., Penzien J. “Dynamic of Structures”, Mc Graw-Hill, Singapore, 1993.
- Dyrbe, Hansen “Wind Loads on Structures”, John Wiley and Sons, 1997.
- Hortmanns M., Sedlacek G. “Wind Tunnel Test-Numerical Simulation”, Aachen, 2003.
- Hortmanns M., Sedlacek G. “Wind Tunnel Tests-Final Report”, Aachen, 2003.
- Larose G.L., Mann J. “Gust loading on streamlined bridge decks” Journal of Fluids and Structures, 12, 511-536, 1998.
- Larose G.L. “The spatial distribution of unsteady loading due to gusts on bridge decks”, Journal of Wind Engineering and Industrial Aerodynamics, 91, 1431-1443, 2003.

- James G., Karoumi R. “Monitoring of the New Svinesund Bridge, Report 1 : Instrumentation of the arch and preliminary results from the construction phase”, Brobyggnad, Royal Institute of Technology (KTH), Stockholm, Sweden, 2003.
- Jin Cheng, Jian-Jing Jiang, Ru-Cheng Xiao, Min Xia “Wind-induced load capacity analysis and parametric study of a long-span steel arch bridge under construction”, Computers and Structures, 81, 2513-2524, 2003.
- Newland D.E. “An Introduction to Random Vibrations and Spectral Analysis”
- Paz “Structural Dynamics : Theory and Computation”, Chapman and Hall, 1991.
- Plos M., Movaffaghi H. “Finite Element Analysis of the New Svinesund Bridge- Design model conversion and analysis of the arch launching”, Report 04:12, Department of Structural Engineering and Mechanics, Concrete Structures, Chalmers University of Technology, Gothenburg, Sweden, 2004.
- Simiu E., Scanlan H. “Wind Effects on Structures”, John Wiley and Sons, New York, 1986.
- Solari G. Lectures notes in Dynamic of Structures, University of Genoa, 2001-2.
- Solari G. Lectures notes in Wind Engineering, University of Genoa, 2002-3.
- Solari G., Piccardo G. “Probabilistic 3-D turbulence modelling for gust buffeting of structures”, Probabilistic Engineering Mechanics, 16, 73-86, 2001
- Wei-Xin Ren, Zhou-Hong Zong “Output-only modal parameter identification of civil engineering structures”, Structural Engineering and Mechanics, Vol. 17, No 3-4, 2004.